Macromolecular Organization of the Rough Endoplasmic Reticulum During Homeostasis and Stress

by

Alyson Marie Hoffman

Department of Biochemistry
Duke University

Date:_____

Approved:

_____
Christopher Nicchitta, Supervisor

_____
Perry Blackshear

_____
Traci Hall

_____
Hashim Al-Hashimi

_____
Michael Boyce

Dissertation submitted in partial fulfillment of
the requirements for the degree of Doctor
of Philosophy in the Department of
Biochemistry in the Graduate School
of Duke University

2019

ABSTRACT

Macromolecular Organization of the Rough Endoplasmic

Reticulum During Homeostasis and Stress

by

Alyson Marie Hoffman

Department of Biochemistry
Duke University

Date:_____

Approved:

_____
Christopher Nicchitta, Supervisor

_____
Perry Blackshear

_____
Traci Hall

_____
Hashim Al-Hashimi

_____
Michael Boyce

An abstract of a dissertation submitted in partial
fulfillment of the requirements for the degree
of Doctor of Philosophy in the Department of
Biochemistry in the Graduate School of
Duke University

2019

Abstract

The endoplasmic reticulum (ER) is an organelle that exists as a patchwork of functional membrane domains with unique protein components. The rough ER is one such domain characterized by associated ribosomal particles and is known as the site of translation for secretory and membrane proteins (SMPs). This has since been extended to include the translation of the entire transcriptome and other diverse functions including autophagosome assembly and miRNA silencing, however, little is known about the macromolecular organization of these complex biochemical processes. Using a proximity labeling technique, BioID, four ribosome associated membrane proteins (RAMPs) were selected to create a rudimentary map of translation on the rough ER by combining the BioID nonspecific biotin-labeling with streptavidin pulldowns and mass spectrometry. This revealed distinct environments surrounding each RAMP in addition to overlap that established spatial organization of these domains with each other. Of the four selected, only two, LRRC59 and Sec61β of the Sec61 translocon, labeled ribosomes *in vivo*. Identification of the mRNAs associated with these labeled ribosomes revealed that translation was spatially distinct between the two sites. This supports the existence of complex sorting mechanisms within this domain that extend to sites of optimized protein synthesis for sub-groups of mRNAs.

Since organisms exist within changing environments and stressors, the next step was to determine if macromolecules associated with the ER during homeostasis change their localization during stress, namely the unfolded protein response (UPR). Combining DTT treatment for UPR stimulation with smFISH for ER chaperones transcriptionally upregulated during this stress, it was determined that only specific transcripts, e.g. GRP94, are localized to cytoplasmic granules during stress while others, e.g. BiP, are not. Combining these observations with the existing literature, the working hypothesis is that transcripts, such as BiP, able to recruit ribosomes during times of inefficient cap-dependent translation, can escape stress granules while the nascent transcript RBP environment, such as that on GRP94, is responsible for its recruitment to these granules. Whether this observation is generalizable to all transcripts being made upon UPR stimulation is the subject of further study.

Contents

List of Tables

List of Figures

List of Abbreviations

ActD	ActinomycinD
ALS-FTD	Amyotrophic lateral sclerosis – frontotemporal dementia
ATF6	Activating transcription factor 6
BiP	Immunoglubulin heavy chain binding protein
B2M	Beta-2-microglobulin
cDNA	Complementary deoxyribonucleic acid
DRB	5,6-Dichloro-1-β-D-ribofuranosylbenzimidazol
DTT	Dithiothreitol
EM	Electron microscopy
ER	Endoplasmic reticulum
ERGIC	ER-Golgi intermediate complex
ERQC	ER quality control
ERSE	ER stress element
FRET	Forster resonance energy transfer
GAPDH	Glyceraldehyde 3-phosphate dehydrogenase
GEF	Guanidine exchange factor
IDR	Intrinsically disordered domain
IF	Immunofluorescence
IRE1	Inositol requiring enzyme 1

IRES	Internal ribosomal entry site
MAM	Mitochondria associated membrane
mNCPs	mRNAs of nucelar and cytosolic proteins
mRNA	Messenger ribonucleic acid
mSMPs	mRNAs of secretory and membrane proteins
NCPs	Nuclear and cytosolic proteins
OST	Oligosaccharyltransferase
PAM	Plasma membrane associated membrane
PERK	Protein kinase R-like endoplasmic reticulum kinase
RAMPs	Ribosome associated membrane proteins
RM	Rough microsome
SG	Stress granules
smFISH	Single molecule fluorescence *in situ* hybridization
SMP	Secretory and membrane protein
SR	SRP receptor
SRP	Signal recognition particle
TOP	Terminal oligopyrimidine
TTP	Tristetraprolin
tRNA	Transfer ribonucleic acid
uORF	Upstream open reading frame

UPR	Unfolded protein response
UTR	Untranslated region
XBP1	X-box binding protein 1
XBP1s	Sliced isoform of X-box binding protein 1

1. Introduction

1.1 Organization of the endoplasmic reticulum

In the first successful attempt at viewing cultured mammalian cells by an electron microscope Porter and colleagues described the presence of a reticular structure extending continuously through its length, this structure later became known as the endoplasmic reticulum (ER)[1,2]. Further imaging studies determined that there were two main compartments of the ER characterized by the presence or absence, rough or smooth membranes, of attached electron dense particles[3]. Through newly developed ultracentrifugation techniques to isolate specific fractions of the cell, it was found that these two fractions are also biochemically distinct as they possess different enzyme activities thus implicating functional division of this continuous membrane by proteins[4]. In the years that followed, studies would place the rough ER, characterized by the electron dense particles, now known to be ribosomes, as the main site of secretory and membrane protein (SMP) synthesis while the smooth ER served as the site of lipid synthesis and detoxification[5–8]. However, further research into the organization of this organelle has expanded their function within the cell. For instance, the smooth ER is actually a patchwork of distinct domains making contact with most other organelles, for instance the mitochondrial associated membrane (MAM), the plasma-membrane associated membrane (PAM), the ER quality control center (ERQC), the ER Golgi intermediate complex (ERGIC), and the site of lipid droplet formation[9]. Similarly, the

rough ER does more than act as the entrance to the secretory pathway. It has been identified as the site of mRNA silencing, autophagosome assembly, and a general center for transcriptome translation[10–13].

That these domains facilitate multiple functions implicates the existence of sorting mechanisms for a higher order protein organization in this membrane; essentially a patchwork of near-neighbor proteins that, together, establish nanoscale domains responsible for a specific process. Techniques such as confocal imaging can localize proteins to specific organelles in the cell but don't tell us how they interact with surrounding proteins. Similarly, high resolution techniques like crystallography and cryo-EM can show us, at atomic resolution, the shape and structure of proteins involved in complexes but do not include information about potentially important heterogeneity in their transient interactors. Biochemical studies can elucidate metabolic pathways and determine how they integrate with each other but how enzymes in metabolic pathways such as glycolysis are spatially organized is unknown beyond a basic localization to the cytosol. As evidence for intricate spatial organization, when cells are lightly permeabilized and the released contents monitored, glycolytic enzymes diffuse at different rates indicating at least partial pathway localization to larger structures[14]. Observations such as these and the fact that enzymatic activities in vivo are much higher than in vitro have led to the idea of metabolons – nanoscale organization of cytosolic proteins involved in the same metabolic process[15]. In support of this, textbooks teach the

process of oxidative phosphorylation as a chain of proteins localized to the inner membrane of the mitochondria in order to facilitate tightly regulated proton transport. Similar observations of functional clustering have been found for tRNA amino-acyl synthetase centers, known as the multi-tRNA synthetase complex, in the cytosol[16]. Furthermore, measured viscosity of the cytosol has shown that individual proteins would experience the cell as a solid, rubbery material implying a crowded environment whereby it would be advantageous for the cell to have enzymes from the same pathway spatially arranged together within the cytoplasm[17].

The field of protein organization in a 2D space such as a membrane, has evolved greatly over the last 50 years. In 1972, the fluid mosaic model of lipid membranes, in which proteins were thought to undergo random diffusion as through a 2D viscous liquid, was proposed by Singer and Nicolson based on experiments from freeze-etching, human-mouse cell membrane fusing, and visualization of different erythrocytic plasma-membrane proteins by radiolabeling[18]. However, as imaging techniques advanced in both single particle speed of tracking and imaging resolution, this view of lipid membranes began to change. Based on these newer data, it is thought that the plasma membrane exists in different organizational domains i) membrane compartments of 40-300 nm anchored by the cytoskeleton in which proteins are corralled and typically hop into other compartments only during a brief separation of the cytoskeleton from the lipid bilayer, ii) raft domains of 2-20 nm that can be heterogeneous depending on the

amount of specialized lipids such as cholesterol (more rigid) or ceramides (more gel-like) and iii) dynamic protein complex domains of 3-10 nm which consist of dimers or oligomers and greater complexes of membrane proteins[19]. This hierarchy of membrane proteins and higher order organization of the membrane has important implications for receptor signaling by oligomerization. First, receptors are present at about 1-15 copies per μm^2, given that actin bound membrane compartments number 2 million assuming a flat, monolayer cell of 60 μm^2, this results in one receptor molecule every 20-200 compartments[20]. The number of events for a protein "hopping" the actin cytoskeletal fence is 1-100 ms but once there are two or more receptors in a compartment, they will readily associate leading to localized reaction bursts[21]. This colocalization of molecules becomes important for the effective propagation of local kinase activity over the phosphatase activity within the cell. Thus, decreasing the diffusion of molecules through the plasma membrane by virtue of both protein and lipid mesoscale organization has been shown to be biologically relevant in this capacity[21]. Another study, using a combination of super-resolution microscopy and metabolic-labeling in live cells, it was shown that plasma membranes exist as patchworks of protein rich domains. These domains were shown to have less mobility with mixing times of protein domains from fused membranes being over an hour[22]. Proteins in these domains were shown to be functionally enriched, for instance proteins involved with vesicle fusion, with protein dependent preferences for internal or external positions within the

nanodomains. These results validate the findings mentioned above by providing structural details about the spatiotemporal organization of difference functions within this membrane.

For intracellular membranes, such as the ER, it is thought that the lower concentration of cholesterol leads to a more homogenous membrane[22]. However, there have been studies determining the composition of separate ultrastructural domains. For instance, using a differential detergent separation, biochemically distinct domains of the rough ER have been excised and characterized ultimately finding that mRNAs encoding ER lumenal proteins and lysosomal proteins are restricted to ceramide rich regions of the ER[23]. Studies of ER ultrastructure have determined that ER shape is highly dependent on the presence of reticulons/DP1 or CLIMP63 to generate tubule or cisternal structures respectively based on the protein's intrinsic structural properties[24–27]. Reticulons and DP1 have wedge-like alpha helices that drive lipid curvature while CLIMP63 lumenal domains link in a 180° manner to stabilize sheets and polysome association on sheets. In support of this model, the advent of super-resolution microscopy has provided clear resolution of RTN4 and CLIMP63 to curved structures and flat sheets respectively, and definitively shown directional as opposed to random lumenal flow of ER resident constructs[28,29]. However, even with these advancements, these techniques cannot determine how the rest of the protein environment is organized

with regards to these different domains since they are limited to antibody availability of previously studied proteins.

To determine in vivo protein interactions and spatial organization de novo, a technique termed proximity labeling has been developed[30,31]. The principle behind these techniques is that an enzyme, fused to a protein of interest, performs a reaction that releases a reactive chemical intermediate with the ability to covalently label specific amino acid residues in a narrow, 10 nm radius. This approach has allowed for the characterization of difficult to purify fractions of the cell such as MAM, PAM, mitochondrial cisternae, neuronal synapses, nuclear lamina and cell signaling pathways[30–35]. In many of these experiments, new interacting partners were found that would not have been identified by standard protein interaction studies such as immunoprecipitation which requires strong binding to a protein of interest. Thus, these studies both extend our knowledge of known proteins function and imply function to unstudied proteins by its protein environment. As 33% of the human proteome has an unknown function, determining how they are spatially organized to proteins of known function will start to bridge this gap in knowledge[36].

For my thesis, I have chosen to use proximity labeling techniques to further interrogate the organization of the rough ER. I have chosen the rough ER as it represents the gateway to the secretory pathway and therefore ultimately controls what is secreted or expressed on the cell surface. My goals for this part of the project were to

determine how translation is organized on the ER in relationship to the Sec61 translocon, the pore-forming complex that allows entry of SMPs into the secretory pathway, and if these proteins can participate in additional functions based on what their near neighbor interactions tell us.

1.2 Translation on the ER

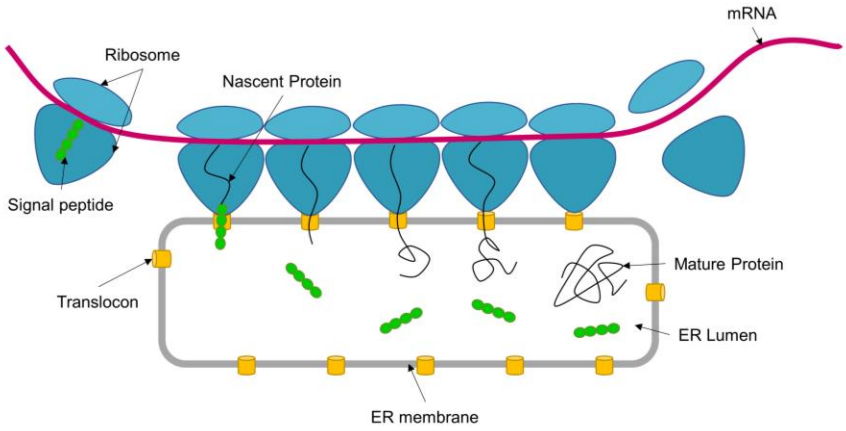

Figure 1: Schematic depicting signal sequence targeting to the ER membrane Adapted from Nobel Prize.org, Nobel Prize in Physiology or Medicine 1999 Press Release.

After the initial discovery of the rough ER, Palade and colleagues demonstrated that the bound ribosomes were integral to the synthesis of SMPs across and into the ER membrane; however, the mechanism by which this selective protein transport occurred remained elusive[37]. In 1975, Günter Blobel first proposed the signal hypothesis describing a mechanism for localizing the synthesis of SMPs to the ER[5,6,38]. Briefly, the model proposed that SMPs possess ER localization signals. These signals are recognized

in the cytosol, and the ribosome/mRNA/nascent protein chain complex is then localized to the ER, where the nascent chain undergoes co-translational translocation to the ER lumen (Figure 1). This hypothesis was validated experimentally in the ensuing decades using immunoprecipitation, biochemical purifications, complementation assays, and genetic knock-downs, uncovering additional molecular components of the signal recognition particle (SRP) pathway in the process[39–43]. This well characterized pathway is the currently accepted model by which ribosomes, proteins, and mRNAs are localized to the ER.

Although SMP biogenesis on the ER is well established, the observation that mRNAs of nuclear and cytosolic proteins (mNCPs) are also translated on the ER is many decades old but has largely been ignored[37]. More recently, this observation has been replicated using transcriptome-wide techniques, such as super-resolution imaging, cDNA microarrays, ribosome footprinting and RNA-seq, in models such as *Drosophila melanogaster*, yeast and mammalian tissue culture cells, indicating this is a significant and conserved phenomenon[11,44–51]. A precise definition of the molecular mechanism describing this unexpected finding remains, however, to be identified.

While mNCPs are translated on the ER, only a small but significant fraction of a given transcript is localized to this membrane. A study from our lab using a sequential detergent fractionation to separate cytosol and membrane fractions to then compare mRNA localization by RNA-seq and localized translational status by Ribo-seq found

that most mNCPs are localized to the cytosol while mSMPs are in the membrane fraction[11]. This is expected. However, when translational status was assessed, while mSMPs were translated exclusively in the membrane fraction, the majority of mNCP translation also occurred in the membrane fraction with an average of about 40% translation on the ER for a given transcript. So, while less than 20% of a mNCP may be localized to the membrane, those that do, associate with a higher number of ribosomes indicative of a higher throughput of translation. This distribution shows a specific pattern where those mNCPs involved in RNA or cell regulatory processes are more likely to be translated on the ER. That there is a notable distribution in functional localization to the ER suggests the existence of a specific mechanism for membrane association in the context of translation. Intriguingly, separate studies have reported that gradient isolated post-termination ribosomes can remain ER-bound and translationally competent for both SMP and NCP mRNAs[52]. These findings illustrate the existence of alternate pathways for mRNA enrichment on the ER[53–55].

The summation of these findings supports a model whereby mNCPs associate stably with the ER via translation on bound ribosomes creating an environment for transcriptome-wide translation. To further examine this idea, it is necessary to first understand the mechanism of ribosome-ER association. Studies characterizing the ribosome-membrane association in the context of the SRP pathway have been published

and these protein candidates can be used to determine how translation is organized on the ER by proximity labeling techniques.

1.2.2 Accessory factors associated with the translocon

The known physical characteristics of ribosome-membrane interactions have been inferred from *in vitro* interaction studies using salt-washed rough microsomes, vesicles derived from rough ER stripped of native bound ribosomes by high salt extraction, and inactive 80S ribosomes[56]. From this model, ribosome binding is known to be high salt and protease sensitive, indicating direct contact by the ribosome with a protein receptor. A variety of experimental approaches, such as crosslinking and affinity chromatography, have been performed using the system described above to identify subsets of ribosome receptors. Candidates have been reconstituted into liposomes where further interrogation with purified 80S ribosomes was performed. Using this model, studies spanning from the late 1970s to early 1990s yielded several candidate membrane proteins with similar ribosome interacting properties. Among these candidates are ribophorins I and II (Ribo1/2), ribosome binding protein 34 (p34/LRRC59), and ribosome binding protein 180 (p180)[57–59]. A turning point in the field came when the Sec61 translocon complex was identified as having both ribosome interacting and protein conducting channel properties in purified liposomes[43,60]. Extending from these studies, Sec61α, a subunit of the Sec61 translocon, has become the accepted ribosome receptor for those translating proteins entering the secretory pathway

[61,62]. Since these discoveries, two additional mammalian proteins, Sec62 and ERdj1, have been shown to interact with ribosomes using more sophisticated techniques such as cryo-electron microscopy and surface plasmon resonance. However, Sec62 has been found to associate with about 10% of Sec61 in mammalian cells and does not always associate with Sec63 and ERdj1 contains a cleavable cytosolic domain that doubles as a transcription factor[63,64]. Thus, like other ribosome interacting proteins, the exact mechanisms for how they regulate translation, their specific interaction with the translocon or its components, and how this integrates with their additional roles in the cell remains to be seen.

By using the proximity labeling technique, BioID, to study a subset these ribosome associating proteins, namely the well-studied components Sec61 and ribophorin I with the under-studied proteins Sec62 and LRRC59, I sought to create a map of the environment surrounding the translocon. From the functional associations of each protein's environment, the map can be used to determine how the under-studied proteins Sec62 and LRRC59 integrate into this environment or exist in unique environments. Overall, this macromolecular map of both proteins and RNAs identified by BioID will be used to reconciliate the idea that all transcripts ultimately share this space for translation and potentially extend to how additional functions attributed to the ER such as autophagy and mRNA silencing are organized around translation.

1.3 Reorganization of the ER during the unfolded protein response

1.3.1 Transition of signaling proteins during stress

As was discussed above, the ER is a vast organelle responsible for many important functions of the cell. As the cytosol and ER lumen are separated by a lipid bilayer, pathways have arisen for communication across the membrane. One such signaling event is stimulated upon accumulation of misfolded proteins[65]. The combined effect of the three known metazoan pathways stimulated by this event is known at the unfolded protein response (UPR).

Each branch of the pathway is controlled by a different ER membrane protein. First, is the protein IRE1 (inositol requiring enzyme 1) which upon detachment of the lumenal chaperone BiP leads to homo-oligomerization and self-transphosphorylation that activates an RNase domain[66]. This RNase domain initiates the cytosolic splicing of XBP1 mRNA to sXBP1 which encodes for a transcription factor that promotes expression of ER chaperones and enzymes responsible for lipid synthesis thus increasing ER folding capacity and the membrane bilayer. The second branch is led by PERK (protein kinase R-like endoplasmic reticulum kinase) which is activated similarly to IRE1. Upon kinase activation by dimerization and autophosphorylation, PERK phosphorylates eIF2α which effectively sequesters its GEF, eIF2B, and halts cap-dependent translation in the cell[67]. This has the effect of reducing additional protein load to the ER. Limiting cap-dependent translation allows for synthesis of the transcription factor ATF4 by using an

upstream open reading frame (uORF). ATF4 enhances the synthesis of transcripts involved in proapoptotic pathways such as CHOP and the regulatory subunit of an eIF2α phosphatase, GADD34. The third branch is led by ATF6 (activating transcription factor 6). This protein is an ER resident during homeostasis due to its interaction with BiP, however, upon the accumulation of misfolded proteins, BiP is removed, exposing a Goli localization sequence on ATF6 where it is cleaved by the two SREBP proteases, S1P and S2P [68]. This creates a 50 kD transcription factor that activates transcription of genes coding for ER chaperones.

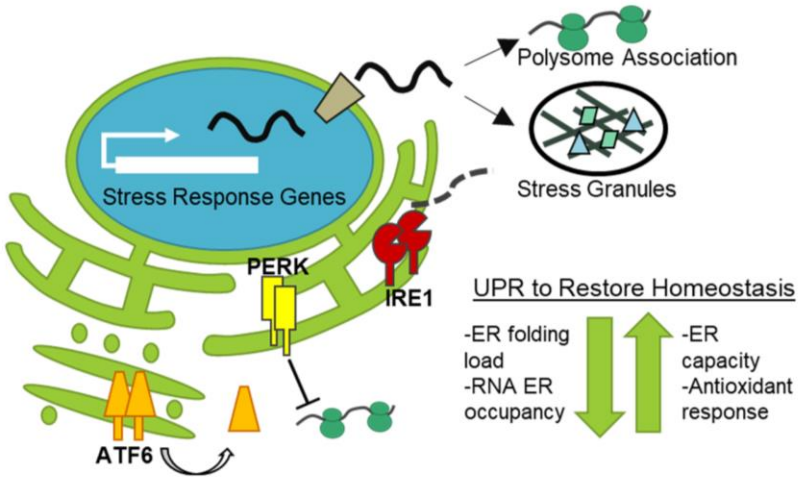

Figure 2: Schematic depicting the three branches of the UPR

The stimulation of the three UPR branches leads to an interesting paradox. If translation is halted by PERK but transcription is upregulated by three transcription factors, how are proteins made that can alleviate the stress? What happens to mRNA processing during this period? A study using Ribo-seq to observe membrane polysome

dynamics during the UPR has shown that polysomes translating secreted and membrane proteins undergo a release from the membrane during the first 30 minutes of stress[69]. Conversely, a study using immunofluorescence (IF) found that mRNAs encoding these proteins remain on the ER during stress while mRNAs encoding for cytosolic proteins undergo a rearrangement to granule structures[70]. Further studies are needed to get a full picture of mRNA localization during the UPR.

This is important because the UPR is a part of normal physiology. For instance, B-cells and pancreatic acinar cells utilize the UPR for ER expansion in order to secrete antibodies and insulin respectively. Prolonged activation of the UPR in pancreatic cells from insulin resistance characteristic of Type II diabetes, can lead to apoptosis, further exacerbating this issue[71]. Additionally, the UPR signaling pathways are responsible for cancer cell survival in tumors and resistance to therapies[71,72]. Understanding differences between cell specific utilization of the UPR and how the pathways interact to trigger apoptosis can provide a basis for a broad range of therapies to treat pathologies like cancer or diabetes. Because distinct changes in transcriptome organization occur, the project I will discuss sought to further the studies mentioned above by observing the localization of actively transcribed mRNAs during the shutdown of translation by PERK.

1.4 Stress associated cytoplasmic droplets

1.4.1 Appearance and physiology of stress granules

In addition to signaling pathways activated upon cellular stress such as hypoxia, nutrient starvation, or increased need for protein secretion, the cell's structure also changes. The most drastic of which is the formation of transient droplet structures, called stress granules (SG) composed of approximately 50% RNA binding proteins (RBPs) and RNA[73]. Appearance of these granules in cells coincides with a block of translation initiation brought on by stress activated signaling pathways such as the UPR. Mechanisms for how these granules form remain unclear. One hypothesis is that ribosome runoff during limited translation leads to an increased surface area of RNA followed by productive binding of RBPs, many of which contain intrinsically disordered regions (IDRs) that allow for multivalent oligomerization[74,75]. This increase in concentration of multivalent interactions between RNA-protein, protein-protein and RNA-RNA leads to an eventual liquid phase transition within the cytoplasm. How specific molecules localize to these structures is an active area of study. With the advent of super-resolution microscopy, it has been shown that these structures are composed of substructures, a less mobile core with a liquid shell surrounding it[73]. These differences are attributed to IDRs of core proteins forming stable amyloid structures during the nucleation of the granules that are tuned by helicases and chaperones occupying the mobile shell to prevent the formation of solid inclusions[76–79].

Through live cell imaging experiments, SG are known to be reversible when the environmental stress – replicated in the lab using chemicals such as sodium arsenite, dithiothreitol (DTT), nutrient starvation or heat shock – is removed[80–83]. ATP is necessary for this reversal and when ATP is depleted, chaperone and helicase activity slows allowing SG to find a solid, crystalline state implicated with cytotoxicity found in Alzheimer's and ALS-FTD[73,84,85]. In accordance with this observation, characterization of SG proteomes shows an enrichment for ATP dependent chaperones such as Hsp40-Hsp70 pairs and CCT, DEAD-box helicases and VCP ubiquitin segregase[73,86]. In the process of transitioning from a liquid condensate to a solid granule, there appears to be a change in SG proteome such as the addition of phosphorylated TDP-43 and p62[83]. Genetic point mutations of SG proteins such as FUS, implicated in ALS-FTD, can spark these pathologies by preventing relaxation of SG upon the lifting of the stressor. This leads to a faster transition from liquid to solid under repeated stress in cells [85]. Since symptoms of neurodegenerative diseases are typically associated with aging, prevention of these pathologies can be driven by a better understanding of their initial formation, earlier detection methods, and methods of reversal.

1.4.2 mRNA trafficking to cytoplasmic granules

While many labs have focused on the protein components of these granules less work has been done characterizing mRNAs within them since the molecule's general flexibility and base-pair annealing properties are thought to be what is needed to

provide the granules with their behavior. To this end, it has been shown that isolated IDRs can form cytoplasmic droplets and gels both *in vivo* and *in vitro* with or without RNAs present[77,82]. Contradictorily, trans-RNA interactions can form stress granules without protein suggesting that both types of interactions are responsible for granule formation *in vivo* and increase the formation of SG with lower IDR concentrations [87]. Interestingly, while specific proteins are known to enrich themselves in stress granules, a transcriptome wide analysis of isolated stress granule cores did not find specific mRNA enrichment[73,88]. Rather while mRNAs accounted for 80% of total granule RNA, enrichments of over 1% were not detected for any given transcript. Furthermore, 10% of bulk mRNAs are found in SG and of these, only 185 have over 50% of their mRNA molecules in SG. The authors conclude a specific program of mRNA selection does not exist but instead is dependent on general properties of the molecule such as length, with longer transcripts being more enriched, and a lack of polysome association[88,89].

This study discredits a small body of work attempting to determine transcript specific SG enrichment. One study found that mRNAs with ARE elements are preferentially recruited to SG by virtue of stabilizing RBPs, such as HuR, in balance with tristetraprolin (TTP) which is responsible for the quick degradation of ARE-rich mRNAs under stressed conditions[90]. However, mRNAs with ARE elements include 5-8% of total coding transcripts, a similar statistic to the study mentioned above[91]. Another study found that localization of mRNAs to either the cytosol or ER can predict its recruitment

to SG. Those mRNAs localized to the ER by a signal sequence are resistant to SG sequestration whereas cytoplasmic mRNAs are not[70]. Additionally, there are two studies that link a transcriptional element of an mRNA to SG localization. One, performed in mammalian cells, looked at mRNAs containing a 5'TOP element which overlaps with a TCT transcription element. These mRNAs code for ribosomal proteins and thus represent about 41% of translation in the cell[92]. Upon nutrient starvation, these mRNAs bind to Tia1/TiaR proteins more tightly and are localized to stress granules[93]. A direct look at transcription was never performed but is implied due to the overlap of the TOP/TCT element. In the second study, performed in yeast, it was found that upon glucose starvation, mRNAs encoding for enzymes within glucose metabolism pathways were not bound to ribosomes and thus recruited to SG while those encoding for chaperones remained in polysomes and were not recruited to granules. The authors traced this back to the heat shock element promoters associated with these chaperone transcripts and showed that changing the transcriptional element alone was responsible for the exclusion of these mRNAs from stress granules[94]. The link between transcription and SG recruitment has not been well validated but presents an intriguing observation. This was investigated further by using IF to monitor actively transcribed ER chaperones during stimulation of the UPR in comparison to transcripts that would show no upregulation during stress. By visualizing the fate of these transcripts, mechanisms will

be uncovered explaining how cells deal with the looming issue of active transcription during a translational shutdown.

1.5 Overview of results

The remaining chapters detail experiments performed to better understand two ongoing questions in the field. First, by using *in vivo* proximity labeling techniques, a preliminary network of the rough ER during homeostasis has been established. By expanding on these findings, the putative ribosome interacting protein, LRRC59, has been confirmed as a ribosome interacting protein *in vivo*. Additionally, I have developed a method to isolate proximity-labeled ribosomes and characterize mRNAs translated by them. Through this, I have established the existence of distinct mRNA distributions to separate sites of the ER, dictated by differences in ribosome binding environments. Tangentially, I propose a potentially novel function for mammalian Sec62 in ER redox sensing by proximity to ER redox chaperones and ATF6.

As all biological systems must deal with a changing environment, ER compartmentalization of membrane localized molecules were interrogated during stress. This project has proposed a mechanism for recruitment to SG based whether an mRNA is actively being transcribed. The new working hypothesis is that newly transcribed mRNAs localize to stress granules whereas incorporation of an internal ribosomal entry site (IRES) element negates this localization by recruiting ribosomes to the transcript during limited cap-dependent translation. From the model, this will remove the coat of

RBPs associated with the nascent mRNA. This establishes a novel pattern for mRNA localization to stress granules and will be tested on additional mRNAs and generalized in the future. This second part of the project is based on an initial observations made by Dr. Sujatha Jagannathan, currently a professor at the University of Colorado Anschutz Medical Campus. These observations and any resulting publications are performed in collaboration with her.

2. Network Analysis of the Translation-Associated Proteome of the Rough ER

2.1 Introduction

The endoplasmic reticulum (ER) is a heterogeneous organelle composed of rough and smooth membrane domains, distinguished by the presence or absence of bound ribosomes respectively, and a diversity of primary cellular functions including secretory/membrane protein biogenesis, lipid biosynthesis, and calcium storage[9,95–97]. In addition to these defining features, the ER engages in communication with different organelles, including mitochondria, endosomes, and the plasma membrane[95,98,99]. The sites of organelle–ER communication are marked by multi-protein assemblies that define areas of regional specialization, e.g., MAMs, and provide evidence for the spatial organization of the ER membrane proteome as a biochemical/biophysical mechanism to accommodate the various structural and functional properties of this critical organelle [32,33,100,101].

In addition to these specific patches of characterized ER-organelle contact sites, there are also several functions that are shared under the broad term of rough or smooth ER. For the rough ER, it is known that the entire transcriptome localizes here in association with mRNA metabolic processes such as translation, degradation and nuclear transport. Given that eukaryotic transcriptomes are substantially weighted to mNCPs, even modest enrichments of 10-20% of a given transcript indicate a broad

representation of these mRNAs on the ER[45,51,102,103]. Although a function for the ER in the translation of mNCPs has been under intermittent investigation for many decades, more recent biochemical and structural biology studies of the ribosome-Sec61 translocon, composed of Sec61α, Sec61β and Sec61γ, would suggest that such a function is unlikely [62,104–108]. The Sec61 translocon serves as a ribosome receptor and translocation channel— displaying an intimate physical coupling of the ribosomal protein exit channel with the translocon pore. Thus, translocon-associated ribosomes would likely need to be dedicated to the translation of secretory and membrane protein-encoding mRNAs to avoid stimulating a stress response from cytosolic proteins translating into the wrong compartment[109]. Recent work suggests an alternative view where a diverse transcriptome localization to the ER could be accommodated by Sec61 translocon-independent ribosome association mechanisms[11,50,51,55,110]. In support of this view, a number of ER resident membrane proteins other than the Sec61 translocon have been proposed to function as ribosome receptors, including ribophorin I— a subunit of the oligosacharyltransferase –LRRC59 (p34), and p180 (RRBP1)[57–59,111]. Although these proposed ribosome receptors have been shown to have a high binding affinity to ribosomes in vitro, very little is known regarding the potential diversity of ribosome-ER protein interactions in vivo. Additionally, many ER membrane proteins such as TRAP, TRAM, signal peptidase, p180 and OST serve as chaperones in the successful synthesis of secretory and membrane proteins[112–115]. Little is known about the dynamics of each of

these protein's translocon association. From cryo-EM studies, it is shown that these components are not stoichiometric with the translocon, nor are all components present in a single complex[62,111,116,117]. The totality of these observations led to the hypothesis that the proteomic landscape of the rough ER might be organized in order to efficiently deal with the diversity of translation.

To test if organization plays a role in the diversity of translation on the ER, I used a proximity labeling technique termed BioID. Briefly, BioID uses a mutant bacterial biotin ligase (BirA*) that catalyzes the formation of a reactive-biotin intermediate (biotin-AMP) which diffuses from the enzyme active site to tag near-neighbor proteins possessing accessible lysines. By fusing this enzyme to a protein of interest, this labeling can occur *in vivo*, thus preserving the spatial interaction information following cell lysis that can be retrieved through streptavidin pulldown of the covalently bound biotin[31]. To make a rudimentary map of the rough ER, four proteins were chosen for our BioID study that are validated RAMPs in mammalian cells, thus localizing them to the rough ER. In summary, these include first, the Sec61 translocon, a well-studied ribosome receptor and so Sec61β was chosen as a subunit that has previously been used to make GFP reporters of functioning translocons[107,118,119]. Second, ribophorin I, a component of the oligosaccharyltransferase (OST), which is proximal to translocating nascent chains and a Sec61 translocon interactor, and thus a high probability candidate for the ribosome interactome analysis[57,111,116]. Third, Sec62 which has an ortholog in yeast that functions in

post-translational translocation. In mammalian systems, Sec62 has a potential gain of function in ribosome binding, with binding interactions mapped to regions adjacent to the ribosome exit tunnel[120,121]. LRRC59, was identified as a mammalian ribosome binding protein through biochemical reconstitution approaches and chemical crosslinking, where it was demonstrated to reside near large ribosomal subunits[58,122]. The four BioID chimera thus include well-studied complexes, e.g., Sec61 translocon (Sec61β) and OST (ribophorin I), as controls that can report on labeling efficiency and incorporation into their respective complexes. The study also includes, proteins with a less established membrane protein interactomes, i.e., LRRC59 and Sec62, where proximity labeling information can be used to further establish their role in mammalian translation.

By performed time courses of biotin labeling with BioID reporters, the existence of stable microdomains surrounding each of the reporters was established, consistent with an active organization of membrane proteins. Upon further interrogation of the specific protein identities of these environments by mass spectrometry, it is shown that LRRC59 is in an RBP-rich environment potentially linking it to mRNA triage on the ER. Furthermore, this study establishes a yet unknown role for Sec62 in ER redox sensing.

2.2 Results

Some of these data are in press at the Journal of Biological Chemistry (Hoffman AM et al.)

2.2.1 Ribosome interactor-BioID chimera are ER-localized and predominately label ER membrane proteins

To assess the subcellular localization and proximity labeling activity of the ribosome interactor-BioID chimera introduced above, reporter cell lines were induced for 16 hours with 50 μM biotin supplementation and expression patterns determined by IF using antisera directed against BirA. Biotin labeling patterns were examined by staining with a streptavidin-AF647conjugate (Figure 3A). A cell line containing the cloning vector backbone served as a negative control (empty vector, EV). As depicted in Figure 3A, all reporter cell lines displayed clear reticular staining with the BirA antisera, consistent with an ER localization for all BioID chimera.

Streptavidin staining of proximal biotin labeled targets mirrored the BirA staining patterns, suggesting that the primary interactomes are largely confined to the ER (Figure 3A,B). These findings were further validated by comparing the streptavidin staining patterns with the resident ER membrane protein TRAPα (Figure 3B). As with the data depicted in Figure 3A, extensive overlap of streptavidin staining pattern with that of TRAPα was observed with little discernible tagging of cytosolic proteins.

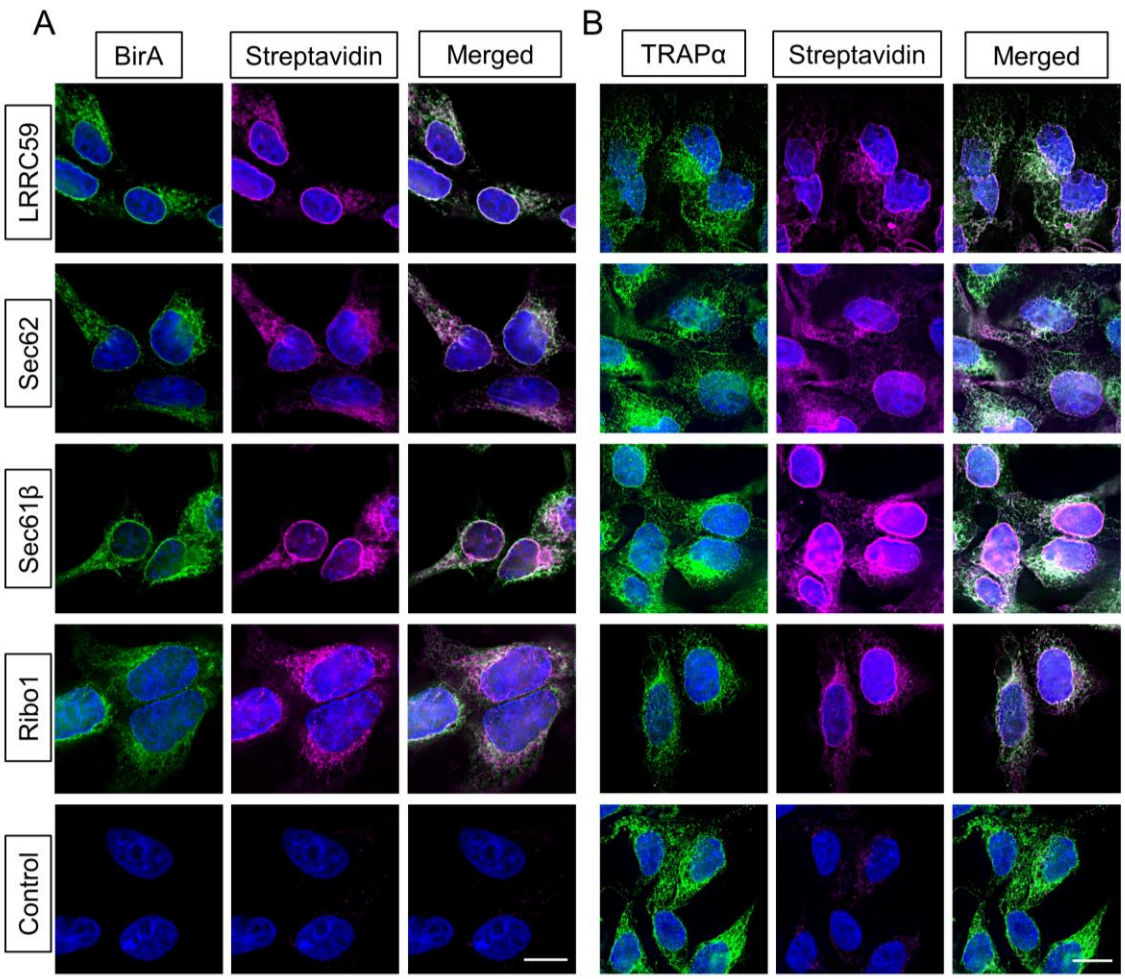

Figure 3: BioID reporters display ER-restricted subcellular localization and biotin-labeling activity.

A) IF micrographs of each cell line after 16 hours of doxycycline induced expression (BirA channel) and 16 hours biotin treatment (streptavidin channel). The merged images reveal high coincidence of a reticular pattern and proximity labeling. B) IF micrographs of each cell line treated as in A showing colocalization of the resident ER membrane protein marker (TRAPα) and the biotin labeling pattern. Scale bar = 10 μm.

The IF data depicting reporter expression and biotin labeling (Figure 3) were

further evaluated in cell fractionation studies (Figure 4). Using a previously validated sequential detergent fractionation protocol[123,124], that releases the cytosolic fraction by digitonin followed by disruption of the membrane fraction, BirA* chimera distributions were assessed by SDS-PAGE/immunoblot analysis. These data are depicted in Figure 4B and demonstrate that all ER membrane protein reporters were wholly recovered in the membrane fraction (**M**) and mobilities consistent with their predicted molecular weights (Figure 4A). Consistent with the IF data shown in Figure 3, biotin labeling was highly enriched in the membrane fractions (**M**) (Figure 4C,D,TRAPα as ER marker), with only modest labeling of cytosolic proteins (**C**) (Figure 4C,D, β-tubulin as cytosolic marker). Interestingly, the biotin labeling patterns of the membrane fractions (Figure 4C**)** were distinguishable from one another, suggesting that the BioID reporters reside in different protein environments. The relative paucity of biotinylated cytosolic proteins, was unexpected because the reactive biotin-AMP intermediate diffuses from the BirA* active site to modify solution-accessible lysines[125]. It was predicted that membrane and cytosolic proteins would be similarly accessible to biotin modification. The bias to biotin-conjugation of ER membrane proteins suggests that the labeling radius for the reactive biotin-AMP intermediate is highly restricted[126].

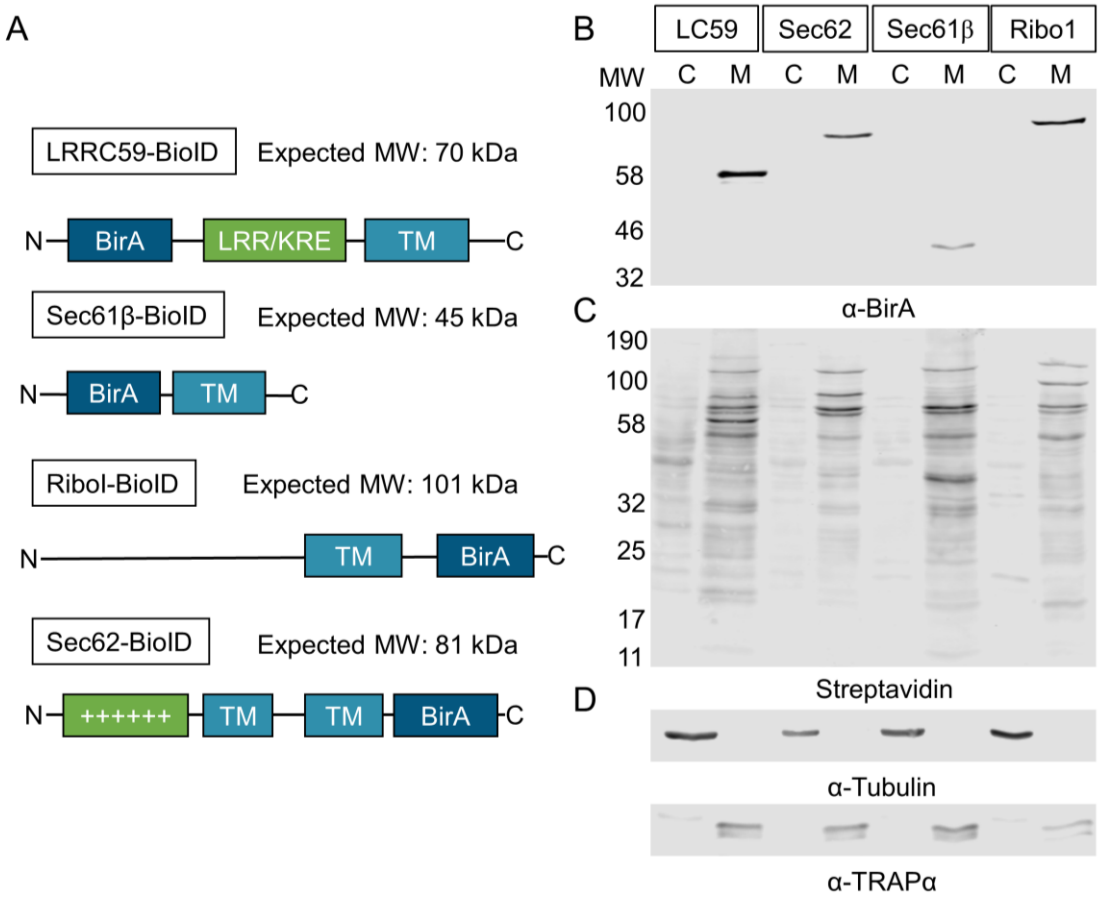

Figure 4: Biochemical fractionation of BioID cell lines confirms correct subcellular localization and demonstrates enriched tagging of membrane proteins.

A) Cartoon schematic of constructs with placement of the BirA tag depicted and predicted molecular weight. TM = transmembrane domain; KRE/LRR = lysine-arginine-glutamate enriched/leucine-rich repeat domain; ++++ = positively charged domain. Schematics are not drawn to scale. B) BirA immunoblot depicting the localization of each construct to the membrane fraction of the detergent fractionated cells described in the text. Cells have been treated as in Fig 1. C) BirA*-mediated biotin labeling of the same samples as in B, depicted by streptavidin blot, reveals distinct labeling patterns for each cell line and high enrichment of the ER fraction over the cytosolic fraction. D) Marker protein immunoblot data depicting efficient fractionation of the cells into cytosol (β-tubulin) and membrane (TRAPα) fractions from ths samples used in B and C. LRRC69 (LC59), Ribophorin I (Ribo1), Molecular weight (MW), Cytosol (C), Membrane (M).

Ribophorin I and Sec61β are subunits of oligomeric protein complexes. To determine if their BioID chimera assemble into native oligomeric complexes, the hydrodynamic behavior of the chimera with the respective natively expressed proteins was observed by glycerol gradient velocity sedimentation[127](Figure 5). As depicted, the sedimentation patterns of all BioID reporters and respective native proteins were similar, suggesting that the chimera were appropriately assembled into native complexes[111]. Comparison of the native protein expression in both BioID cell lines and the empty vector cell line are similar suggesting that overexpression of the chimera does not affect membrane protein expression. In yeast, such chimera complement genomic deletions of the parent gene, also indicative of native-like function[128]. To further ensure the incorporation of the chimera into their respective complexes streptavidin pulldown of biotinylated proteins from the membrane fraction of each cell line was performed and blotted with antisera against the proteins indicated in Figure 5B. As shown, the chimera labeled known interactors within their respective complexes and labeling was limited to the direct complex interactors. For example, the Sec61β chimera labeled Sec61α whereas the ribophorin I chimera labeled the OST subunits STT3A/B. Additionally, the LRRC59 chimera appeared to label SRP54, a key component of the SRP, thus suggesting an *in vivo* role for LRRC59 in ER-associated translation. Combining this observation with that in Figure 4B, that labeling is restricted to the membrane fraction, it is shown that the BioID labeling radius is highly restricted and thus if these proteins are in stable

nanodomains, a labeling time course would show little change in the biotin labeling pattern.

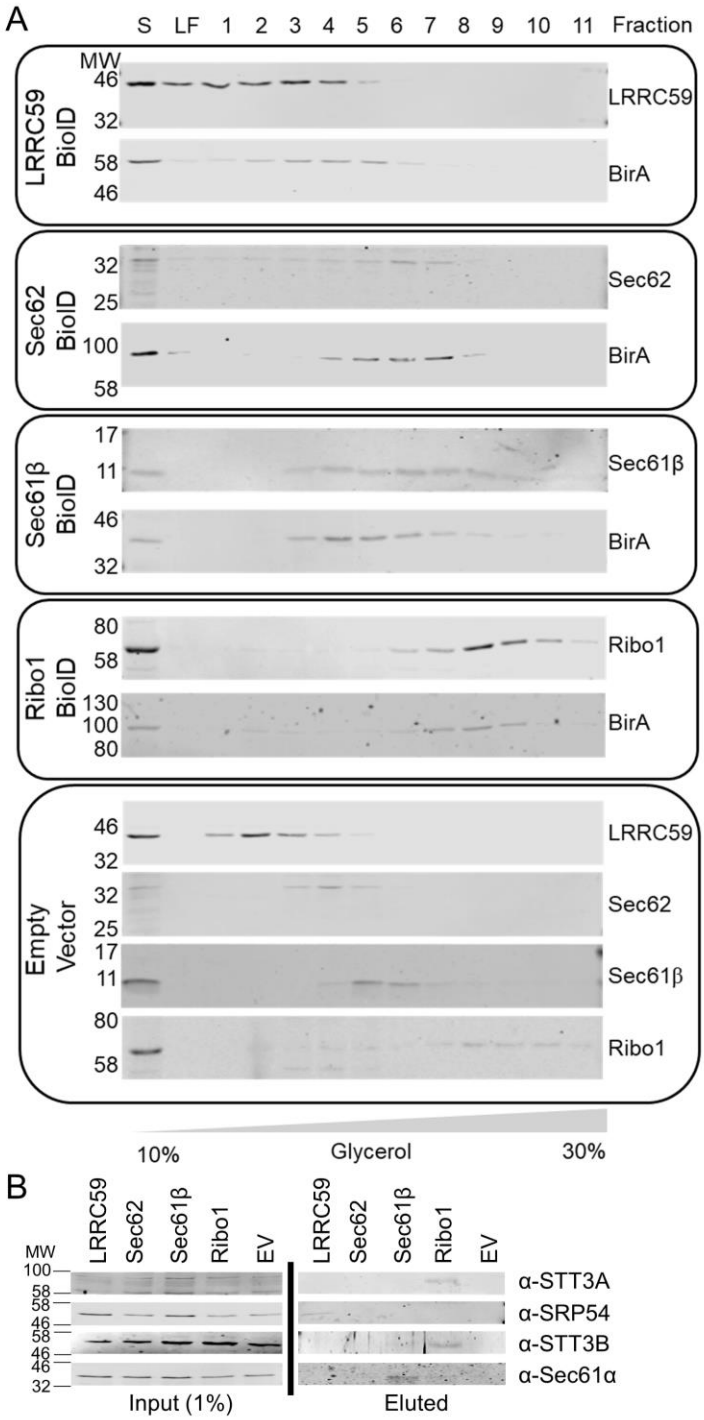

Figure 5: BioID constructs display hydrodynamic behavior similar to native complexes in glycerol gradient sedimentation analyses.

A) Western blots of each fraction of the gradients to determine the centrifugation pattern and expression of the corresponding native protein in each BirA*-chimera cell line as labeled on the left. Antibodies used are labeled to the right of each plot, either the indicated native protein or BirA antisera. The bottom panel depicts an empty-vector control cell line to compare migration patterns of native proteins tested in one of the above two panels. Ribosome depleted supernatant is loaded in the first lane (S) followed by the light fraction (LF) encompassing the first 0.8 mL of material unincorporated into the gradient, the numbers refer to the remaining gradient fractions collected (1-11) B) Biotinylated proteins of the membrane fraction from each cell line were pulled down by streptavidin beads as described in the Methods and immunoblots performed for proteins in known complexes as an orthogonal validation of BioID chimera incorporating into known complexes. Antibodies used are indicated to the right of the blots against the input and eluted proteins. Vertical black line indicates these are separate gels. Percent of input is based on volume. Molecular weight in kDa (MW).

2.2.2 Evidence for meso-organization of ER membrane protein assemblies.

BioID proximity labeling experiments are typically conducted over many hours (e.g. 16-24h), a reflection of the biotin-AMP slow release kinetics from the BirA* active site[129,130]. Because this time scale is substantially slower than that of most cellular processes, the specificity of the labeling reaction is formally a concern, though it has been demonstrated that neighboring proteins can be distinguished from random interactors by their higher relative labeling over non-specific controls[31,126,131–133]. In the context of the experiments with ER membrane-localized BioID reporters, one concern is that reporter diffusion in the constrained 2D environment of the ER membrane over such extended labeling times could confound identification of near-neighbor and interacting proteins. To address this concern, the biotin labeling patterns produced by the BioID chimera were determined as a function of labeling time. The prediction was

that the biotin labeling patterns would diversify as labeling times increased, a consequence of the expected random diffusion within the membrane. The results of these experiments are shown in Figure 6A. Depicted are streptavidin blots of the cytosol and ER protein fractions from the four BioID reporter cell lines, sampled over a time course of 0–6 hours. Two observations are highlighted here. First, as noted above, the relatively enhanced labeling of membrane proteins (**M**) to cytosolic proteins (**C**) is evident throughout the time course examined, with modest levels of cytosolic protein labeling throughout the time course for all constructs. Second, contrary to our expectations, the membrane protein biotin labeling patterns did not substantially diversify over the labeling time course (Figure 6A). Rather, the labeling pattern intensified as labeling time increased. The biotin labeling patterns revealed by SDS-PAGE were further analyzed by densitometric analysis (Figure 6A), where it can be appreciated that the biotin labeling patterns intensify, but only modestly diversify, as a function of labeling time. These data suggest that the BioID interactomes comprise largely stable membrane protein assemblies (Figure 6B**),** rather than the presumed diffusion-driven random mixing (Figure 6B)[18–20,134].

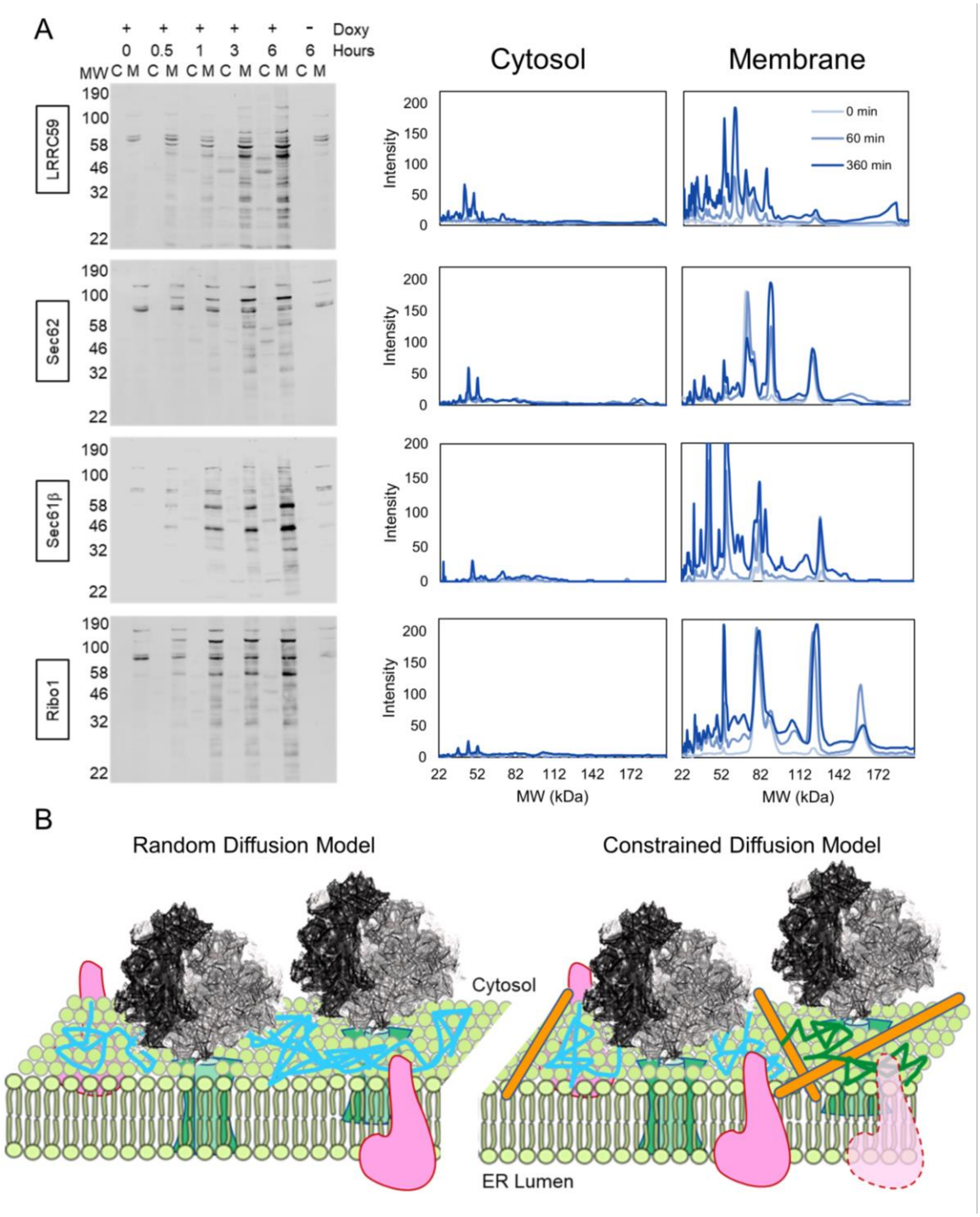

Figure 6: The BioID labeling patterns of the reporter cell lines largely intensify, rather than diversify, over time.

A) Streptavidin blots of biotin labeling time courses are shown for each reporter cell lines. Also provided are line-intensity plots of selected time points through the six hour (hr) labeling period. Indicated are the biotin treatment time periods. -D represents a six hr biotin treatment without prior doxycycline treatment, to test for leaky expression. B) Cartoons depicting the two predicted models of membrane protein diffusion. The first (random diffusion) model depicts a biological membrane in which proteins diffuse freely in the 2-D membrane plane, encountering targets by random collision. The second (constrained diffusion model), predicts that an organizing force, be it protein-protein interaction, lipid-enriched domains, or both, enables the formation of distinct compartments where protein diffusion is restricted.

The data presented above (Figure 6A) are consistent with a model where the mobility of the BioID reporters is constrained (Figure 6B), perhaps reflecting mesoscale organization of the ER via biomolecular interactome networks, as has been extensively studied in the plasma membrane[19,20,134]. Labeling patterns could be influenced by either ER distribution biases (e.g., ER tubules vs. sheets) or protein-specific differences in reactivity to the biotin-AMP reactive intermediate. To examine these possible scenarios, proximity labeling time course experiments were performed using canine pancreas rough microsomes (RM), which lack the native topological structure of the ER, and a soluble, recombinant BirA*. Using this system, the reactive intermediate was delivered in *trans* and accessible to the ER surface by solution diffusion. The results of these experiments are shown in Figure 7 and demonstrate that when delivered to RM in *trans*, biotin labeling is pervasive and monotonic, with a diversity of proteins undergoing labeling and relative labeling intensities increasing as a function of labeling time to less resolved protein peaks (compare Figure 7B to 6D). Taking results from both Figure 6 and Figure 7, it can be concluded that these BirA* chimera are restricted to specific

protein microdomains of the ER *in vivo* that can be seen in the specific labeling patterns present for each cell line.

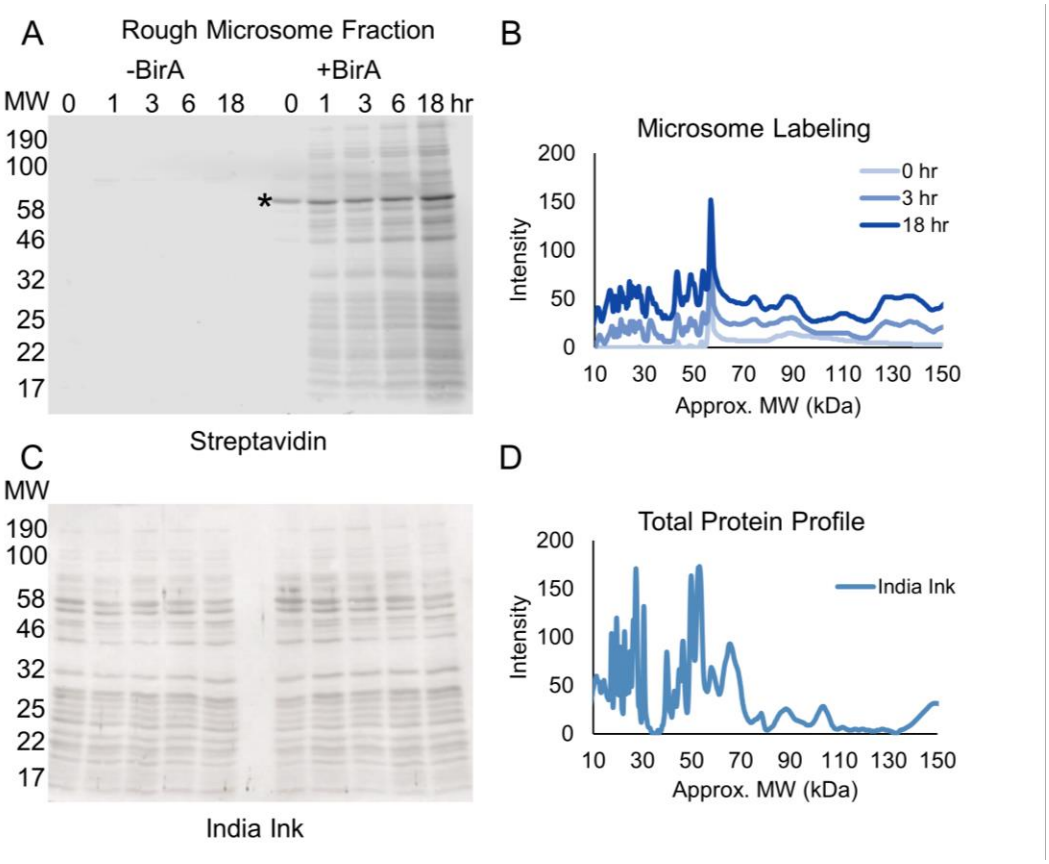

Figure 7: In the absence of ER membrane organization and with trans-delivery of the reactive biotin intermediate, proximity-based selective labeling is abolished.

A) SDS-PAGE gel depicting an in vitro labeling experiment conducted with canine rough microsomes (RM) incubated in the presence of soluble, recombinant BirA*. RM were incubated in the presence of an ATP regenerating system, biotin, and either BirA* or PBS as indicated. Note that the general avidin labeling pattern mirrors the total protein when the reporter is present in trans. Asterisk indicates the BirA*-GST fusion protein, which is biotinylated during its induction in E.coli. A) Lane intensity plots demonstrate a general increase at all molecular weights, indicating loss of specificity when the reporter is presented in trans. B) India ink stain of the blot above to show equivalent protein loading levels. C) Lane intensity plot of the India ink stain, illustrating the overall similarity in the labeling of total accessible protein.

To gain molecular insight into the protein neighborhoods of the reporters, cell lines were supplemented with biotin for 3 hours, the time point at which labeling intensity was highest compared to background as illustrated in Figure 6, and biotinylated proteins captured from membrane extracts by streptavidin-magnetic bead affinity isolation. Elution was performed by biotin competition at high pH to select against non-specific background, with protein composition determined by mass spectrometry of the eluted samples. A summary of the analysis schema is depicted in Figure 8A. In brief, spectral counts of proteins meeting high confidence (1% FDR) cutoffs were normalized to those of natively biotinylated proteins and the subset with enrichments of $\geq$ 2.5-fold over an empty vector control were selected. For these, two categories were defined; "enriched", displaying an enrichment of > 2-fold over the combined normalized value, and "shared", for those below this selection threshold. For all reporters, the majority of the labeled proteins meeting initial significance criteria were membrane proteins, corroborating the data presented in Figure 4, Figure 5, and Figure 6. In the shared category, representing those proteins that met selection criteria and were present at similar normalized levels in two or more reporter datasets, about 80% were membrane proteins, 10% were cytoplasmic proteins, and 10% were nuclear proteins. Upon preliminary analysis of the screened proteins, many prominent ER resident membrane proteins were identified in the reporter datasets to varying levels and included signal peptidase complex subunit 2, the eIF2⍺ kinase PERK, DNAJC1, the

ERAD-associated E3 ubiquitin ligase TRIM13, ERGIC-53, ER calcium ATPase 2, and reticulon-4. Other prominent ER resident proteins present in at least 3 of the 4 reporter datasets included Sec63 homolog, calnexin, and NADPH cytochrome P450. With respect to the enriched datasets, the candidate ribosome interactors LRRC59 and ribophorin I returned identical numbers of neighboring/candidate interacting proteins (35), with Sec61◎ returning 19 enriched hits, and Sec62, 11 enriched hits; these specific interactomes are discussed further below. In summary, proteomic analysis of the neighboring proteins for the indicated BioID chimera revealed a high enrichment in ER membrane proteins and within this category, proteins with established functions in canonical rough ER functions such as protein translocation/protein processing, the unfolded protein response (UPR), and ER-associated protein degradation[10,135–137].

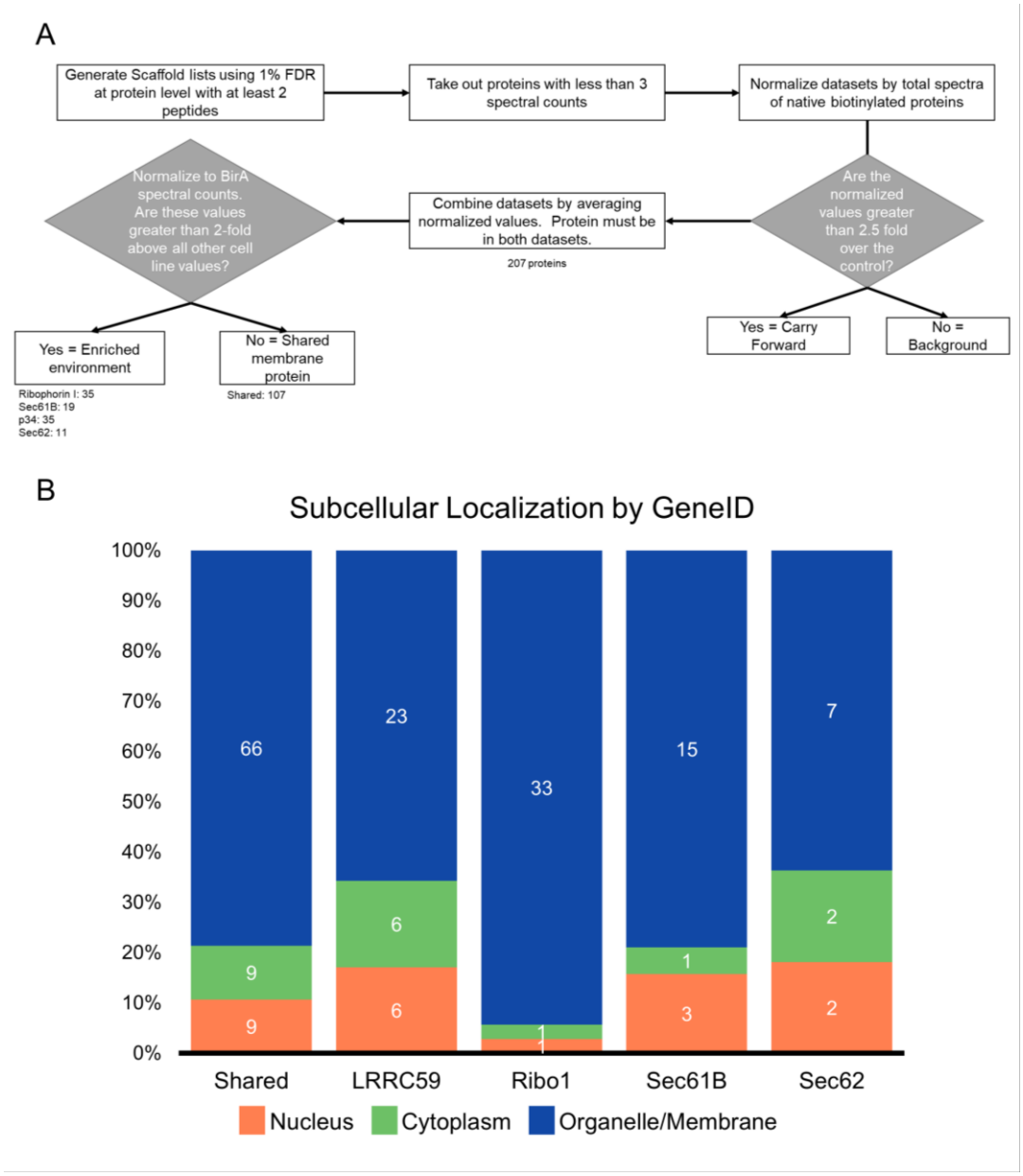

Figure 8: MS analysis of BioID-labeled proteins demonstrates a high labeling enrichment of membrane vs cytoplasmic proteins.

A) Schematic depicting the data analysis pipeline and significance selection criteria. All MS experiments were performed in duplicate. B) Stack plots depicting the relative distributions of cellular localization for enriched and shared proteins from each cell line. The number of genes in each category is shown on the bar graph for a more accurate comparison of each cell line.

2.2.3 Candidate Ribosome Interactors Reside In Distinct ER-Protein Neighborhoods

To further evaluate the subsets of neighboring proteins scoring in the enriched category, the datasets were visualized in Cytoscape[138], cross-referenced via the STRING Protein-Protein Interaction Network resource[139], and functional enrichments for each reporter neighborhood determined by GO analysis. For clarity, the Cytoscape-generated plots depicted in Figure 9A-D include the top unique hits, with screened, shared interactors included as Figure 10A-B. The plots provided in Figure 9A-D are coded to illustrate interactions with soluble proteins (yellow border) and membrane proteins (turquoise border). Centered and uncolored nodes indicate the chimera protein from each cell line and reporter spokes identify candidate interactor or near neighbor proteins. Direct protein-protein interactions that have been previously experimentally demonstrated via STRING annotation are represented by additional edges between colored nodes and, in the cases of Sec61⊙ and Ribophorin I, green nodes for members of their native heterooligomeric complexes which serve as important internal controls. Dark blue nodes and green nodes with asterisks by the gene name are proteins comprising the top GO category indicated underneath each plot and in the included table at the bottom of the figure. For Sec61⊙⊙⊙Figure 9A), a prominent interactor was Sec61⊙, as would be expected if the reporter was assembled into the native Sec61 translocon. The enriched BioID neighborhood set for Sec61⊙ also included membrane biogenesis enzymes, e.g., the stearoyl desaturase SCD, the IP_3 receptor/calcium channel

ITPR3, and the calcium ATPase ATP2B1. GO analysis of the enriched Sec61◎ BioID interactome set yielded the category "organelle membrane" as a high probability functional gene set. The enriched interactome set for ribophorin I (RPN1 in figures) ◎Figure 9B) includes STT3A, STT3B, and RPN2, (subunits of the oligosaccharyltransferase complex), accessory components of the translocation machinery, such as SSR1, the IP_3 receptor/calcium channel ITPR2, and the stearoyltransferase SOAT1. GO analysis of the enriched ribophorin I BioID interactome set yielded the category "transport" as a high probability functional gene set. The LRRC59 (Figure 9C) unique interactome was particularly interesting as it included ER membrane proteins either predicted or demonstrated to function as RNA binding proteins, include MTDH (AEG-1), RRBP1 (p180), and CKAP4, as well as SRP68[140–142]. This functional enrichment is consistent with recently published work demonstrating a function for AEG-1 and RRBP1 in RNA anchoring to the ER, and implicate LRRC59 in translational regulation on the ER[110,143,144]; the GO category "poly(A)RNA-binding" reflects this enrichment. The Sec62 (Figure 10D) BioID chimera unique dataset was of interest for its relative abundance of soluble and membrane proteins functioning in redox regulation in the ER, including DLD, PDIA3, and PRDX4. This enrichment is reflected in the GO category assignment "cell redox homeostasis".

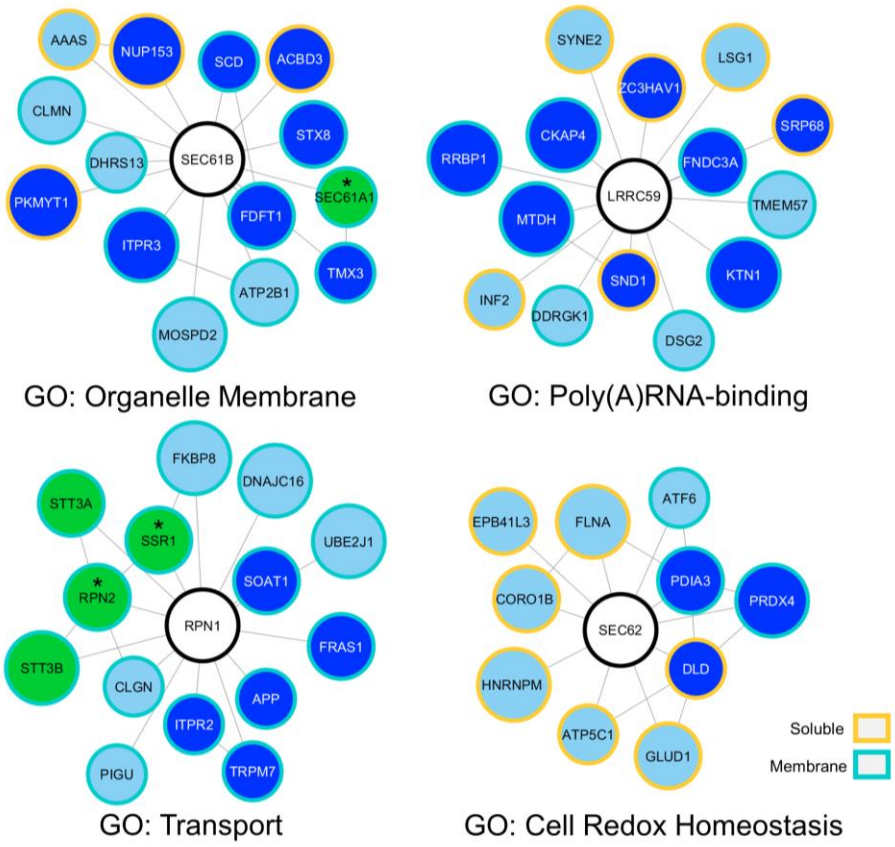

BioID Cell Line	Top GO Enrichment	FDR
LRRC59	Poly(A) RNA-Binding	$7x10^{-5}$
Sec61β	Organelle Membrane	$1x10^{-4}$
Sec62	Cell Redox Homeostasis	$4x10^{-2}$
Ribophorin I	Transport	$9x10^{-3}$

Figure 9: BioID reporters reside in distinctive protein neighborhoods.

Cytoscape plots of enriched proteins for each cell line reveal distinct functional enrichments for proximally labeled proteins, indicative of higher order organization. Center nodes indicate the chimera protein from each cell line while the surrounding nodes develop from the proteomic datasets. Sizes indicate ranked normalized counts with the largest nodes having the highest values. Green nodes indicate stable, well-characterized protein complexes on the ER, dark blue nodes are proteins comprising the top GO category indicated underneath each plot and in the table at the bottom of the figure. Asterisks denote proteins that are in both established complexes and GO categories. Borders indicate whether the protein is a membrane or soluble protein.

The binning scheme ("enriched" and "shared") is useful for highlighting enriched near-neighbor interactions and their functional enrichments. As noted, however, the proteomics dataset also revealed crosstalk between the BioID chimera and the wild-type candidate ribosome interacting proteins, though these interactions were not above the high stringency cutoff used to define near proximity interactions. The Cytoscape plot illustrated in Figure 10A depicts these interactions, with the reporter nodes illustrated in yellow, green and red, representing Sec61β, LRRC59, and Ribophorin I, respectively, with the remaining "shared" dataset illustrated in Figure 10B. In summary, mass spectrometric analysis of the protein neighborhoods/interactomes identified by the BioID method confirm that for two of the candidate ribosome interactors, Sec61◎ and Ribophorin I, the reporter chimera reside in proximity to their established native oligomeric complexes and surprisingly, all chimera reside in distinct protein neighborhoods whose residents are enriched in for different ER functions, such as poly(A)RNA-binding (LRRC59) and redox homeostasis (Sec62).

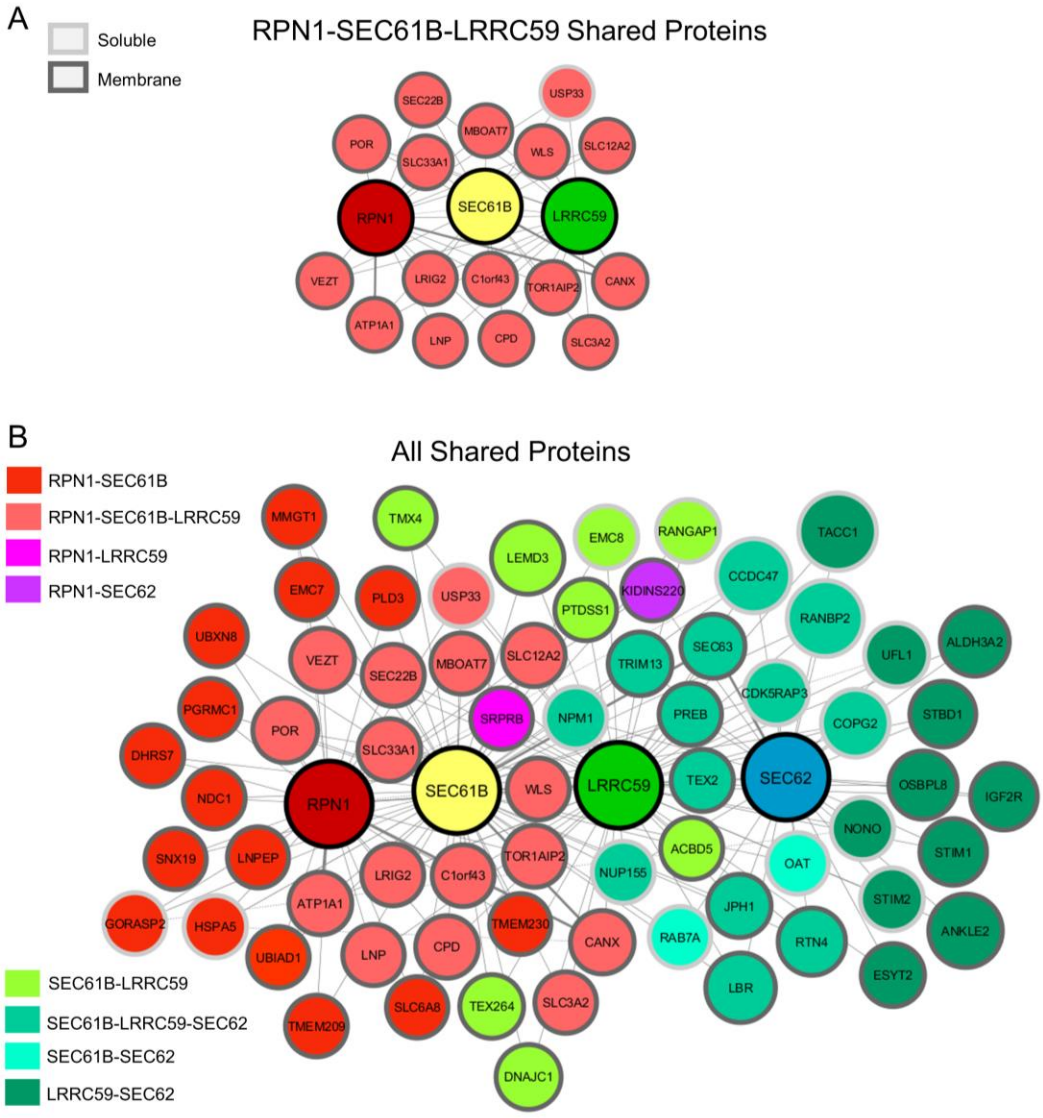

Figure 10: Shared proteins comprise the majority of the proteomic datasets and define common components of mesoscale-ordered ER membrane domains.

A) The three chimera proteins, Ribophorin I (RPN1), LRRC59 and SEC61β (SEC61B), implicated in ribosome binding, with common, shared proteins. B) Cytoscape plot of shared proteins confirms several established protein-protein interactions from experimental evidence (dotted edge lines, bold lines if connected to a reporter node). Size of the nodes are based on highest normalized count from the shared reporters. Proteins shared by specific chimera are distinguished by the indicated color scheme. LRRC59 share more proteins with the SEC61B and RPN1 reporters than SEC62. Files containing all membrane protein IDs are placed in Appendix A.

2.3 Discussion

In this study, the translational landscape of the ER was investigated from the perspective of RAMPs and their protein interactome networks. An unbiased proximity labeling approach, BioID, was used to investigate the near-neighbor environments of both established (Sec61β and ribophorin I) and unknown ER (LRRC59 and Sec62) membrane proteins. Two primary conclusions can be drawn from these studies; i) the proteins examined reside in stable, mesoscale-ordered ER membrane domains; and ii) these domains appear to have functional significance based on the known functions of the protein components identified. Combined, these data reveal a higher order organization of the ER, which are referred to as mesoscale organization by analogy to current understanding of the domain organization of the plasma membrane[19,20,134], and provide early experimental evidence for a higher-order organization of subdomains in the ER.

Two largely unexpected observations were made from this work. The first was that the near-neighbor environments of the different BioID reporter constructs did not diversify as a function of labeling time. According to the Singer-Nicolson model of membranes, the reporter interactomes would diversify as a function of labeling time to reflect random diffusion in the plane of the ER membrane. To the contrary, their environments became more densely labeled over labeling time courses of many hours, with only a modest increase in labeling diversity. The remarkable stability of the protein

labeling patterns is consistent with a model where low affinity interactions between functionally related proteins enable a mesoscale organization of the membrane. In support of this interpretation, GO analysis of the enriched sets of labeled proteins revealed distinct and functionally related gene categories. Importantly, those BioID reporter chimera that are known to be subunits of oligomeric proteins (e.g., Sec61◎, ribophorin I) tagged key subunits, Sec61◎ in the case of Sec61◎ and RPNII and STT3A/B in the case of ribophorin I, indicating that the chimera assembled into native oligomers and reporting on the environments of these oligomeric complexes. Perhaps more persuasively, extensive studies of plasma membrane architecture have provided strong evidence for such mesoscale organization with roles for biophysical contributions from distinct lipid species and interactions with cytoskeletal components as important organizing determinants[145]. Whether lipid species or cytoskeletal components contribute to mesoscale ER membrane organization remains to be determined, although there is substantial evidence for ceramide/sphingolipid domains in the ER as well as both microtubule and actin cytoskeleton interactions with ER resident proteins[47,146,147].

The second unexpected observation from this work was the strong biotin labeling bias to the ER membrane over cytosolic proteins. Given the diffusion-based mechanism of BioID labeling, significant labeling of both cytosolic and membrane proteins was expected. While, the exact reason for this bias remains to be determined, it is tempting to speculate that it reflects both high local concentrations of reactive sites

and high residence lifetimes of ER membrane proteins proximal to the reporters, as contrasted with a soluble protein undergoing three-dimensional diffusion. This work supports a model of the rough ER as organized in mesoscale domains actively partitioning its functions to clustered areas of the organelle. Since the main function of the rough ER is translation, I next sought to use these BioID reporters to determine how mesoscale membrane organization partitions this function between different environments.

3. Higher Order Organization of RNA by Translation Dependent Ribosome Association

3.1 Introduction

Recent reports identify a transcriptome-wide function for ER-associated ribosomes in proteome expression[11,51,128,148]. Given the central role of the Sec61 translocon as both the protein-conducting channel and ribosome receptor for membrane and secretory proteins[62,149], it can be argued that ER membrane proteins other than the Sec61 translocon participate in ribosome-ER interactions, to support broad transcriptome expression on the ER[62,102,107]. To test this hypothesis, a BioID proximity labeling approach was used, where BioID chimera of known ribosome interacting proteins were used to map ER membrane protein interactions described above. In the studies reported below, the BioID reporter translational interactomes are studied by subcellular fractionation combined with mass spec and RNA-sequencing analyses of biotin-tagged ribosomes.

For this study, the same four ER membrane protein reporters were used as in Chapter 2. In summary, these are: Sec61β, a subunit of the Sec61 translocon and gate to the secretory pathway[107,118,119]; Ribophorin I, a component of the oligosaccharyltransferase (OST) which acts as the site of N-glycosylation of membrane proteins[57,111,116]; Sec62, participates in post-translational translocation in yeast but has an established gain of function as a ribosome binding protein in mammalian cells [120,121]; and

LRRC59, identified as a ribosome binding protein through biochemical reconstitution approaches and chemical crosslinking[58,122].

The following section details results that show, of the four candidate ribosome receptors examined, two (Sec61β and LRRC59) labeled ribosomes. Intriguingly, the ribosomal protein labeling patterns of the two reporters were distinct, consistent with differential spatial interactions with ribosomes. RNA-seq analysis of mRNAs from the different ribosome populations revealed both highly enriched and shared transcriptome cohorts. Taken together, these data are consistent with a nanoscale organization of ER translation into distinct centers. In addition, these data suggest mechanisms whereby the ER could serve a broad role in proteome expression.

3.2 Results

Some of these data are in press at the Journal of Biological Chemistry (Hoffman AM et al.)

3.2.1 Proximity labeling of ER-bound ribosomes by candidate ribosome interactors

To examine proximity interactions between ribosomes and the BioID reporters, biotin labeling experiments were conducted, fractionated cells, enriched for the ribosome fraction by ultracentrifugation, and analyzed the ribosome fractions by streptavidin blot. As ribosome exchange on the ER is thought to be functionally coupled to the translation cycle[150,151], a biotin labeling time course was performed and examined

labeled ribosome distributions in the cytosol and ER compartments (Figure 11) to determine if ribosome interactions might vary after many rounds of translation.

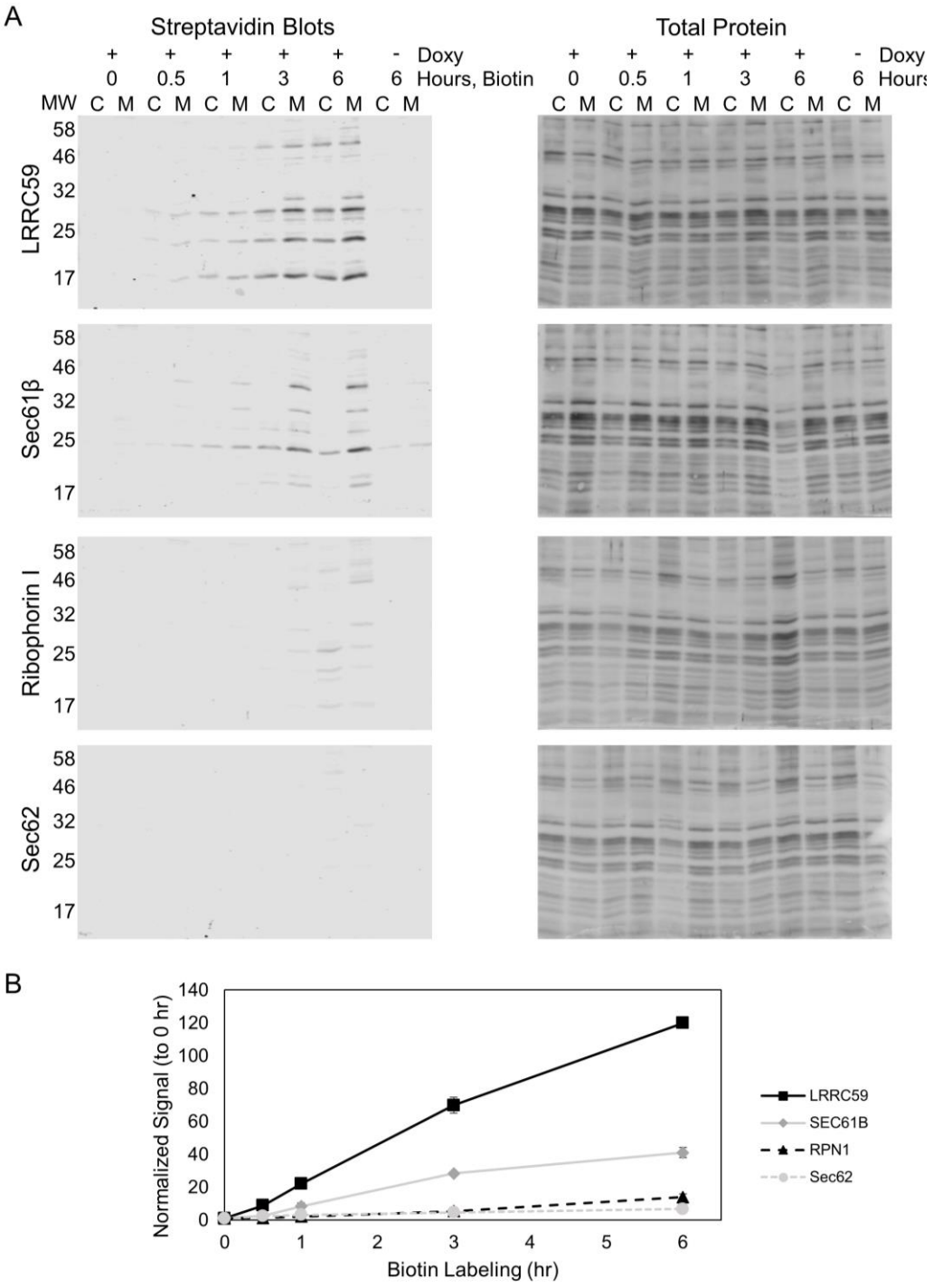

Figure 11: Labeling Time Course of ER bound Ribosomes.

A) Streptavidin blots and related total protein analysis (india ink stains) of ribosome pellets made from BioID cell lines that have been treated with doxycycline for 16 hours (+) or not (-) before being treated with biotin for the indicated amount of time (hours). B) Quantification of the signal intensity in both fractions from the 25 kDa biotin labeled band in each blot, plotted against time of added biotin from the blots shown in A. Error bars represent the range in signal intensity between the two experiments. Cytosol (C), membrane (M), Molecular weight in kDa (MW), doxycycline (Dox).

Ribosomal proteins, being highly basic and lysine-rich, should be highly receptive to BioID labeling, however, SDS-PAGE analyses of ER-derived biotinylated ribosomes revealed that, of the two chimera that showed distinct ribosome labeling, only a subset of ribosomal proteins were targets for BioID labeling (Figure 11**).** As shown, distinct ribosome labeling patterns seen for the LRRC59 and Sec61β BioID reporters were evident within 0.5 hour of biotin addition, and enriched in the ER-bound ribosome fraction over the labeling time course monitored. The labeling pattern and relative ratio of ER to cytosolic ribosome labeling, most evident in the LRRC59 BioID reporter line, did not vary substantially over the 6-hour time course of the experiments (Figure 11). Ribosome labeling was observed at extended labeling periods for the ribophorin I BioID chimera, though relatively modestly. Under these experimental conditions, ribosome labeling was not observed for the Sec62 BioID chimera. In the case of the ribophorin I reporter, the ribosome-OST interaction may be too short lived for efficient labeling. Consistent with this interpretation, recent cryoEM studies of ER microsomes have reported two distinct Sec61 translocon environments distinguished by the presence or absence of OST, where it is noted that OST recruitment to the translocon may be

transient, being present for the brief interval of N-linked sugar addition (Figure 11). [107,116]. In addition, the possibility cannot be ruled out that the ribophorin I and Sec62 chimera may be compromised in their ability to associate with the Sec61 translocon and thus to report on translocon-bound ribosomes[152].

Interestingly, ribosomal protein labeling patterns evident at early time points intensified as a function of labeling time, but did not diversify, suggesting a preferred spatial orientation of the BioID reporter-ribosome interface. This phenomenon is further characterized in the analysis depicted in Figure 11B, which illustrates the increase in labeling of the biotinylated ribosomal proteins, for all BioID reporters. Notably, the ribosomal protein labeling of the LRRC59 and Sec61β BioID reporters are similar, suggesting that the two reporters undergo similar near-neighbor lifetime interactions with membrane-bound ribosomes.

To determine if the LRRC59 and Sec61β BioID reporters were labeling translationally active ribosomes and to assess whether biotinylation perturbed ribosome function, sucrose gradient sedimentation analyses of the polysome fractions were performed (Figure 12). Subunit identification was confirmed by sucrose gradient centrifugation and RNA gel analysis of 18S and 28S rRNA distributions. One strongly labeled band (S-R1) was identified for LRRC59 and two strongly labeled bands (S-B1/2) for Sec61β in the 40S subunit (Figure 12A) and the inverse for the 60S subunit, two bands (L-R1/2) in the LRRC59 set and one band (L-B1) in the Sec61β analysis. These

bands may represent more than one protein but, as they are highly reproducible patterns, each band was labeled as indicated to facilitate comparisons between experiments (Figure 12A). In comparing the patterns of ammonium chloride washed and puromycin treated ribosome fractions from the respective cell lines, the S-B1 and S-B2 bands are reduced upon ammonium chloride/puromycin treatment leading us to believe these may be 40S associated ER membrane proteins. As the biotin tagged-ribosomal bands were evident throughout the polysome profile shown in Figure 12B, it can be concluded for both reporters that BioID tagging did not compromise ribosome function.

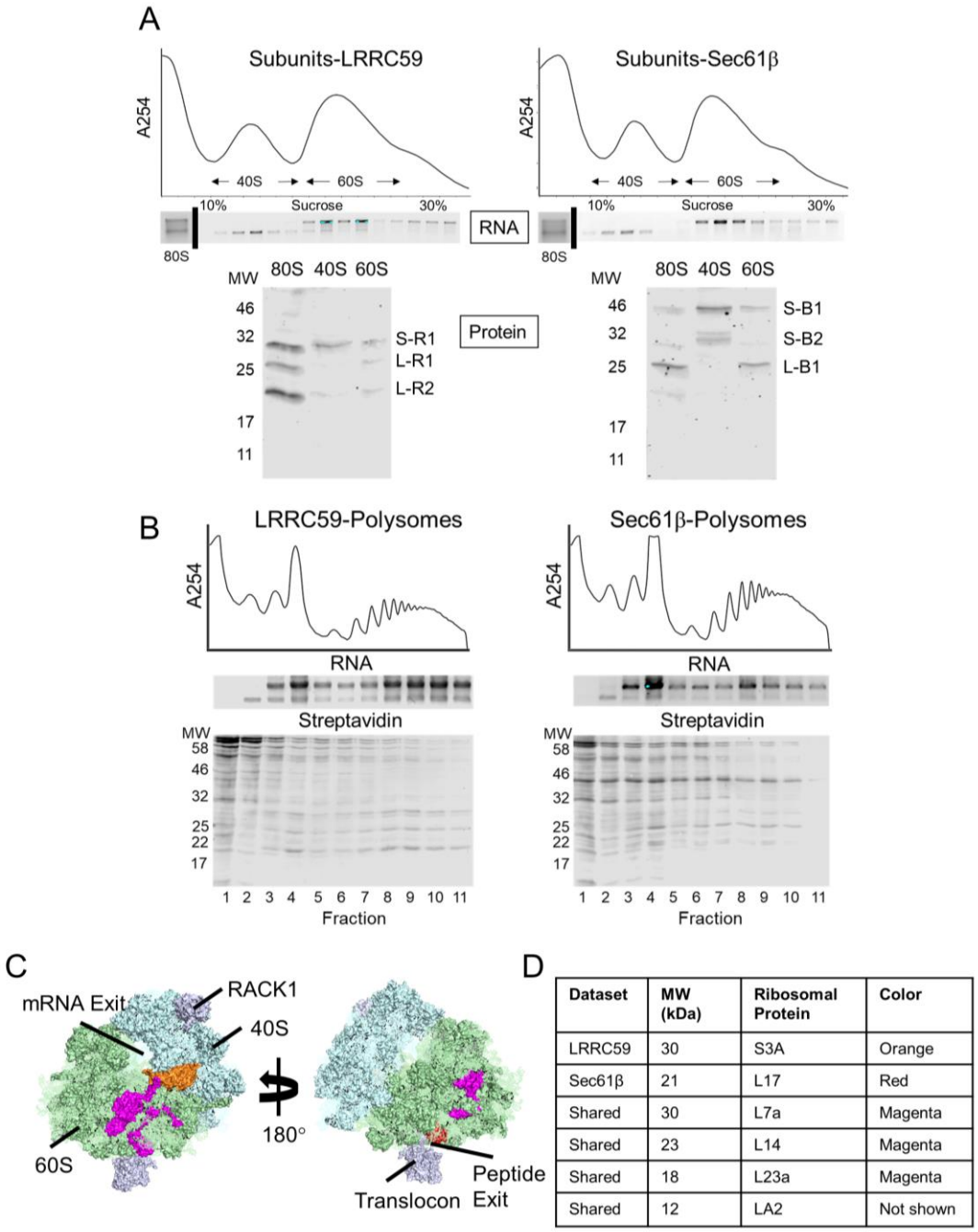

Dataset	MW (kDa)	Ribosomal Protein	Color
LRRC59	30	S3A	Orange
Sec61β	21	L17	Red
Shared	30	L7a	Magenta
Shared	23	L14	Magenta
Shared	18	L23a	Magenta
Shared	12	LA2	Not shown

Figure 12: Biotin labeling of ER-associated ribosomes in LRRC59 and Sec61β BioID reporter cell lines is distinct and occurs on translating ribosomes.

A) To compare ribosomal protein labeling patterns in the LRRC59 and Sec61β translation domains, ribosomal subunits were separated on sucrose gradients and

compared to ammonium salt and puromycin treated 80S ribosome pellet. Vertical line indicates separate gels. B) To determine if BioID-mediated biotinylation altered ribosome function, polyribosomes were examined by sucrose gradient centrifugation and rRNA and biotin-labeled protein distributions analyzed. C) MS/MS identified ribosomal proteins were mapped onto a PDB structure of the ribosome bound to the translocon (PDB: 3J7R). MS experiments were performed in duplicate. D) Table of the five ribosomal proteins identified from the mass spec datasets with high confidence.

To identify the proteins labeled by the LRRC59 and Sec61β BioID reporters, biotin-labeled ribosomes were captured by Neutravidin agarose beads, subjected to on-bead digestion, and peptides analyzed by mass spectrometry. As summarized in Figure 12C, only a subset of the 80 ribosomal proteins were identified in these analyses. Consistent with the overall streptavidin labeling patterns, both BioID reporters labeled a common set of ribosomal proteins whose locations on the ribosome seen in magenta on Figure 12C, are regionally clustered. Intriguingly, the shared proteins distribute in regions adjacent to the peptidyl transferase and nascent peptide exit site[153]. Two ribosomal proteins were highly enriched in only one dataset. RPL17 (red), enriched in the Sec61β dataset, is located near the nascent chain exit site and has been demonstrated to serve important roles in transmembrane domain sensing and signaling to the peptidyl transferase, a function consistent with its appearance in the Sec61β interactome[154,155]. RPS3A (orange), enriched in the LRRC59 dataset, is located near the mRNA exit site and has been shown to interact with the transcription factor CHOP[156]. These data are consistent with cryoEM data depicting a specific interaction between the ribosome and the translocon consistent with the data shown for the Sec61β BioID reporter[62]. The

LRRC59 BioID reporter, a known poly(A)-mRNA binding protein, also resides in proximity to bound ribosomes, consistent with a potential function in coupling translating ribosomes to translocons[102,140]. These data place LRRC59 in an important ER locale for translation. The precise role(s) performed by LRRC59 in this environment awaits further study.

3.2.2 Ribosome exchange is multiphasic and correlated to the membrane environment

Extending from the data depicted in Figure 11A, ribosome exchange between the ER and cytosol compartments was examined, and the contribution of translation to the exchange kinetics. To this end, a pulse-chase assay was established where cells were labeled with biotin for one hour (pulse) followed by incubation in non-biotin supplemented media for the indicated amount of time (chase). Figure 13A depicts plots of ribosome labeling kinetics in control (continuous labeling, dashed line) and experimental (biotin removal at one-hour, solid line) conditions. The cessation of labeling upon biotin washout indicates that this approach is suitable for pulse-chase analyses. In the data reported in Figure 13B, ribosome exchange for both reporters is comprised of a relatively rapidly exchanging pool, evident in the first 30 min of chase, and a slowly exchanging pool, which remains membrane associated after 1 hour of chase. Subsequently, ribosome exchange was interrogated under different translational states utilizing cycloheximide (Figure 13B) and harringtonine treatment (Figure 13C) to stall translating ribosomes and inhibit initiation respectively[157,158]. Inhibitors were added

at one hour, when the biotin supplemented media was removed from the cells. Figure 13B depicts the ribosome exchange by densitometry analysis of the streptavidin blotsfrom cycloheximide treated cells, for both cell lines. Here it is shown that the exchange behaviors of the labeled ribosomes were like the untreated control (Figure 13A) with a fraction of the labeled ribosomes recovered in the cytosol and a fraction remaining membrane bound. Notably, exchange patterns were also mirrored in analyses of the total ribosomal pools (Appendix C). In contrast, upon the harringtonine block of translation initiation showed a divergence in behavior of the labeled ribosomes (Figure 13C). Ribosomes labeled by the LRRC59 reporter went into the cytosol to a substantially lesser degree than those labeled by the Sec61β reporter. In the Sec61β reporter cells, ca. 15% of L-B1 remains on the membrane after 30 minutes of harringtonine treatment versus 35% of the large subunit protein band L-R2 in the LRRC59 reporter cells. Throughout treatment for each of these inhibitors, the two Sec61β bands S-B1 and S-B2 remain exclusively on the membrane. As the S-B1 and S-B2 interactions are restricted to the small ribosomal subunit (Figure 12A), these bands may represent integral membrane 40S subunit binding proteins. In summary, LRRC59 labeled ribosomes associate with the ER membrane in a manner that is largely independent of translation (i.e., cycloheximide-insensitive exchange) whereas Sec61β labeled ribosomes are sensitive to a global block in initiation, consistent with an SRP pathway targeting model where cytosolic initiation is necessary for recruitment of ribosomes onto the membrane. For the Sec61β labeled

ribosomes as well, a fraction of the labeled ribosomes underwent translation-independent exchange to the cytosol.

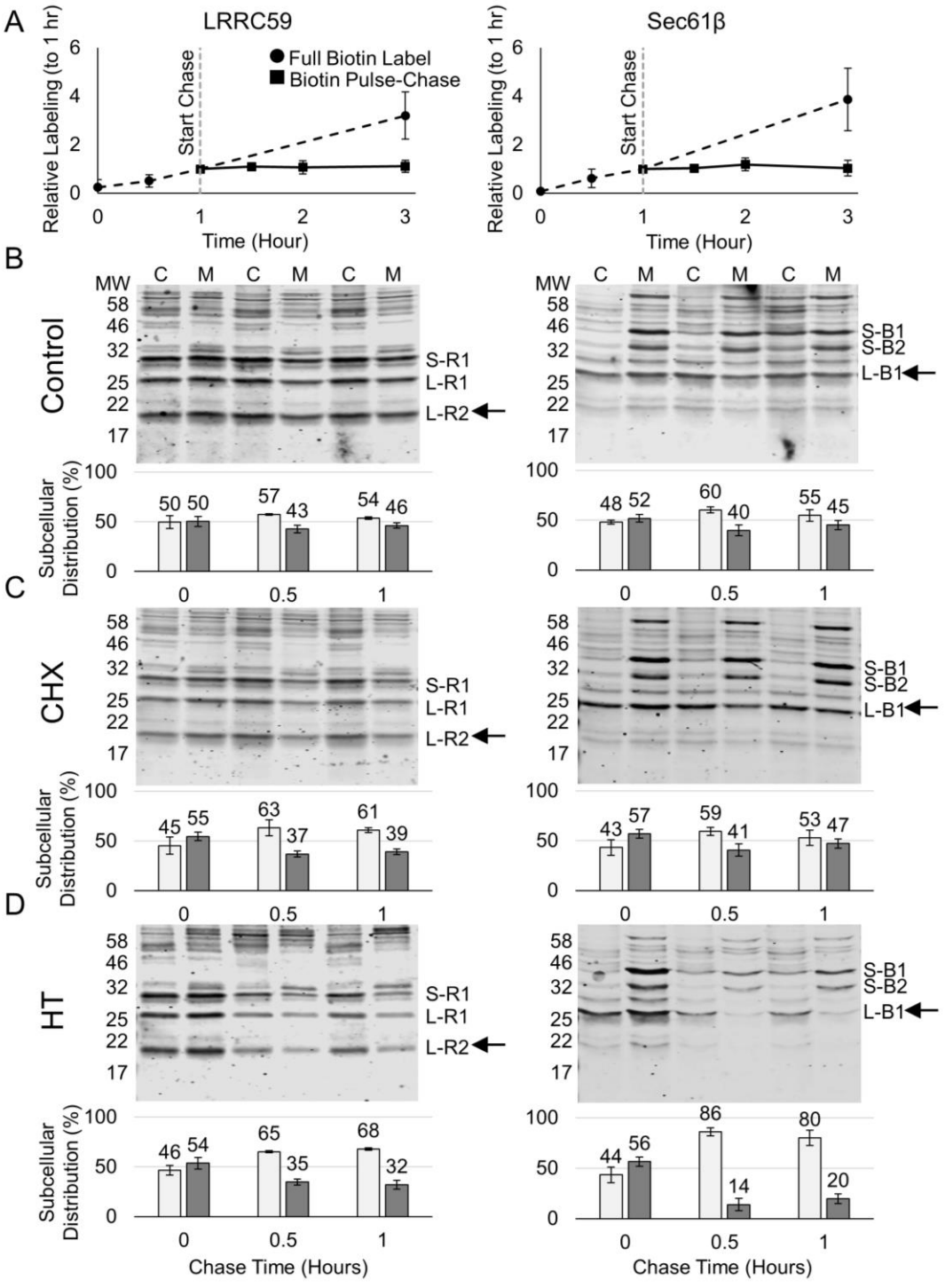

Figure 13: Differences in subsets of membrane bound ribosomes revealed under global disturbance of cellular translation.

A) Establishing a pulse-chase system to study ribosome exchange shows no significant increase in biotin labeling after biotin is washed out and no significant change in exchange rates between the two sets of reporter-labeled ribosomes. Compared to cells with biotin in the media after three hours (dashed line with circle markers), labeling appears to stop after being washed out after one hour (solid line with square markers). Relative intensity is the ratio to streptavidin signal at 1 hr. B) Streptavidin blot of untreated control cells with times indicating the pulse chase. C) Streptavidin blot showing treatment of cells with cycloheximide, which stalls ribosomes in the process of translation shows similar exchange patterns as the untreated control indicating that actively processing ribosomes is not necessary for membrane association. D) Streptavidin blot showing treatment of cells with harringtonine, which prevents elongation of initiating ribosomes, shows a divergence between the two pools of ribosomes where Sec61β labeled ribosomes require active initiation to maintain association with the membrane whereas LRRC59 labeled ribosomes are largely unchanged. Bar charts below each of the blots depicts the percentage in each cellular fraction, cytosol (C) or membrane (M), of the lowest MW labeling ribosomal protein band (L-R2 or L-B1). Shown is the best of two replicates performed as independent experiments. Error bars shown in all graphs mark the high and low measurements of streptavidin signal intensity from each experiment determined by densitometry analysis. Performed by Dr. Chen Qiang.

3.2.3 Domain-specific RNA-seq reveals regional mRNA enrichments and broad translation functions for ER-bound ribosomes

A primary objective of this study was to examine the translational landscape of the ER including whether mRNAs are non-randomly distributed across the membrane. Interactions between ER-bound ribosomes were identified by, the translocon subunit Sec61β, and the candidate ribosome receptor LRRC59. To extend these findings to the translational landscape of these domains, biotin-tagged, ER-associated ribosomes were purified from the Sec61β and LRRC59 BioID cell lines and the associated mRNAs identified by RNA-seq (Figure 14). In brief, following a 4-hour biotin labeling period, the cytosolic, free ribosome fraction was released via sequential detergent extraction and the

membrane fraction kept. The ribosomes were then separated from the co-solubilized membrane proteins by size exclusion chromatography on Sephacryl S-400 gel filtration. Biotinylated ribosomes, which are recovered in the S-400 void fractions, were isolated by avidin-magnetic bead capture, the total RNA fraction depeleted of rRNA isolated, and cDNA libraries prepared for deep sequencing. To correct for background mRNA contributions, parallel isolations were performed with empty vector cell line and cDNA libraries from these mock purifications deep sequenced in parallel. Three biological replicates are represented (Figure 14).

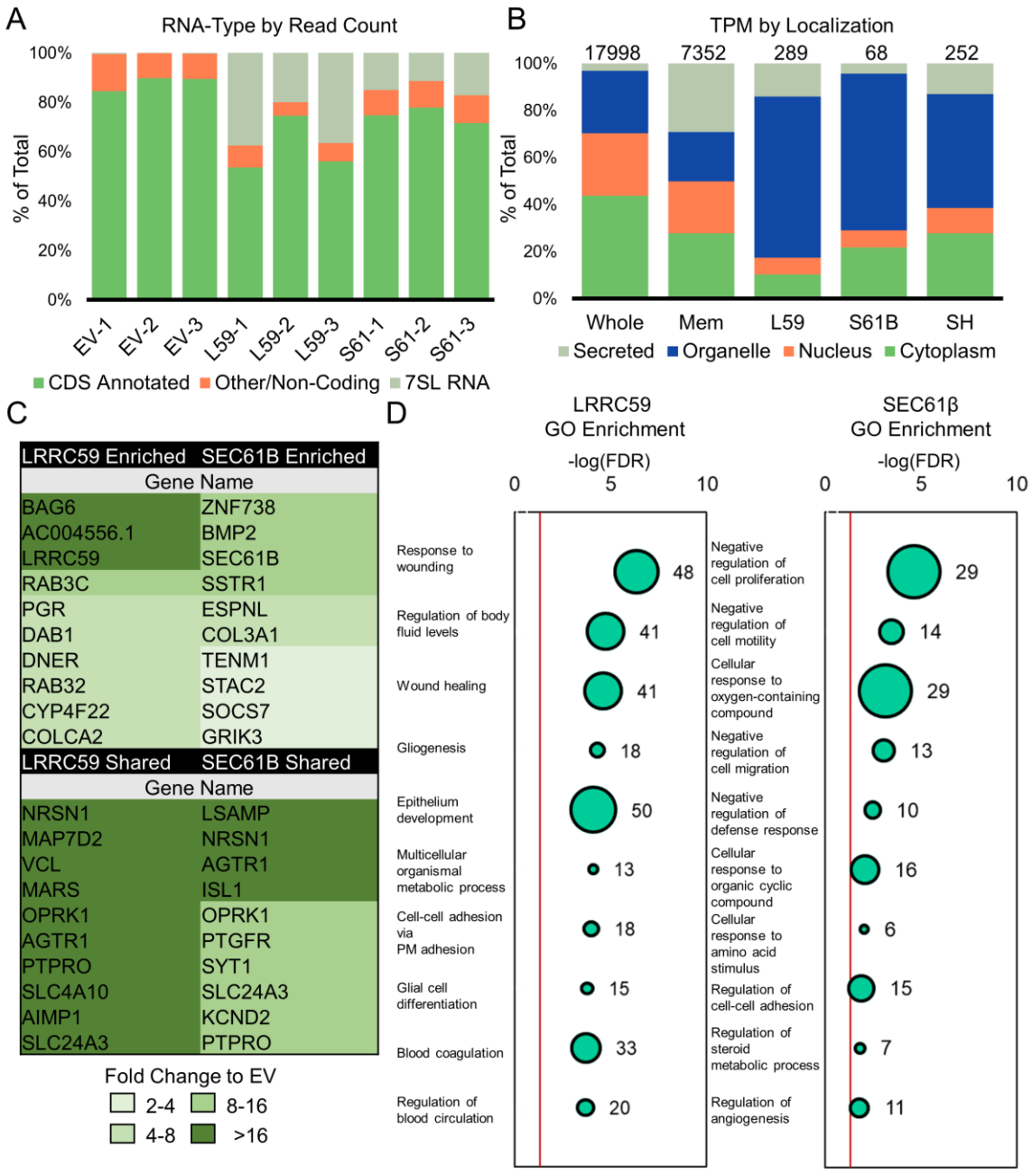

Figure 14: RNA-seq analysis of biotin-labeled polysomes shows divergent membrane bound transcriptomes of cytosolic and secretory protein-encoding RNAs.

A) Analysis of raw counts shown for each of the datasets by percentage of those that aligned to a single site in the human genome B) Final subcellular distributions of proteins encoded by ribosome-associated RNAs represented as a percentage of the

total. Stack plots of RNA-seq TPM reveal an enrichment for organellar proteins (DeepLoc1.0) compared to the total mRNA distribution by TPM for membrane and total cell (LocTree3, using datasets from (Reid and Nicchitta, 2012 and Human Protein Atlas respectively). Intriguingly, the transcriptomes from Sec61β (S61), LRRC59 (L59), and shared (SH) labeled ribosomes diverge from the whole cell (Whole) and secretory/membrane distributions (Mem), but less so from one another. Organelle category encompasses coded proteins localized to the ER, Golgi, lysosomes/vacuoles, cell membrane and mitochondria. C) Table of top ten genes by log_2 fold change value for enriched and shared datasets color coded by fold enrichment over the control datasets. D) Bubble plots depicting the -log(FDR) of diverging GO Molecular Function enrichments for the transcriptome identified by each chimera. Red line indicates FDR cutoff of 0.05. Analyzed data found in Appendix B.

As expected, coding RNAs comprised the majority of the counted reads (Figure 14A). However, an interesting difference in noncoding mRNAs was observed between the datasets. For the purposes of this study, focus was placed on the non-coding 7S RNA of the signal recognition particle[159]. 7S RNA is enriched over control in the BioID reporter translation domains, with a higher representation in the LRRC59 vs Sec61β datasets. Consistent with the 7S RNA enrichment in the LRRC59 translation domain, SRP54, the 54kDa SRP protein subunit, was enriched in the LRRC59 mass spec data in Figure 9B and serves as orthogonal validation for the specific enrichment of SRP.

Figure 14B depicts the mRNA subcellular category distributions in the Sec61β-enriched, and LRRC59-enriched pools, as compared to the total mRNA transcriptome and total ER-associated mRNA transcriptome. As expected, the ER-associated mRNA transcriptome (Figure 14B, Mem) differs substantially from the total cellular mRNA transcriptome by enrichment in mSMPs but still contains a substantial representation of mNCPs[11,128,148]. Intriguingly, the datasets from the BioID reporters further enrich for

mRNAs encoding organelle associated proteins which comprise over 60% of their datasets. This finding suggests that the BioID reporters reside in specific ER environments enriched in organelle-encoding vs. secretory cargo-encoding mRNAs. Consistent with this view, each mRNA cohort contained a subset of genes that were substantially enriched (e.g. 8-16-fold) relative to the shared gene cohort. Furthermore, of the shared genes, some were highly enriched relative to the control datasets (Figure 14C).

Displayed in Figure 14D are the highest confidence divergent GO Biological Process enrichments for the two reporter gene sets, which demonstrate that the two examined reporter domains display specialization. For example, genes identified in the LRRC59 data sets are enriched in GO terms associated with cell contact, cell adhesion, wound healing, and blood coagulation. Conversely, Sec61β shows an enrichment for regulatory processes associated with signaling pathways and transcription factors, reflecting some of the mNCPs associated with its dataset. This finding corroborates previous findings from our lab that cytosolic mRNAs non-canonically associated with the ER are enriched in these GO categories[11]. Intriguingly, for both translation domains, one of the most enriched genes is the parent reporter gene. Thus, ribosomes engaged in the translation of the reporter reside in proximity to their translation product (Figure 14C). Such an intimate association may arise if the reporter parent genes encode or

associate with an interacting RNA binding protein. Consistent with this view, both LRRC59 and Sec61β have been identified as poly(A) RNA binding proteins[160].

In summary, RNA-seq analyses of mRNAs undergoing translation on ribosomes proximal to the Sec61β and LRRC59 BioID reporters revealed translational specialization, where specific GO category gene sets were enriched in the two domains, and shared translation functions, where numerous genes were common to the two translation domains. Combined with the ribosome exchange and ribosomal proteomic data reported above, these data suggest a higher order organization of the ER, with membrane-bound ribosomes and mRNAs, displaying discrete enrichments, which is consistent with a model where the ER is comprised of interacting membrane neighborhoods engaged in the translation of enriched subsets of mNCPs and mSMPs.

3.3 Discussion

Here the translational landscape of the ER from the biochemical perspective of candidate ribosome interacting proteins is reported. The rationale for this study is rooted in the growing number of reports demonstrating that mNCPs undergo translation on ER-bound ribosomes. Indeed, recent analyses indicate that mNCPs comprise the majority of the translation activity of total ER-bound ribosomes[11,148,161]. These reports raise a number of intriguing questions regarding mechanisms and specificity for RNA localization to the ER as well as mechanisms of ribosome localization and exchange on the ER, which is accepted to be functionally linked to SMP synthesis[162].

Indeed, there is a fundamental cell biology element to these questions, where a dedicated role for the ER in the biogenesis of SMPs is well established though the question of the exclusivity of this role has been raised for many decades and continues to be debated[11,45,103,161]. An unbiased proximity labeling approach, BioID, is used to investigate the near-neighbor environments of both established and candidate ribosome-interacting ER membrane proteins, including Sec61β, a subunit of the Sec61 translocon, ribophorin I, a subunit of the OST complex, and which resides in proximity to Sec61 translocons, and LRRC59, which displays ribosome binding activity *in vitro* [58,111]. Four primary findings can be proposed from these studies; i) the ribosome interactors examined reside in interactome-distinguishable ER membrane protein environments; ii) LRRC59 resides proximal to ER-bound ribosomes and thus likely contributes to the totality of ribosome association on the ER; and iii) ribosomes residing next to different reporters are engaged in the translation of both mSMPs and mNCPs, including commonly shared and selectively enriched transcripts; and iv), ribosome exchange rates are slow, relative to translation, and can be distinguished by exchange rates under different translational inhibition. Combined, these data suggest that multiple ribosome interacting proteins contribute to ribosome association on the ER and by virtue of their slow exchange rates, are spatially disposed to perform a general function in translation.

A particularly intriguing observation from these studies is the finding that LRRC59 is near translating ribosomes. Although LRRC59 had previously been reported

to function as a ribosome binding protein *in vitro*, a function in ribosome association *in vivo* has not been demonstrated[58,122,163]. Indeed, after a decades long search for the ribosome receptor, which yielded the identification of the ribophorins, LRRC59, p180, and Sec61α, among others, research interest has largely focused on the Sec61 complex as the sole ribosome interacting ER protein[60,62,107,149]. Substantial structural data supports this functional assignment, but these data do not exclude the possibility that additional ER proteins contribute to the totality of ribosome association with the ER[120,144,164–166]. In support of this view, many ER membrane proteins including LRRC59 have been found to bind poly(A)-RNA including MTDH (AEG-1), which was recently demonstrated to be an ER RNA binding protein enriched in membrane protein-encoding mRNAs[143], p180 and CKAP4, which have also been demonstrated to have a poly(A)RNA binding function[110,140,144]. Taken together, these findings suggest LRRC59 may have a role in coupling ER-associated translation to translocon engagement of the translation product. These data fit with a previously proposed model suggesting ribosome interacting proteins might diffuse in the ER membrane to allow nascent chain engagement with unoccupied translocons[102,167,168].

Since the two BioID reporter chimeras, Sec61β and LRRC59, tagged ER-bound ribosomes in readily distinguishable patterns, it was determined whether such differences were informing of a transcriptome organization to the ER. As noted, a primary role for the ER in SMP biogenesis is well established by many studies

examining the subcellular distributions of mRNAs between the cytosol and ER compartments have strongly affirmed this role[11,51]. Although the interpretation of these data has been debated, studies of mRNA distributions between the cytosol and ER compartments in yeast, by ER localized BirA-AVI tag labeling or by SRP-directed immunoprecipitation, demonstrate that many mNCPs display $\log_2$ cytosol enrichments of < 1-2, and are thus substantially represented on the ER[128,148]. This mRNA distribution is similar to data reported in mammalian cells[11,51]. In the current study, the associated transcriptomes of biotin-tagged, ER-bound ribosomes were examined. Although enriched in mSMPs as in earlier studies, ribosomes residing in proximity to both the Sec61β and LRRC59 BioID chimera contained a fraction of mNCPs. The RNA populations for the two cell lines displayed both shared and enriched transcripts and, of high interest, the enriched transcript cohorts differed in GO enrichments, with the Sec61β cohort being enriched in mRNAs encoding ER proteins and the LRRC59 cohort being enriched in mRNAs encoding integral plasma membrane proteins. Particularly interesting was the finding that one of the most enriched transcripts for both reporters was the "self mRNA". These findings support the concept of translation centers on the ER, where mRNAs encoding proteins of related function are coordinately translated in a coherent, localized manner. It remains to be determined how individual mRNAs are targeted to distinct sites or whether mRNAs may be directly recruited to such sites via

binding interactions with additional ER RNA binding proteins such as AEG-1 or by stably associated ribosomes potentially with heterogeneous composition[143,169–172].

While there is a significant overlap of transcripts between the two reporters, the two ribosome populations showed differences in exchange upon global shutdown of translation initiation where a subset of LRRC59 labeled ribosomes remain bound to the membrane whereas ribosomes labeled by Sec61β are released entirely to the cytosol and unable to regain access to the membrane (Figure 13D). These data raise two interesting points i) subsets of ribosomes appear to require different mechanisms of membrane association and ii) subsets of ribosomes are restricted to a specific membrane environment potentially through heterogeneity of the ribosome interactome within the cell. The latter can be inferred by the fact that membrane bound ribosomes that leave to the cytosol do not return potentially due to the crucial function of initiation in the SRP pathway supporting the findings for ribosomes labeled by the Sec61β reporter. Further identifying the mechanism of ribosome association close to LRRC59 and its apparent role in membrane bound translation awaits further study.

In summary, biochemical and transcriptomic data are presented supporting the view that translation on the ER is subject to higher order organization where cohorts of ribosomes and their respective mRNAs are localized to distinct spatial environments. These data also provide additional evidence in support of a transcriptome-wide function for the ER in translation. The remaining questions are many, but given emerging data on

the nanoscale structural organization and translational organization of different regions and compartments of the cell, notably dendrites, mitochondria, stress granules, and P bodies, these data are consistent with higher organization of transcriptome expression and regulation as an evolutionarily conserved cellular strategy[95,100,173–176].

3.4 Methods

Generation of BioID Chimera Plasmids were from the following sources: pCMV-Sport6-RPN1 (Transomic ID: pCS6-BC010839, TransOMIC, Hunstsville, AL), pCMV-Sport6-LRRC59 (Transomic ID: pCS6-BC017168), Sec61β (Transomic ID: pOTB7-BC BC001734), Neo-IRES-GFP-Sec62 (Richard Zimmerman, Saarland University, Homburg, Germany), pEYFP-N1-BirA* (Scott Soderling, Department of Cell Biology, Duke University Medical Center). Gibson assembly master mix (NEB E2611S, Ipswich, MA) was used with the specified amplified fragments using the primers below to generate all constructs with the indicated BirA* tag including a Gly-Ser-Gly-Ser linker between the protein of interest and BirA*. All resulting constructs were cloned into pcDNA5-FRT/TO for downstream generation of HEK293 Flp-In T-REx cell lines (Thermo Fisher Scientific, Waltham, MA).

Table 1: List of BioID Cloning Primers

Primer Name	Primer Sequence (5′ to 3′)
Vector-RPN1-Fwd	CTCTAGCGTTTAAACTTAAGCTTATGGAGGCGCCAGCCGCC
RPN1-BirA*-Rev	CCACTGCCCAGGGCATCCAGGATGTGGTCG

RPN1-BirA*-Fwd	ATGCCCTGGGCAGTGGCAGTAAGGACAACACCGTGCCC
BirA*-Vector-Rev	ATCCGAGCTCGGTACCTATGCGTAATCCGGTACATCG
Vector-BirA*-Fwd	CTCTAGCGTTTAAACTTAAGCTTATGAAGGACAACACCGTGC
BirA*-LRRC59-Rev	CCACTGCCCTCGAGCTTCTCTGCGCT
BirA*-LRRC59-Fwd	AGCTCGAGGGCAGTGGCAGTACCAAGGCCGGTAGCAAG
LRRC59-Vector-Rev	ATCCGAGCTCGGTACCTCACTGCTGAGAGTCGGTC
BirA*-Sec61β-Rev	CCACTGCCCTTCTCTGCGCTTCTCAG
BirA*-Sec61β-Fwd	CAGAGAAGGGCAGTGGCAGTCCTGGTCCGACCCCCAGT
Sec61β-Vector-Rev	GGGTTTAAACGGGCCCTACGAACGAGTGTACTTGCCC
Vector-Sec62-Fwd	GCGTTTAAACTTAAGCTTATGGCGGAACGCAGGAGA
Sec62-BirA*-Rev	CTTACTGCCACTGCCTGATTTTTCATGTGAAGATTTAGGTGTTTCTC
Vector-C terminal-BirA*-Rev	AAGCTTAAGTTTAAACGCTAGAGTC
Vector-C terminal-BirA*-Fwd	GGCAGTGGCAGTAAGGA

Sequences were confirmed using a CMV-Forward and BGH-Reverse sequencing primers supplied by Eton Biosciences (Research Triangle Park, NC).

Generation of HEK293 Flp-In T-Rex cell lines. HEK293 Flp-In T-REx cell lines were generated according to the manufacturer's instructions (Thermo Fisher Scientific). Cells

were transfected in 6-well culture dishes at 80% confluence using 7.5 μL of Lipofectamine 3000 (Thermo Fisher, L3000001) with 0.4 μg of plasmid containing the desired fusion protein and 4 μg of pOGG4 plasmid. Selection with 100 μg/mL of hygromycin (MediaTech, 30-240-CR, , Manassas, VA) and 15 μg/mL of blasticidin (Thermo Fisher, R21001) was started 48 hours after transfection and continued for 2 weeks at which point colonies were identified. A control cell line was generated by recombination of an empty vector pcDNA5-FRT/TO and antibiotic selection for an empty vector matched control.

Expression of BirA fusion proteins Expression levels were examined by doxycycline (Sigma Aldrich, D9891, St. Louis, MO) titration and the following doxycycline concentrations were used for each construct: 10ng/mL LRRC59-BioID, 5 ng/mL Sec61β-BioID, 50 ng/mL Ribophorin I-BioID, 100 ng/mL Sec62-BioID. Expression of BioID constructs was performed for at least 16 hr before addition of biotin unless otherwise noted.

IF Analyses Cells were plated on poly-lysine coated 22 mm #1.5 coverslips (Globe Scientific, 1404-15, Paramus, NJ). Reporter expression was induced by doxycycline addition and 50 μM biotin added for an overnight labeling. After 16 hours, cells are washed twice with PBS, fixed in 4% paraformaldehyde for 10 min on ice and 10 min at room temperature then washed 3 times with PBS for 5 min each. Cells were permeabilized with a blocking solution of 3% BSA and 0.1% saponin (Sigma Aldrich, S-

2149) in PBS for 1 hr at room temperature. Primary staining was performed in the identical solution supplemented with 1:200 BirA antibody (Sino Biological Inc., rabbit IgG, Wayne, PA) or 1:50 TRAPα antibody [177] (polyclonal, rabbit IgG) at 4°C overnight. Following 5 x 3min washes of 0.1% saponin in PBS, coverslips were incubated with 1:200 goat anti-rabbit IgG AlexaFluor488 (Thermo Fisher, A-11034), 1:1000 streptavidin-Alexafluor647 (Thermo Fisher, S21374) and 1:10000 DAPI (0.5mg/mL stock solution) mixed in blocking solution at room temperature for 45 min in the dark. Coverslips were washed 5X as above, rinsed and mounted in FluorSave hard mount (CalBioChem, 345789, Burlington, MA) and cured at 4°C overnight prior to imaging.

Fluorescence Imaging All imaging was performed on a Deltavision deconvolution microscope (Applied Precision, Issaquah, WA) equipped with 100x NA 1.4 oil immersion objective (UPlanSApo 100XO; Olympus, Tokyo, Japan) and a high-resolution CCD camera (CoolSNAP HQ2; Photometrics, Tucson, AZ). Images were acquired as Z-stacks (at 0.2μm intervals) at identical exposure conditions across the samples for a given protein. The data were deconvolved using the SoftWoRx program (Applied Precision, Mississauga, ON) and processed further on ImageJ/FIJI software to render maximum intensity projections (as required), merge channels and pseudo color the images. Only linear changes were done to the brightness/contrast values of the images, as required and such changes were applied uniformly across all images in a given experiment.

Sequential Detergent Fractionation and General Cell Lysis Cells were washed twice with ice-cold PBS containing 50 μg/mL of cycloheximide (CHX) (VWR, 94271, Radnor, PA) for 3 min each wash. Permeabilization buffer (110 mM KOAc, 25 mM HEPES pH 7.2, 2.5 mM $Mg(OAc)_2$, 0.03% digitonin (CalBioChem, 3004010), 1 mM DTT, 50 μg/mL CHX, 40U/mL RNAseOUT (Invitrogen, 10777-019, Carlsbad, CA), Protease Inhibitor Complex (PIC) (Sigma Aldrich, P8340)) was added to cells and incubations performed for 5 min at 4°C. The supernatant fraction (cytosol) was collected and cells rinsed with wash buffer (110 mM KOAc, 25 mM HEPES pH 7.2, 2.5 mM $Mg(OAc)_2$, 0.004% digitonin, 1 mM DTT, 50 μg/mL CHX, 40U/mL RNAseOUT, Protease Inhibitor Complex (PIC)). Cells were then lysed in NP-40 lysis buffer (400 mM KOAc, 25 mM HEPES pH 7.2, 15 mM $Mg(OAc)_2$, 1% NP-40, 0.5% DOC, 1 mM DTT, 50 μg/mL CHX, 40U/mL RNAseOUT, Protease Inhibitor Complex (PIC)) for 5 min at 4°C. Both cytosolic and membrane fractions were cleared by centrifugation (15,300 x g for 10 min). Total cell lysis was performed in the ER lysis buffer by incubating cells at 4°C for 10 min. Lysates were cleared by centrifugation as above.

***In Vitro* BirA* Labeling of Microsomes** Canine pancreas rough microsomes (RM) [178] were adjusted to a concentration of 4 mg/mL protein in 500 μL of BirA reaction buffer (20 mM Tris pH 8, 5 mM $CaCl_2$, 100 mM KCl_2, 10 mM $MgCl_2$, 3 mM ATP, 1.5 mM biotin, 5 mM phosphocreatine (Sigma-Aldrich, P7936-1G) and 5 μg/mL of creatine kinase (Sigma-Aldrich, C3755-3.5KU)). Purified recombinant BirA*-GST fusion protein was

added to a concentration of 10 μg/mL. At 0, 1, 3, 6, and 18 hrs, 100 μL of reaction was removed, flash frozen in an ethanol bath and stored at –80°C prior to Western blot analysis.

Western blotting Lysate protein concentrations were determined using a Pierce BCA Protein Assay Kit (ThermoFisher, 23225). SDS-PAGE was performed in 12% acrylamide gels containing 0.5% of trichloroethanol. Gels were UV irradiated for 5 min and imaged using an Amersham Imager 600 (GE Life Sciences, Pittsburgh, PA) to verify protein loading. Gels were then equilibrated in Tris-gycline transfer buffer for 5 min and transferred using a Trans Blot SD Semi-Dry Transfer apparatus (Biorad, Hercules, CA). Blots were blocked in PBS, 3% BSA for 1 hr before primary antibody was added at the indicated dilution and incubated for 2 hr at RT or overnight at 4°C. Goat secondary antibodies (Li-Cor, Lincoln, NE) were matched to the species of the primaries used and diluted 1:10,000. Streptavidin was used at a dilution of 1:20,000. Secondary reagents were incubated for 45 min, washed 5x with TBST and imaged on the Odyssey Clx (Li-Cor). Primaries used: BirA (Abcam #14002, polyclonal, chicken IgG), TRAPα [177](polyclonal, rabbit IgG), tubulin (Iowa Hybridoma Bank, E7, monoclonal, mouse IgG, Iowa City, IA), Sec61β (Gift of Ramanujan Hegde, University of Cambridge, polyclonal, rabbit IgG), LRRC59 (Bethyl Labs A305-076A, polyclonal, rabbit IgG, Montgomery, TX), Sec62 (gift from Richard Zimmerman, polyclonal, rabbit IgG), Ribophorin I [177](polyclonal, rabbit IgG), streptavidin-RD680 (Li-Cor, P/N 925-68079).

RNA Extraction As adapted from [179], RNA was extracted from 1 volume of lysate using 2 volume of GT buffer to 0.5 volumes of water-saturated phenol, pH 4.5 and incubated for 5 min at RT before adding 0.8 volume of chloroform. Following centrifugation for 15 min at 10,000xg, 4°C for 15 min, the aqueous phase was recovered, and RNA precipitated by addition of 1.2 volumes of isopropanol and 0.15 volume of 3M sodium citrate pH 5.2. Following incubation at -20°C for 1 hr, RNA was recovered by centrifugation at 10,000xg, 4°C for 20 min. RNA pellets were washed in 70% ethanol, dried, and resuspended in TE buffer (10 mM Tris pH 8.0, 1 mM EDTA). RNA concentrations were determined using a NanoDrop ND-1000 Spectrophotometer (Thermo Fisher Scientific). RNA quality was examined by denaturing formaldehyde gel electrophoresis.

Glycerol Gradients As adapted from [127], reporter construct expressing BioID lines were lysed in 1 ml/10cm dish of homogenization buffer (20 mM Tris pH 7.4, 500 mM NaCl, 1.5% digitonin, 1mM $MnCl_2$, 1 mM $MgCl_2$, 1mM DTT, PIC) for 30 min at 4°C. Lysates were cleared by centrifugation in a TLA 100.2 rotor at 40,000 rpm for 10 min, 4°C (TL-100 Ultracentrifuge, Beckman Coulter, Brea, CA). 850 µL of the supernatant was then loaded onto a 8-30% glycerol gradient and centrifuged in an SW-41 rotor at 35,000 rpm for 15.5 hr, 4°C (L5-50B Ultracentrifµge, Beckman). Gradients were fractionated into 12 fractions using a Teledyne Isco gradient fractionation system and analyzed by immunoblot.

Polysome Gradients Cells expressing BioID constructs were lysed in 50 mM HEPES, pH 7.2, 200 mM KOAc, 1 mM DTT, 2% dodecylmaltoside (ChemImpex Intl Inc, 21950, Wood Dale, IL), 5 mM EGTA, PIC, 1mM DTT, 50 μg/mL CHX for 10 min at 4°C. Cell lysates were cleared at 15,300xg for 10 min, 4°C. 0.8 mL of lysate was loaded onto 15-50% sucrose gradients and centrifuged for 3 hours at 35,000 rpm, 4°C (L5-50B Ultracentrifuge, Beckman). Gradients were fractionated into 12 fractions using a Teledyne Isco (Lincoln, NE) gradient fractionation system and analyzed by immunoblot and denaturing RNA gel electrophoresis.

Biotin Pulldowns Adapted from [180]: Constructs are expressed as above, with biotinylation reactions performed for 3 hours prior to sequential detergent fractionation. The membrane fraction was obtained and volume adjusted to a protein concentration of ca. 1.3 mg/ml an diluted 1:1 with 100 mM NaCl, 50 mM HEPES pH 7.4 to reduce detergent concentratons. Pierce NeutrAvidin Agarose (Thermo Fisher, 29200) resin was blocked for 1 hr with 1% BSA and washed three times in HEPES buffer. Pulldown reactiosn were performed overnight at 4°C. Beads were washed with the following buffers twice each for 10 min at RT. Buffer 1: 2% SDS in 50 mM HEPES pH 7.2 Buffer 2: 0.1% DOC, 1% Triton X-100, 1mM EDTA, 500 mM NaCl, 50 mM HEPES pH 7.5 Buffer 3: 0.5% DOC, 0.5% NP-40, 1mM EDTA, 250 mM LiCl, 10 mM Tris pH 7.4. Beads were then suspended in 50 μL of biotin elution buffer, vortexed, and heated for 15 min at 70°C.

Supernatant fractions were combined and concentrated to 50 μL in a Savant SpeedVac Concentrator (Thermo Fisher Scientific).

Ribosome Pulldowns Cells were washed with PBS and lysed in NP-40 lysis buffer (above). Lysates were cleared at 15,300xg for 10 min and the supernatant fraction overlaid onto a 1M sucrose cushion (2:1, load:cushion). Samples were centrifuged at 80,000 rpm for 25 min (TLA 100 rotor in TL-100 Ultrcentrifuge, Beckman). Ribosome pellets were washed with PBS before being suspended in 50 mM HEPES, pH 7.4, 100 mM NaCl, 1% SDS, 10 mM EDTA, 1 mM DTT, by dounce homogenization. Ribosome concentration was determined by the A_{260} absorbance and calculated using the extinction coefficient: $5x10^7$/cm*M [181]. Equal amounts of ribosomes were used for pulldowns, as above. Binding reactions were performed by end-over-end mixing for 90 minutes at room temperature. Beads were washed as above and suspended in 20 μL of HEPES buffer and submitted to the Duke Proteomics Core for on-bead digestion.

Mass Spectrometry On-Resin Trypsin Digestion. Samples for on-resin digestion were delivered to the DPMSR at 4°C in 1.5 mL tubes containing streptavidin-coupled Dynabeads (Thermo Fisher Scientific) conjugated to biotin and the protein of interest. The Dynabead complexes in solution were washed three times with 500 μL of 50 mM ammonium bicarbonate (AmBic, Millipore Sigma, Burlington, MA). Twenty microliters of 1.0% acid labile surfactant (RapiGest, Waters, Milford, MA) in AmBic was added to each sample followed by an additional twenty microliters of AmBic. Samples were

subsequently reduced with 10 mM dithiothreitol (DTT, Millipore Sigma) for 30 minutes at 40°C with shaking, and alkylated using 20 mM iodoacetamide (IAM, VWR Scientific) for 30 minutes at room temperature. Digestion was performed using 500 ng sequencing grade trypsin in AmBic (5 uL at 0.1 ug/uL, Promega, Madison, WI), at 37°C overnight with shaking. Peptides were extracted by decanting supernatant into a separate 1.5 mL Eppendorf (Hamburg, Germany) LoBind tube, and washing the resin with 50 uL additional AmBic, which was also combined with digested peptides. The combined extract was acidified to 1% v/v trifloroacetic acid (Thermo Fisher Scientific), heated to 60°C for 2 hours to cleave the RapiGest surfactant, and lyophilized to dryness.

Gel Electrophoresis. The six samples of approximately 45 uL in loading buffer were delivered for one dimensional sodium dodecyl sulfate polyacrylamide gel electrophoresis (1D-SDS-PAGE) to the DPMSR on dry ice and stored at -80°C until analysis. Upon thawing, twenty five microliters was pipetted from each sample into a new, labeled 0.5 mL protein low-bind tube (Eppendorf). Five microliters of 100 mM DTT and 10 uL of NuPAGE™ (Thermo Fisher Scientific) 4X loading buffer was added to each sample, and samples were then heated to 70°C for ten minutes with shaking at 750 rpm. 1D-SDS-PAGE separation was performed using a 1.5 mm a 4-12% Bis-Tris pre-cast polyacrylamide gel (Novex, Thermo Fisher Scientific), 1X MES SDS NuPAGE™ Running Buffer (Thermo Fisher Scientific) including NuPAGE™ antioxidant. Forty microliters of each sample was loaded into the gel with a gel loader tip (Eppendorf), and PAGE

separation was performed at a constant 200V for five minutes then gels were removed from the box and proteins fixed for 10 minutes, stained for 3 hours, and destained overnight following manufacturer instructions.

Gel Band Isolation and Trypsin Digestion. Gel bands of interest were isolated with the assistance of a light box, using a sterile scalpel with minimal water while still in the gel staining box with a small amount of the destaining solution. Each gel band was placed into a protein low-bind tube (Eppendorf) labeled with the sample name and split into pieces using a pipette tip. The gel pieces were washed with five hundred microliters of 40% LCMS grade acetonitrile (MeCN, Thermo Fisher Scientific) in AmBic, with shaking at 30°C. Gel pieces were shrunk with neat LCMS grade MeCN, then the solution was discarded and the gel pieces were allowed to dry at 50°C for three minutes with no shaking and the caps open to promote evaporation. Reduction of disulfides was performed using 100 uL of 10 mM DTT at 80°C for thirty minutes with shaking, followed by alkylation with 100 uL of 55 mM IAM at room temperature for twenty minutes in the dark. This liquid was aspirated from the samples and discarded, and gel pieces were washed twice with 500 uL AmBic, and these washes were also discarded. LCMS grade MeCN was added to shrink the gel pieces in each sample, then samples were swelled in AmBic and this process was repeated a second time, finally the gel pieces were shrunk a final time by adding two hundred microliters of LCMS grade MeCN, and tubes were left open with no shaking for 3 minutes at 50°C to promote evaporation. Trypsin digestion

was performed with addition of 30 uL of 10 ng/μL sequencing grade trypsin (Promega, Madison, WI) in AmBic plus 30 uL microliters of additional AmBic. The samples were incubated overnight at 37°C with shaking at 750 rpm. Finally after overnight digestion 60 microliters of 1/2/97 v/v/v TFA/MeCN/water was added to each sample and incubated for thirty minutes at room temperature and 750 rpm to extract peptides, and the combined supernatant is transferred to an autosampler vial (Waters). Gel pieces are shrunken in 50 uL additional MeCN for 10 minutes to extract the maximum amount of peptides, and this is combined with the previous supernatant. The samples were dried on the Vacufuge (Eppendorf) and stored at -80°C until ready for LC-MS/MS analysis.

Qualitative Analysis of On-Resin and Gel Electrophoresis Samples. All on-resin and gel band samples were resuspended in 20 uL of 1/2/97 v/v/v TFA/MeCN/water. The samples were analyzed using by nanoLC-MS/MS using a Waters nanoAcquity LC interfaced to a Thermo Q-Exactive Plus via a nanoelectrospray ionization source. Two microliters of each on-resin sample, while one microliter of each gel band sample was injected for analysis. Each sample was first trapped on a Symmetry C18, 300 μm x 180 mm trapping column (5 μl/min at 99.9/0.1 v/v H2O/MeCN for 5 min), after which the analytical separation was performed using a 1.7 μm ACQUITY HSS T3 C18 75 μm x 250 mm column (Waters). The peptides were eluted using a 90 min gradient of 5-40% MeCN with 0.1% formic acid at a flow rate of 400 nl/min with a column temperature of 55 °C.

Data collection on the Q Exactive Plus mass spectrometer was performed with data dependent acquisition (DDA) MS/MS, using a 70,000 resolution precursor ion (MS1) scan followed by MS/MS (MS2) of the top 10 most abundant ions at 17,500 resolution. MS1 was performed using an automatic gain control (AGC) target of 1e6 ions and maximum ion injection (max IT) time of 60 msec. MS2 used AGC target of 5e4 ions, 60 ms max IT time, 2.0 m/z isolation window, 27 V normalized collision energy, and 20 s dynamic exclusion. The total analysis cycle time for each sample injection was approximately 2 h. The sample run order was chosen to minimize potential carryover and is detailed as follows for the on-resin and gel band samples, respectively: 125-EV, 125-LR59, 125-S61, 1210-EV, 1210-LR59, 1210-S61, EV, LRRC59, SEC62, SEC61B, and RPN1.

Database searching. Proteome Discoverer (Thermo Fisher Scientific) was used to generate mgf files from the DDA analyses and the data was searched using Mascot v 2.5 (Matrix Science) with a custom database containing the human proteome downloaded from UniProt combined with common proteins found in BirA experiments and common contaminants. The data was searched using trypsin enzyme cleavage rules and a maximum of 4 missed cleavages, fixed modification carbamidomethylated cysteine, variable modifications biotinylated lysine, deamidated asparagine and glutamic acid and oxidated methionine. The peptide mass tolerance was set to +/- 5 ppm and the

fragment mass tolerance was set to +/- 0.02 Da. False discovery rate control for peptide and protein identifications was performed using Scaffold v4 (Proteome Software, Inc).

Analysis of Scaffold data. Method adapted from [182]. For the membrane protein data sets of each biological replicate, hits with 1% FDR at the protein level, 50% peptide match with a minimum of 2 peptides and 2 spectral counts were used for subsequent analysis. Each dataset is first normalized by summing spectral counts for the natively biotinylated proteins-acetyl-CoA carboxylase, propionyl CoA carboxylase, pyruvate carboxylase, and methyl crotonyl-CoA carboxylase subunits – and dividing all spectral counts by this number. Proteins less than 2.5-fold above the same proteins in the control dataset for the specific run were removed. The remaining protein spectral counts for each dataset were averaged and normalized by dividing by the BirA protein spectral counts to account for any differences in enzyme expression. Analyses were performed so that any proteins with average normalized counts higher than 2-fold above the same protein in the three other datasets was assigned to the specific cell line as "enriched." Remaining proteins were analyzed by covariance of normalized counts with a cut-off of 50.0. These proteins were shared between at least two of the cell lines with higher than 2-fold normalized counts of the lowest count. For localization prediction, a FASTA file containing the protein sequences was generated and processed on the TMHMM Server v2.0 (DTU Bioinformatics) to identify membrane vs soluble proteins. Localization by

organelle (Fig 6B) was determined by running the datasets through DeepLoc v1.0 (DTU Bioinformatics) using the Profiles algorithm.

For ribosomal protein data sets, spectral counts were retrieved for only ribosomal protein hits with 90% protein identity, 50% peptide identity with at least 2 peptides. Each experiment dataset was divided by the control, and those exceeding a 2-fold difference were further analyzed. For each candidate, sample spectral counts were divided by the control and proteins with greater than 2-fold difference are termed "enriched" and those below the cutoff are termed "shared". Those proteins with the same term between the two datasets are kept and mapped onto PDB file 37JR, of the translating ribosome on the translocon.

Biotinylated Polysome Isolation and Sequencing. Ribosomes were purified from the membrane fractions of sequential detergent fractionation of the indicated BioID cell lines by gel filtration chromatography, collecting void fraction of a Sephacryl S400 column operating at a flow rate of 0.7 mL/min. Dynabeads M-270 Streptavidin beads (ThermoFischer, 65305) and 0.05% Triton X-100 are added to each sample and incubated overnight at 4°C. Beads are washed three times for 10 min at 4°C in high-salt wash buffer followed by suspension in low-salt buffer and extraction of bound RNA using an RNAEasy Kit (Qiagen, 74104, Hilden, Germany). RNA was quantified by Bioanalyzer 2100 analysis (Agilent, Santa Clara, CA) and like samples combined to provide 10 ng of total RNA total. RNA samples were concentrated to 12 μL using E.Z.N.A. MicroElute

RNA Cleanup Kit (Omega Bio-Tek, R6247, Norcross, GA) and libraries constructed using MLtra II RNA Library Kit (NEB, E7645S) for biological duplicates.

Illumina Hi-Seq. Libraries were submitted to the Duke Sequencing and Genomic Technologies for sequencing. Concentration of each library was estimated using Qubit assay and run on an Agilent Bioanalyzer for library size estimation. Libraries were then pooled into equimolar concentration. Final pool was clustered on a HiSeq 4000 Paired-End flow cell. Sequencing was done at 150bp Paired-End. Bcls files generated by the sequencer were then converted into fastq files using Illumina bcl2fastq v2.20.0.422 and reads demultiplexed using the molecular indexes incorporated during library preparation.

Sequencing Analysis. FASTA files were adapter trimmed using Trimmomatic v0.32 [183], aligned to the human genome, build GRCh38/h38, using HISAT2.0.5 default options for unpaired reads [184]. Aligned read files were then counted using htseq-count v0.5.4p3 [185] using options for non-stranded reads, intersection-strict mode, and 'exon' as the feature to be counted using a UCSC hg38 GTF annotation file. This GTF file with unique gene IDs and transcript IDs was generated to a genePred file for hg38 using the genePredtoGTF script from kentUtils. Data sets from the two cell lines were analyzed for differential expression versus the control experiments using DESeq2v1.18.1 [186]. Gene lists were generated by taking the subset with greater than or equal to 2-fold change over the control data set with an adjusted p-value of 0.05 [187]. Genes coding for protein

products were selected for interaction and GO analysis using the STRING database. Localization predication analysis was performed using the DeepLoc1.0 Profiles algorithm [188]. Transcript per million (TPM) analysis was performed by first calculating reads per kilobase (RPK), summing the RPK values and dividing by 1 million to use as the scaling factor (SF). Individual RPK values were divided by the SF to obtain a gene specific TPM value for the given subset of data for better comparison of the datasets.

4. Selective Recruitment of mRNA to Stress Granules by Specific Transcriptional Responses

4.1 Introduction

The results presented in this chapter are based on initial observations made by Dr. Sujatha Jagannathan. These observations and any resulting publications are performed in collaboration with her.

When the demand on the ER protein folding machinery exceeds its capacity, unfolded proteins accumulate in the lumen of the ER, triggering a conserved stress response pathway mentioned in Chapter 1, the UPR (Figure 2)[189]. The UPR is mediated by three ER transmembrane proteins: ATF6, PERK and IRE1. Upon ER stress, ATF6 is proteolytically processed in the Golgi to yield a transcription factor that induces expression of multiple ER chaperones and quality control proteins to increase the folding capacity of the ER. PERK phosphorylates the translation initiation factor, eIF2α, causing an acute shortage of the functional initiator eIF2–GTP–$tRNA^{Met}$ complex, effectively stopping translation. The dramatic slowdown of protein synthesis allows the ER to deal with the unfolded proteins in its lumen, without adding to the burden. The reduced amount of translation allows a subset of RNAs containing an uORF to translate their full-length proteins. One of these proteins, ATF4, is a transcription factor that induces the expression of ER chaperones and other stress response proteins including CHOP, which promotes apoptosis upon accumulation, and GADD34, the regulatory

subunit of PP1 that dephosphorylates eIF2α-P, creating a negative feedback loop to restore protein synthesis. IRE1, the third branch of the UPR, oligomerizes in response to ER stress, auto-phosphorylates to activate its endonuclease activity. This catalyzes the splicing of XBP1 mRNA (XBP1s) which produces a transcription factor that induces expression of ER chaperones and lipid biosynthesis proteins to facilitate ER expansion. Another function of IRE1 is to promote decay of ER-localized RNAs to additionally reduce the folding load on the ER. Thus, ATF6, PERK and IRE1, together help decrease the folding load on the ER, while also building ER capacity.

A key unanswered question in the field is how the ER achieves the seemingly paradoxical goal of both reducing the protein folding load and yet increasing the folding capacity of the ER – the latter requiring synthesis and folding of new chaperone proteins by the ER. All three major pathways involve a transcriptional response, many of these for transcripts that are traditionally ER localized however, with the absence of general translation and, as a consequence, co-translational localization, it remains to be seen how newly transcribed RNAs are localized during the translational attenuation phase of the UPR. One possibility is the recruitment of these mRNAs to transient cytoplasmic condensates known as SG as a method for protecting or possibly staging these transcripts for translation upon the dephosphorylation of eIF2α.

By visualizing specific classes of mRNAs via single molecule fluorescence *in situ* hybridization (smFISH), the data show that actively transcribed but translationally

attenuated transcripts such as GRP94 localize to granules that share protein components with SG. When transcription is inhibited during DTT exposure, these transcripts are no longer localized to granules that form suggesting only newly transcribed mRNAs are capable of this recruitment. The recruitment to SG allows for concentrated contact with translation initiation factors so a quick rise in translation for these important proteins can occur upon dephosphorylation of eIF2α.

4.2 Results

4.2.1 UPR-induced stress granules show selective recruitment of ER-localized mRNAs

To study the effects of the UPR on localization of mRNAs, DTT was chosen because it is a membrane permeable molecule that acts by reducing the redox potential of the ER lumen thereby preventing re-oxidation of the disulfides in protein disulfide isomerases and disulfide bond formation in SMPs leading to misfolding thus stimulating protein aggregation in the ER. In addition to acting quickly, DTT treatment is reversible which allows us to easily study system recovery by simply replacing media. To determine a suitable time frame for studying the UPR's effects, time course studies were performed on tissue culture cells to determine when translation is attenuated in the cell upon addition of 1mM DTT. First, the phosphorylation state of eIF2α was performed over the course of DTT treatment for 360 minutes by western blot and found it most pronounced from 0.5-2 hours (Figure 15A). Second, [^{35}S]cystine/methionine labeling was

used to ensure eIF2α phosphorylation led to a concurrent attenuation of nascent protein synthesis over the same course of time (Figure 15B). The date demonstrate that these two methods correlated well with each other and provided the optimal treatment time for our studies to be kept between 30-60 minutes of DTT treatment.

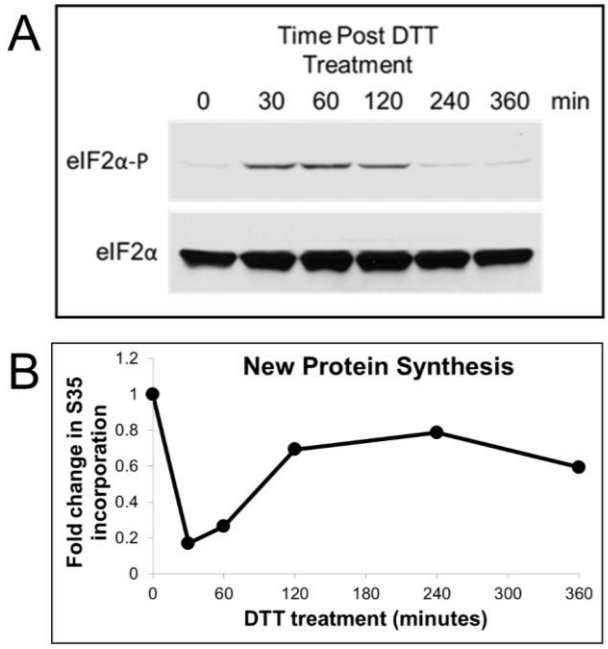

Figure 15: Protein synthesis during 1 mM DTT treatment

A) Monitoring eIF2α phosphorylation (eIF2α-P) during a 360 min time course of 1mM DTT treatment in relation to eIF2 B) Monitoring of [^{35}S]methionine/cysteine incorporation over the same time course as A to determine when protein synthesis was most attenuated. Data from Dr. Sujatha Jagannathan.

To see if mRNA localization is affected upon UPR induction, smFISH was performed using labeled probes that bind to distinct subclasses of mRNAs – cytosolic (GAPDH) and three ER-bound mRNAs: B2M, GRP94 and BiP. It is expected that ER-localized mRNAs would not enter SG, or do so weakly, while the cytosolic mRNA

would be dominantly recruited to SG, as previously shown for studies using oxidative stress[70]. Since both BiP and GRP94 are actively transcribed during the UPR, it was expected that the fraction unable to engage in productive translation may be recruited to SG and thus a portion of the mRNAs would be recruited to these granules as well. Surprisingly, upon stimulation of the UPR with 1 mM DTT for one hour, only GRP94 is recruited to SG while GAPDH, B2M and BiP mRNAs maintained a diffuse localization through the cell (Figure 16).

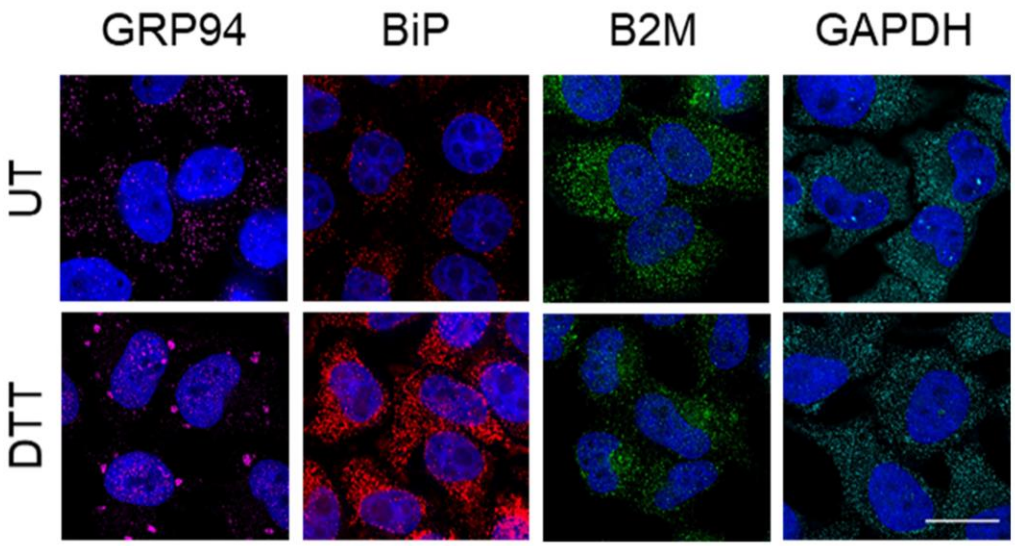

Figure 16: Selective localization of mRNAs to cytoplasmic granules during the UPR.

smFISH micrographs of the indicated mRNAs with (DTT) or without (UT) 1 mM DTT for 120 min. Scale bar = 20 μM. Data from Dr. Sujatha Jagannathan.

To ensure that transient formation of SG had not been missed before the cell reaches a new homeostasis, the localization of B2M and GRP94 mRNA was followed over time during DTT treatment and quantitatively determined that GRP94 SG form and

grow larger over two hours while the distribution of B2M puncta do not change significantly in size (Figure 17). Additionally, these granules were reversible, as they were seen only in the first 2 hours of treatment and not detectable after treatment times of 3 hours indicating they form only during times of limited cap-dependent translation. This finding implicates a protective role of SG formation for GRP94 transcripts during the stress response in a very selective fashion.

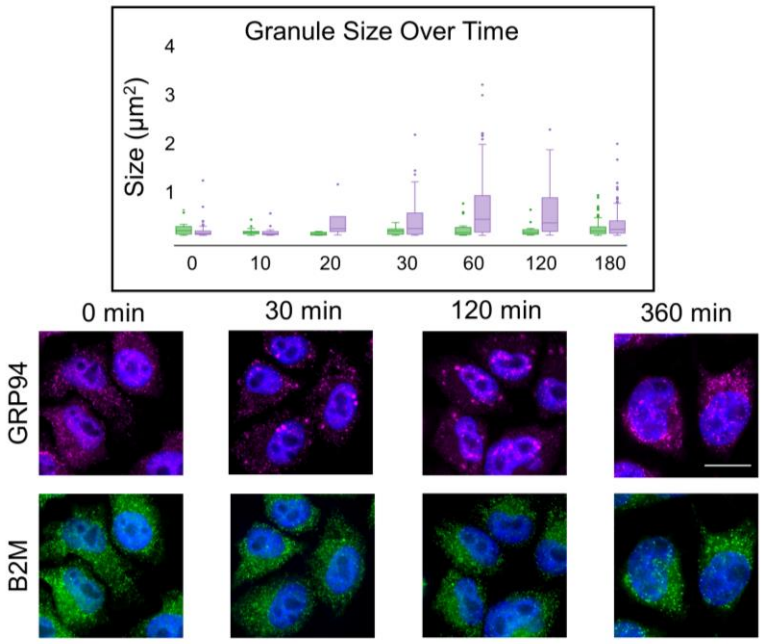

Figure 17: Granules form over the same time as eIF2α-P appearance and are reversible.

A) Quantification of granule size over time during translation attenuation caused by 1 mM DTT treatment. B) smFISH of cells during different time points of 1 mM DTT treatment to 360 min. Scale bar = 20 μM Images from Dr. Sujatha Jagannathan, quantitation by Alyson Hoffman.

Furthermore, to determine the observed granules are bona fide SG, IF-FISH was performed using GRP94 probes with proteins previously determined to be in SG and saw co-localization with canonical SG markers such as HuR, PABP, and Tia1 but not the P-body marker DDX6 (Figure 18)[190]. From these data, it can be concluded that recruitment of mRNAs to SG during the UPR is surprisingly selective and the rules of localization need to be further understoodt.

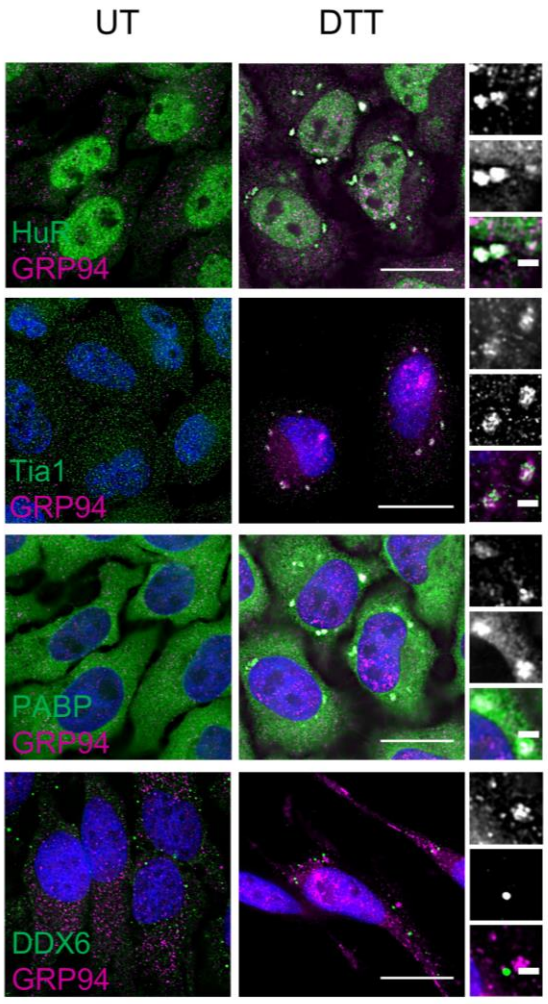

Figure 18: GRP94 mRNA is colocalized with canonical stress granule markers.

HeLa cells were treated for two hours with or without DTT before being analyzed by IF-FISH for the indicated protein markers (green) against the GRP94 transcripts (purple). Scale bar = 20 μM, insets = 2 μM. Images with PABP and DDX6 from Dr. Sujatha Jagannathan, images with HuR and Tia1 from Alyson Hoffman.

4.2.2 Translational status of an mRNA only partially determines recruitment to SG

As actively translated mRNAs are known to escape SG sequestration, the difference in SG recruitment between the three ER localized mRNAs could be explained by their translation status. In fact, it is known that BiP can initiate translation in an eIF2α-independent manner via an IRES element, though no such element is known to be present in the B2M 5′ UTR[191]. To look further into this, cells were treated with DTT for one hour and looked at the distribution of B2M, GRP94 or BiP mRNAs within polysomes. As expected, upon treatment with 1mM DTT there is a breakdown of polysomes to monosome peaks shown in Figure 19A. By performing qPCR for B2M, GRP94 and BiP on the collected fraction from each polysome gradient, the data show that B2M and GRP94 mRNAs shifted away from heavier polysomes (Figure 19B) towards the subunit and free mRNA fractions after DTT treatment (Figure 19C), while BiP mRNAs remained associated with polysomes upon DTT treatment, however, less so than before. Interestingly, there remains a fraction of each transcript pool that remains on polysomes or within the free fraction for GRP94 and BiP respectively (Figure 19C). This implies that although there is an enrichment of free or sequestered mRNAs, neither

is mutually exclusive from the other adding a layer of complexity to the model that may allow us to study both the process of sequestration and process of escape during stress.

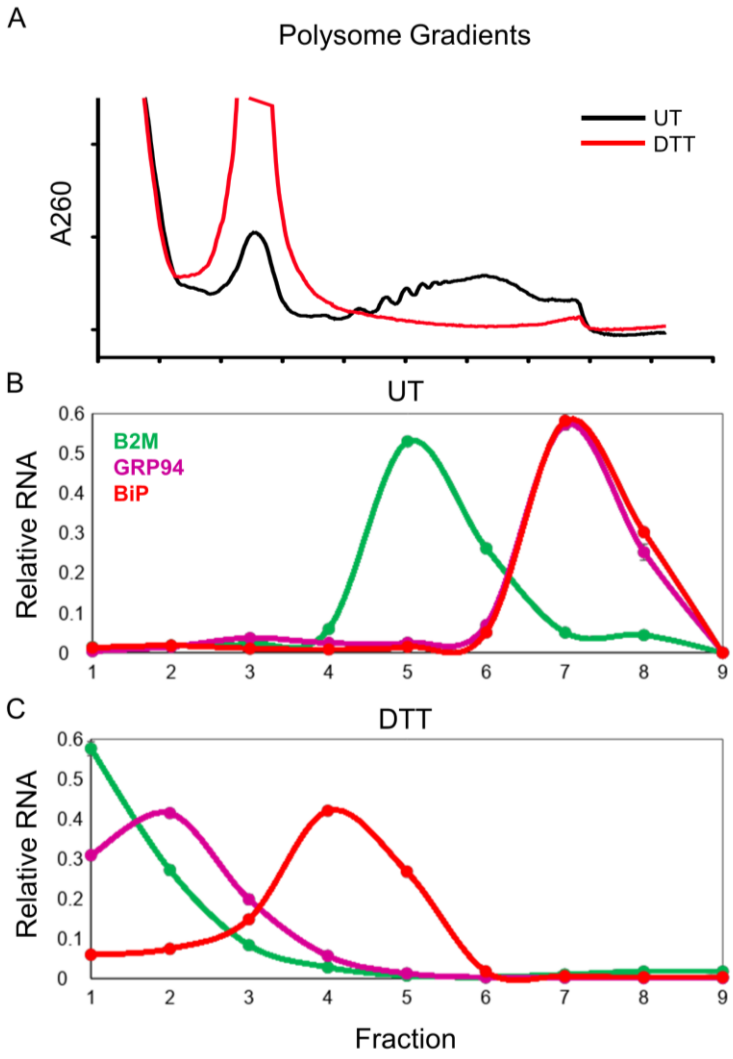

Figure 19: BiP remains polysome associated and thus presents a potential mechanism to escape from SG sequestration.

A) Polysome profile of cells treated or untreated by 1 mM DTT for one hour. B) qPCR of the indicated mRNAs represented as a fraction of 100% of the transcript found in all fractions of the gradient for untreated (UT) cells. C) Same as B but after 1 hr of 1 mM DTT treatment. Data from Dr. Sujatha Jagannathan, plotted by Alyson Hoffman.

4.2.3 Active Transcription Plays a Crucial Role in Recruitment of GRP94 to SG

One crucial difference between B2M and GRP94 is the ER stress element (ERSE) promoter that allows for transcription of GRP94 during the UPR. Genes with an ERSE promoter generally encode for chaperones and proteins that will resolve the burden on the ER lumen and thus would need to be actively translated at some point during the response[192]. However, their translation paradoxically means increased translational and protein folding load on the ER during this stress. Selectively recruiting to and releasing these mRNAs from SG could be a method for attenuating the protein folding load on the ER while allowing for the right concentration of transcript specific translation at the appropriate response time. This is hinted at by the small fraction of GRP94 transcripts that remain in the polysome fraction with BiP transcripts (Figure 19C). It was hypothesized that the nuclear RBP signature on the mRNA from active transcription allows recruitment of specific mRNAs to these granules. To test this, transcription needed to be halted during the UPR, and second, GRP94 transcripts would be monitored to see if there was a difference in granule localization with and without redox stress when a transcriptional response was silenced. The transcriptional inhibitor used for these studies is actinomycin D (ActD). First, it is shown that the ActD concentration used, 10 μM, was sufficient to halt transcription of the specific mRNAs for periods of time similar to DTT treatment as shown in Figure 20A. Cells were pretreated with ActD for 30 minutes before treating with DTT for 1 hour and IF-FISH performed to examine

the effects of transcriptional halting on SG formation. These data confirm our hypothesis, GRP94 mRNA already in the cytosol is not recruited to SG as can be seen in Figure 21B similar to B2M transcripts during DTT treatment (Figure 17). Surprisingly, SG containing HuR still formed indicating a change in the RNA signature of SG upon transcription termination with stress treatment.

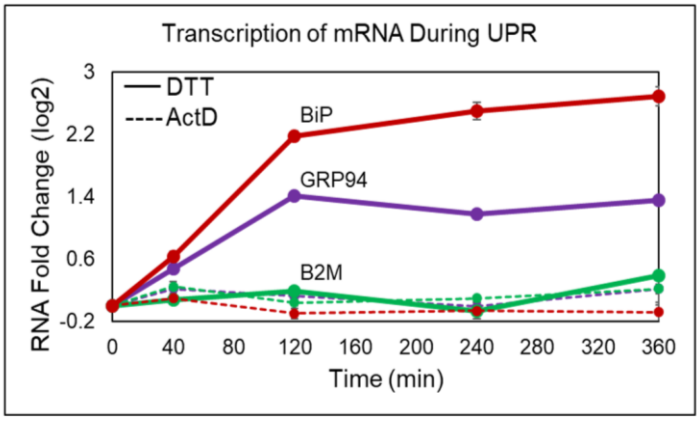

Figure 20: ActD pre-treatment silences transcriptional upregulation of BiP and GRP94 during redox stress.

Line plot of log2 fold change to total RNA calculated from qPCR data from the labeled transcripts. Solid line indicates treatment of cells with 1 mM DTT for the indicated amount of time. Dashed line is the DTT treatment with a pre-treatment of ActD for 30 minutes prior to DTT treatment. Data from Dr. Sujatha Jagannathan.

To control for potential off-target effects of ActD, these experiments were repeated with a second transcriptional inhibitor, 5,6-Dichloro-1-β-D-ribofuranosylbenzimidazole (DRB)[193]. Repeating the IF-FISH experiments replacing 100 μM DRB for ActD, the results are shown to be reproducible (Figure 21**)**. The new working model is one where active transcription plays a role in the recruitment of

nascent transcripts to stress granules, potentially by the nuclear RBP signature that coats them.

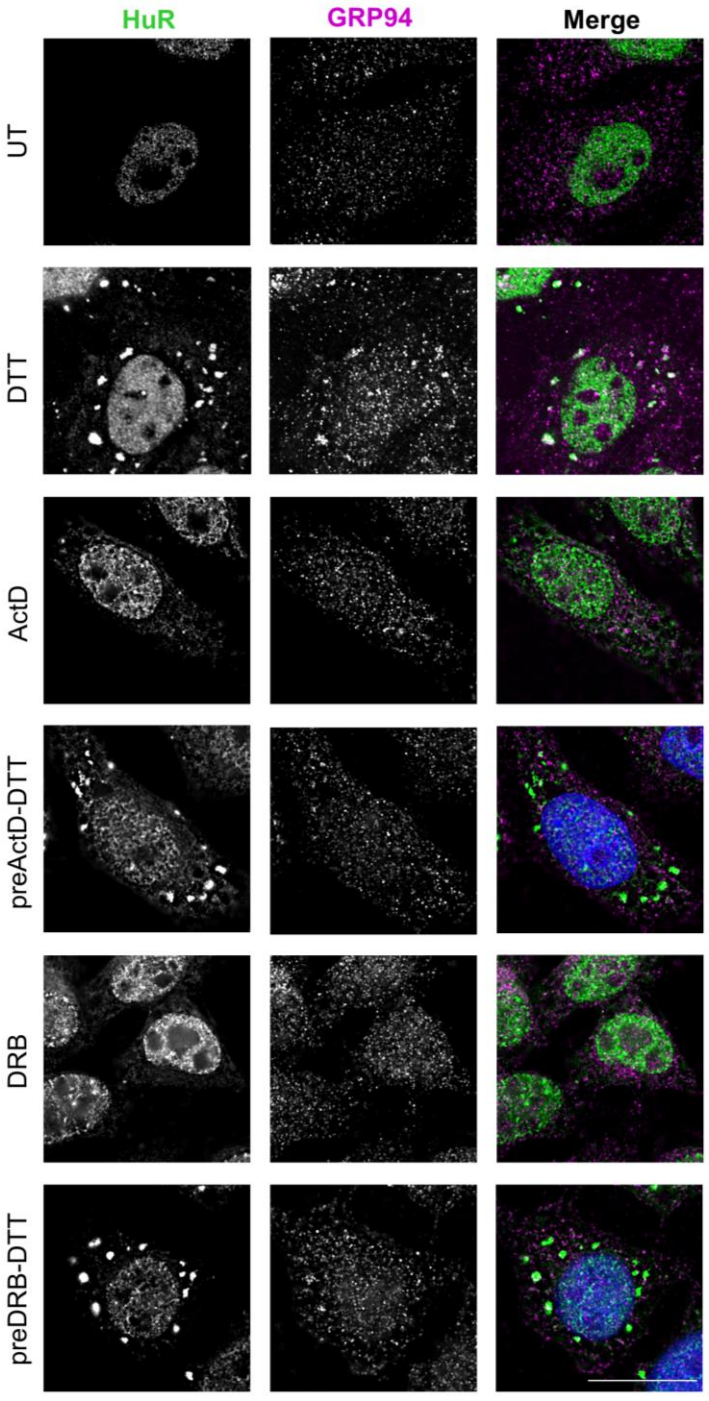

Figure 21: Active transcription of GRP94 is needed for its recruitment to SG during redox stress.

Micrographs showing HuR protein as a stress granule marker and GRP94 mRNA to monitor recruitment to stress granules during 60 min of DTT induced stress with or without a 30 minute pretreatment of a transcriptional inhibitor, ActD or DRB. These transcriptional inhibitors were used on their own to ensure they are not responsible for the formation of any granules seen. Scale bar = 20 μm. Data from Alyson Hoffman.

4.3 Discussion

Our data show that actively transcribed but translationally attenuated transcripts localize to SG upon UPR induction. Initially this was surprising given that previously shown work suggests transcripts with ER localization signals remain upon the ER upon stress induction however, these transcripts may have been localized to the ER prior to stress induction since GRP94 has diffuse signal upon stress in experiments when new transcription has been blocked (Figure 21). Instead, these data support a nuclear RBP coat provides localization to SG for preferentially transcribed transcripts such as ER chaperones. These protein signals would be stripped away following the first round of translation which would explain why previously transcribed mRNAs are immune to recruitment. The exception to this appears to be transcripts harboring an IRES element such as BiP that allows for cap-independent translation, stripping away of the nuclear protein signature, and separation from SG. A schematic depicting the described working model is shown in Figure 22. A similar phenomenon has been shown in yeast during glucose starvation where the promoter a gene was under determined whether it would be localized to SG and translationally inept or diffuse through the cytoplasm and actively translated[94]. While the protein signature that determined these differences in

localization were not studied, they were able to demonstrate, using constructs under engineered promoters, that they could shift the localization of these transcripts solely by changing the promoter they were under. To understand how active transcription might serve as a broad mechanism for transcript recruitment to stress granules, ongoing studies have been planned to look at the specific contributions of transcription factors, ATF6 and XBP1, produced during the UPR that are known to bind to ERSE promoter elements. I am currently using siRNA to known down each transcription factor and test the effect on GRP94 SG recruitment. To test for efficient localization to granules by an increase in transcription activity, I am modifying a method developed in Roy Parker's lab to isolate granules and sequence their contained mRNAs to determine how general this phenomenon is[88].

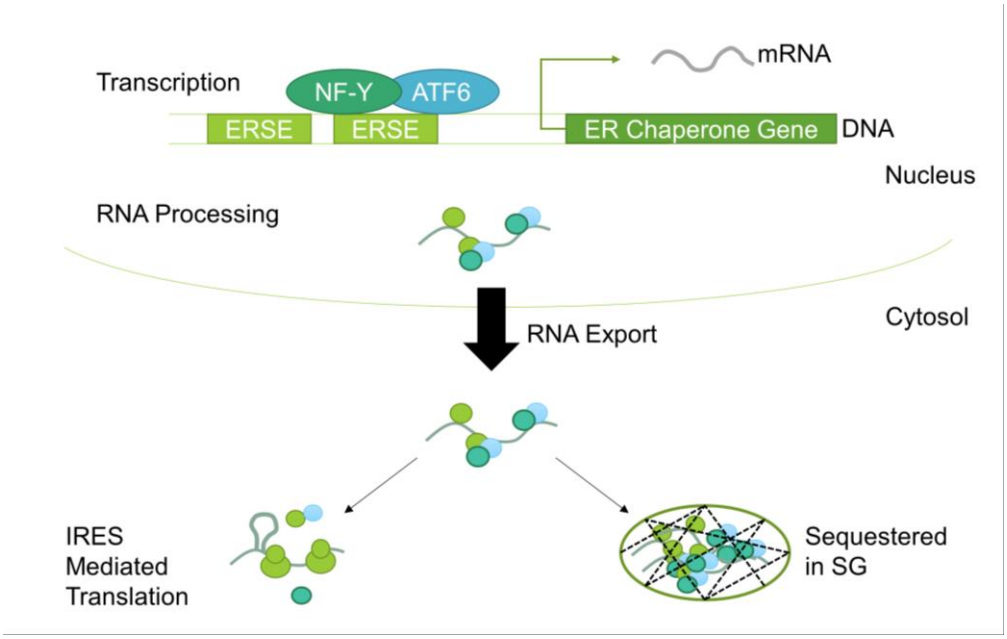

Figure 22: Untranslated RNA-linked sequences dictate specific localization in the cell during the stress response.

4.4 Methods

Cell culture, metabolic labeling and UPR induction. HeLa cellsor HEK 293T cells were maintained at 37ºC and 5% CO2 in Dulbecco's modified Eagle's medium (DMEM; Mediatech), supplemented with 10% fetal bovine serum (FBS; Gibco). For studies on protein synthesis rates, cells were typically labeled for 10 minutes in methionine- and cysteine-free media containing 100μCi/ml of [^{35}S] Met/Cys. Cells were treated with 1mM DTT from 30 minutes to 2 hours as indicated to induce ER stress.

RNA isolation and RT-qPCR. RNA was extracted by the standard acid guanidinium thiocyanate (GT)-phenol-chloroform extraction procedure [179], using GlycoBlue (Ambion) as a carrier to ensure quantitative precipitation of the RNA. The samples were then

treated with Turbo DNAse (Ambion) or DNAseI (NEB) and RNA recovered using RNeasy® mini kit (Qiagen) or by re-extraction in GT: phenol. RNA samples were quantified by UV spectrometry (Nanodrop). Cell-equivalent amounts of RNA were used to synthesize cDNA using M-MLV reverse transcriptase (Promega) or Superscript II (ThermoFisher) and random hexamers as primers (Roche). Quantitative RT-PCR was performed on a 7900HT Sequence Detection System (Applied Biosystems) or on a CFX Connect (BioRad) using Power SYBR® green PCR mastermix (Applied Biosystems) and primers shown below.

GRP94 F: CTGGAAATGAGGAACTAACAGTCA R: TCTTCTCTGGTCATTCCTACACC

BiP F: CAACCAACTGTTACAATCAAGGTC R: CAAAGGTGACTTCAATCTGTGG

B2M F: TTCTGGCCTGGAGGCTATC R: TCAGGAAATTTGACTTTCCATTC

18SrRNA F: CACGGGAAACCTCACCCGGC R: CGGGTGGCTGAACGCCACTT

Protein extraction and immunoblotting: Proteins in cell extracts were concentrated by TCA precipitation. The protein pellets were resuspended in a sample buffer containing 0.5M Tris base and 5% SDS. [S^{35}]-Met/Cys-labeled samples were quantified by scintillation counting. Protein concentrations were determined by BCA assay (Pierce). Either cell-equivalent or equal amounts of protein samples were analyzed by reducing SDS-PAGE. Immunoblotting was conducted by standard protocols using antibodies against HuR (a gift from Jack Keene, Tia1 (Santa-Cruz sc166247, DDX6 (a gift from Debra Silver), PABP (a gift from Debra Silver).

Immunofluorescence (IF). HeLa cell monolayers were fixed in 10% formalin for 10 minutes at room temperature. After blocking with 1% bovine serum albumin (BSA) in PBS, the cells were incubated in a primary antibody solution for 1 hour, extensively washed and incubated in secondary antibody solution for 45 min. Cell monolayers were again washed and the nuclei stained using DAPI. The cells were then mounted in a mounting solution containing 0.4% glucose in PBS, supplemented with glucose oxidase and catalase and imaged on a Deltavision deconvolution microscope.

Single molecule RNA fluorescence in situ hybridization. Single RNA molecules were visualized using Stellaris FISH probes (Cell Search Technologies) as per the manufacturer's instructions. All reagents were made up in DEPC-treated deionized water and standard precautions were taken to prevent RNA degradation. Briefly, HeLa cell monolayers were fixed in 10% formalin in PBS for 10 minutes at room temperature. After three 5-minute washes in PBS, the cells were permeabilized overnight in cold 70% ethanol. The cells were equilibrated in 2X saline-sodium citrate (SSC) buffer and hybridized with fluorescently labeled oligonucleotide probe mixture for 4-12 hours at 37ºC. Excess probes were washed by two 30-minute incubations in 2X SSC containing 10% formamide at 37ºC. The cells were then washed in 2X SSC containing DAPI and equilibrated in GLOX buffer (0.4% glucose in 2X SSC and 1mM Tris HCl, pH 7.4) before mounting in GLOX buffer supplemented with glucose oxidase and catalase. For costaining protein and RNA, cells were first blocked in RNAse-free UltraPure BSA

(Ambion) and proteins immunolabeled with fluorescent antibodies under RNAse-free conditions. The cells were then fixed a second time in ice-cold methanol for 5 min and then smRNA-FISH was performed as described above.

Fluorescence imaging and analysis. All imaging was performed on a Deltavision deconvolution microscope (Applied Precision) equipped with 100x NA 1.4 oil immersion objective (UPlanSApo 100XO; Olympus) and a high-resolution CCD camera (CoolSNAP HQ2; Photometrics). Images were acquired as Z-stacks (at 0.2μm intervals) at identical exposure conditions across the samples for a given protein, RNA or lipid molecule. The data were deconvolved using the SoftWoRx program (Applied Precision) and processed further on ImageJ/FIJI software and Adobe Photoshop (Adobe Systems) to render maximum intensity projections (as required), merge channels and pseudo color the images. Only linear changes were done to the brightness/contrast values of the images, as required, and such changes were applied uniformly across all images in a given experiment. For smRNA-FISH data, the brightness/contrast was adjusted to ensure optimal visibility of the RNA molecules, while not altering the number of molecules in a given sample. The number of RNA molecules per cell was measured using the spot-counting module of the Imaris 7.3 software (Bitplane) with automated thresholding. The mean number of RNA spots/cell was calculated for 10-45 cells in each sample and plotted using GraphPad Prism, with the error bars representing standard error of mean. The final figures were assembled on Adobe Illustrator (Adobe Systems).

ImageJ software was used to determine granule size distributions over time as follows. For the deconvolved image, converge the middle 3 slices to median intensity using the Z-stack function. Select area to analyze by tracing the cell outline (9 cells per time point). Convert the image to 8-bit, set threshold and make the image binary. From the binary image, choose the "Analyze Particles" macro to analyze the particles within the previously traced cell. A cut-off area was chosen at 20 nm3 and the final distributions for each channel and time point plotted by box-blot.

5. Conclusions

In the above three chapters, I presented data in support of higher order organization and mechanisms of recruitment into mesoscale domains within the cell in two contexts. First, using BioID proximity labeling, I have data that support the existence of functional nanodomains on the ER of which I will discuss the implications of these and propose a model of SMP translation within heterogenous translocons. Second, we have observed the behavior of several macromolecules within the context of the UPR and noted both specialized transcripts and proteins that accumulate in SG during translational attenuation within this response. Specifically, the data show a link between transcription and the accumulation of GRP94 mRNAs in SG while other mRNAs, e.g. BiP, do not show this link. These data support the possibility that if the coat of IDR-containing RBPs on newly transcribed mRNAs is retained by lack of translation, these are recruited to stress granules. This is discussed below. There are several other interesting observations that were made, notably the behavior of HuR, which strongly exits the nucleus upon dual PolII and translation inhibition. Possible explanations for this behavior are discussed below.

5.1 Evidence for protein and mRNA microdomains on the ER

BioID protein network analysis of four RAMPs has confirmed known positioning and function of well-studied proteins, ribophorin I and Sec61β, while integrating knowledge about their interactions with understudied proteins, LRRC59 and Sec62. It is

shown that Sec62 is in the vicinity of the translocon without OST machinery and was shown to uniquely interact with proteins involved with redox homeostasis (Figure 9 and Figure 10). This aligns with previous reports of Sec62 being in the smooth ER 50% of the time, not necessarily complexed with the other post-translational translocation protein Sec63, which is present in the ER at an amount 30-40% less than Sec62. Additionally, Sec62 was measured to be in the vicinity of the translocon about 10% of the time[63]. Together, this suggests a function for mammalian Sec62 that varies from the post-translational translocation function assigned to its ortholog in yeast. Indeed, in mammals, there is an additional positively charged region on the N-terminus which is thought to associate with ribosomes although evidence of this is not seen in the BioID studies above[120]. Further work will be performed to affirm these initial observations and uncover the role of Sec62 in redox homeostasis.

Secondly, LRRC59 is vicinal to environments similar to the translocon and OST as depicted in Figure 10 aligning with a potential role in translation. Visible biotin labeling of ribosomes shown in Figure 11 support a role in membrane translation and affirm a role for LRRC59 as a ribosome receptor *in vivo*. To further support its role in mRNA processing and translation, the unique environment around LRRC59 is enriched for RBPs. From screens performed in the Hentze group, LRRC59 is known to be an RBP so this finding is suggestive of a domain with high RNA enrichment either for storage or triage[140]. The latter is supported by the observation that LRRC59 interacts with both

translation machinery and SND1, a micrococcal nuclease associated with miRNA mediated mRNA degradation, and CKAP4, which forms a high MW complex containing Dicer within the ER lumen that is excreted from the cell[12,194]. More work is needed for validating the link between miRNA silencing and this RBP rich interactome of the rough ER. Presumably, these interactions could be mediated by RNA or activity of the micrococcal nuclease, both of which could be tested by an immunoprecipitation with or without RNAse and/or a nuclease inhibitor.

Most surprisingly biotin-labeled polysomes from different protein environments were shown to translate subsets of mRNAs although there were many shared transcripts. Additionally, the entire dataset was highly enriched for mSMPs, more so than an RNA-seq dataset for the total membrane fraction (Figure 14B). This suggests the BioID constructs are labeling highly specific membrane domains further supporting a mesoscale organization of the ER. Surprisingly, mNCPs are associated with Sec61β and LRRC59 RNA-seq datasets although to a lower extent than the enrichment found on the whole membrane. Perhaps a quality control mechanism exists actively sorting these mRNAs away from the translocon which would explain the lower enrichments of mNCPs to these domains.

5.2 Heterogeneous translocons and potential effects on RNA organization

Overall, our findings of mesoscale organization within the ER suggests the organization of secretory and membrane protein mRNAs into RNA-regulons by the existence of heterogeneous translocons[195]. There is evidence in the literature to support this. The first line of evidence is based on the number of RAMPs that have been found implicated in different aspects of protein maturation; at least 33 proteins including those in complexes[196]. If the translocon is the predominant ribosome binding protein, accounting for 60% of the association with the membrane, many of these other proteins likely encounter ribosomes by association with the translocon[121]. In the case of ERdj1 and Sec62/Sec63 complex, ribosome interactions are thought to be transient as they shuttle translating peptides to the translocon only when BiP is bound to their lumenal domains to help with co-translocational protein folding[120,167]. This is similar to the SRP receptor (SR) which transiently binds the ribosome nascent chain complexes bound by SRP while locating them to an empty translocon[197]. Many RAMPs do not actively bind ribosomes but pellet with ribosomes due to tight association with the translocon. By FRET analysis of the translocon with several RAMPs, including TRAP and TRAM these associations do not appear dependent on the status of translation[198]. Additionally, a study of native OST by Blue-Native PAGE showed three predominant molecular weight complexes ranging from 500-700 kDa each with different mechanisms of ribosome release indicating a heterogeneity of the translocon environment[164].

Many of these RAMPs are close to the translocon in order to function as post-translational chaperones for specific subsets of proteins. For instance, the OST is involved in N-glycosylation with different components of this complex involved in the modification efficiency of specific proteins[115]. A different complex, TRAP, chaperones the C-terminal insertion of specific membrane proteins[112]. TRAM, a protein with 7 transmembrane domains, is thought to function early in translocation by associating with proteins containing a specific signal sequence pattern and controls domain specific modification by cytosolic exposure during pausing of transmembrane protein synthesis [113,199]. The signal peptidase complex cleaves soluble signal sequences and is not needed for certain classes of transmembrane domains[200]. The ribosome binding candidate p180 mediates collagen synthesis by binding to and organizing the translation of the mRNAs that produce this complex protein[144]. This is in addition to the transient interactors mentioned above – SR, Sec62 and ERdj1 – and now LRRC59 which appears to associate with mRNAs involved in wound healing and cell adhesion (Figure 14D). Due to many RAMPs having chaperone functions for specific subsets of proteins it is plausible that heterogeneity in translocons exist to better facilitate the synthesis of the entire transcriptome at any given time.

Furthermore, from cryo-EM studies, it is know that accessory complexes are not in translocon proximity 100% of the time. For instance, OST associates with translocons 35-70% of the time depending on the system used[111,117]. In clinical glycosylation diseases

associated with deletion of TRAPγ or TRAPδ, TRAPα and TRAPβ are still in a complex with each other but association with the translocon drops to less than 20% suggesting a translocon independent function for at least two proteins outside of this complex although their association could also be saturated to the number translocons available[117]. In conclusion, the lack of 1:1 stoichiometric association for translocons with different proteins argues for specified sites of translation based on the surrounding protein environment.

As a second line of evidence for organized translation, co-translational assembly of complexes occurs in eukaryotes and bacteria[201–205]. For bacteria, smFISH experiments have shown distinct mRNA localization to either the nucleoid or the inner membrane, depending on the species used, and fluorescent probes have detected the clustering of membrane proteins in a heterogeneous manner[206,207]. Computational modeling of bacterial translation dynamics determined that mRNA localization to the membrane depends on both rates of initiation and translation for short transcripts – faster rates were associated with higher membrane localization – while long transcripts are predicted to be tethered to the membrane regardless of rate[203]. In this model, long polycistronic mRNAs encoding for different membrane proteins could undergo bursts of translation nucleating membrane protein clusters and facilitating the formation of membrane complexes. Eukaryotic organisms do not have many polycistronic mRNAs, however, a report using RNA immunoprecipitations and microarray analysis of 30

randomly selected proteins in yeast has shown association of 1-3 mRNAs encoding for proteins of similar function with 38% of the proteins tested[201]. A second study furthered this observation by using selective ribosome profiling on 12 complexes in yeast. Of these, 9 complexes show co-translational association with at least one of the subunits that are localized to specific interacting domains[202]. When this interaction was disrupted *in vitro*, proteins whose mRNA interacted with fully translated subunits, formed aggregates implying that this process is important for proper complex assembly *in vivo*.

An interesting observation from the work described in Chapter 3 shows that the bait proteins, LRRC59 and Sec61β, label ribosomes translating their own mRNAs. This could be due to ribosome labeling during translation of the BioID reporters, however, translation of the average eukaryotic protein is 2 minutes while the labeling time of BirA* is on the order of hours (Figure 6). Therefore, co-translational ribosome association would not last long enough for robust labeling unless there are multiple rounds of translation of the reporter mRNA lasting for extended periods of time, but even that would presumably be from a fully formed, membrane-integrated reporter. Similarly, on comparison of RNA-seq and proteomics data, not much overlap is found, probably because many of the proteins being translated are destined for locations in the cell away from the endoplasmic reticulum(Figure 14B).

On this last point, intentionally heterogenous translocon protein environments could be a method for sorting mRNAs on the ER membrane. The data generated from

the BioID reporters supports this possibility by i) establishing the existence of stable protein labeling over a time period of hours, ii) identifying unique and shared macromolecular environments around each reporter, and iii) unique enrichments of specific mRNAs on biotin-labeled ribosomes. Speaking to this last point, both datasets share many mRNAs and most encode for secretory and membrane proteins compared to mRNAs found in the whole membrane fraction (Figure 14B). Intriguingly, LRRC59 shows an enrichment for plasma membrane and secreted proteins involved in wound healing. LRRC59 is an oncoprotein involved in metastasis, and a knock-down of this gene in metastatic breast cancer cells reduces migration in a wound healing assay[208]. Thus higher order sorting of mRNAs encoding functionally related proteins may be a mechanism for translational efficiency that could lead to measurable phenotypes in disease models.

5.3 Regulation of mRNA transport to and from stress granules

In experiments described in Chapter 4, the status of ER chaperone mRNAs was monitored by smFISH during initial stages of the UPR. Interestingly, the two chaperone transcripts monitored, BiP and GRP94, exhibited divergent localization patterns upon addition of 1 mM DTT. While BiP was evenly distributed through the cytoplasm, GRP94 was sequestered to SG. BiP has an IRES that allows for cap-independent translation, since transcripts must be free of ribosomes to enter stress granules, this explains its diffuse localization pattern[89]. Indeed, polysome traces during stress show

that BiP remains in a polysome bound state (Figure 19). However, both polysome gradient analysis and smFISH, show that GRP94 exists in two pools, those that are sequestered and those that are free in the cytosol (Figure 19 and Figure 21). By blocking transcription with two different small molecules before inducing stress, GRP94 sequestration to granules is shown to be dependent on active transcription presumably by ERSE-promoter binding transcription factors ATF6 and XBP1. What remains to be seen is precisely how transcription changes the RBP association of GRP94 to induce its inclusion in SG compared to those mRNAs in the cytosol. One hypothesis is that mRNAs encoding for membrane or secreted proteins exhibiting diffuse smFISH patterns during stress have undergone at least one round of translation which would secure the mRNA to the ER by a combination of the SRP pathway and membrane RBPs. RNAs tethered to the ER are resistant to SG recruitment[70]. Those cytosolic mRNAs that remain diffuse, such as GAPDH which is not actively transcribed (Figure 16), remain an enigma but could undergo conformational changes preventing IDR containing proteins from accessing them after the initial round of translation[209]. Whereas, nascent mRNAs bound by nuclear RBPs containing IDRs would be actively contained in SG, potentially even serving as nucleation sites since nuclear shuttling is restricted during the stress response by the concurrent sequestration of importins[210]. HuR, a nuclear RBP, is also found in small cytoplasmic structures during times of homeostasis, potentially nucleating SG when a stress response is stimulated. In a similar vein, two studies using proximity

labeling techniques with known stress granule proteins show the proteome labeled in unstressed cells is almost identical to the proteome seen during stress implying the appearance of SG is due to increased concentration of similar proteins and not necessarily a change in environment[175,211]. Thus mRNAs with an intact nuclear RBP signature compounded by increased concentration in the cytoplasm from impaired nuclear transport could be a defining factor in SG formation.

Another unexpected observation from these studies is the almost complete localization of HuR to the cytosol upon a transcription block during DTT treatment. This effect is not due to the transcription inhibitor alone and so is the response to the combination of both events. HuR is known to become cytosolic during PolII inhibition, and this has an effect on stabilization of transcripts, such as c-fos, normally targeted for ARE-mediated decay by binding of TTP[212,213]. Interestingly, TTP is known to segregate to stress granules but only during proton uncoupling in mitochondria through FCCP treatment[90]. Upon stimulation of oxidative stress through sodium arsenite treatment, TTP is no longer recruited to granules by its phosphorylation and subsequent binding of 14-3-3[90]. Perhaps HuR becomes more prominent in the cytosol by PolII inhibition but then binds more effectively to mRNAs with AU-rich elements unbound by TTP under conditions of oxidative stress. It would be interesting to see if this holds true for stress induction by mechanisms other than oxidative stress such as increase in Ca2+ concentration, blocking N-glycosylation or heat shock. This increase in RNA binding

would increase the local concentration of RBPs and essentially stimulate a phase transition. However, without effective translation or transcription of mRNAs, the release of HuR would be lower perhaps because its function as an mRNA export chaperone is not required. It could be that active binding to mRNAs hides a site for nuclear import since these two functions are localized to the same part of the protein[214]. The specifics for how this could happen needs to be investigated, perhaps by developing a method to interrupt this RNA-protein interface.

5.4 Closing thoughts

Within a single cell, there exists a complex network of biochemical processes that must be regulated in space and time. In eukaryotes, spatial organization of the cell is clearly seen by a microscope through organelles such as the Golgi apparatus, nucleus, mitochondria, ER and various vacuole compartments, all of these bound by a phospholipid bilayer. However, on both sides of these membranes, a myriad of functions occur through the coordination of extensive protein networks. A great example of this is the ER, the cell's largest organelle stretching from the nucleus to the plasma membrane and integral to many cellular functions ranging from drug detoxification to the processing and sorting of one-third of the proteome. Thus the question remains, how does the cell organize its processes around these lipid bilayers in a productive manner? Recent work in super-resolution microscopy under changing cellular conditions has led to the characterization of molecular condensates and the

heterogenous composure of cellular compartments such as the Golgi and ER[28,29,73,215,216]. Fast-tracking single molecule techniques coupled with super-resolution microscopy on the plasma membrane has led to an updated Singer-Nicolson model of mesoscale membrane organization[20,22]. Proximity labeling techniques have led to a better understanding of the key players involved in a myriad of cellular processes within previously hard to isolate structures of the cell[129,131]. With these advances we are now beginning to understand how spatial organization of the cell can lead to neurodegenerative disease, protein complex assembly, and receptor oligomerization and signaling. The work in this dissertation focuses on determining the nanoscale organization of translation on the ER membrane and the reorganization of ER localized macromolecules to the cytoplasm during stress. It was found that i) domain organization of proteins and mRNAs exist on the cytoplasmic face of the rough ER and ii) that specific transcripts coding for ER chaperones specifically relocate to SG during perturbations to the cell's redox state. Together, these findings together support the general emerging field of mesoscale cellular organization. Within the field of membrane bound translation, these findings support other work within the field of client-based translation dictated by the translocon protein environment and provides new methods for interrogating this in the future. Within the field of molecular condensates, our findings support a view of transcript specific recruitment to SG in conjunction with their

active transcription. This is a novel finding and elucidating the mechanisms behind how this occurs is ongoing work in the lab.

Appendix A

List of all proteins associated with each BioID reporter used to make Figure 8, Figure 9, and Figure 10.

LRRC59 Unique				
UniProt_ID	Molecular Weight	Localization	Type	LRRC59-Normalized
ATLA1_HUMAN	64 kDa	Endoplasmic reticulum	Membrane	2.054191
CAMLG_HUMAN	33 kDa	Endoplasmic reticulum	Membrane	7.060908
CKAP4_HUMAN	66 kDa	Nucleus	Soluble	44.26274
DDRGK_HUMAN	36 kDa	Endoplasmic reticulum	Membrane	12.06763
DSC2_HUMAN	100 kDa	Cell membrane	Membrane	2.619541
DSG2_HUMAN	122 kDa	Cell membrane	Membrane	8.141296
FND3A_HUMAN	132 kDa	Cell membrane	Membrane	31.04523
GGT7_HUMAN	70 kDa	Cell membrane	Membrane	2.054191
VIGLN_HUMAN	141 kDa	Cytoplasm	Soluble	3.800551
HNRPK_HUMAN	51 kDa	Nucleus	Soluble	4.516835
INF2_HUMAN	136 kDa	Cytoplasm	Soluble	8.555712
T131L_HUMAN	179 kDa	Cell membrane	Membrane	6.602144
KTN1_HUMAN	156 kDa	Cytoplasm	Membrane	78.32273
LRC59_HUMAN	35 kDa	Endoplasmic reticulum	Membrane	56.06558
LSG1_HUMAN	75 kDa	Cytoplasm	Soluble	27.8663
MDN1_HUMAN	633 kDa	Nucleus	Soluble	3.18489
LYRIC_HUMAN	64 kDa	Cell membrane	Membrane	54.69656
MXRA7_HUMAN	21 kDa	Endoplasmic reticulum	Membrane	3.310668
NSDHL_HUMAN	42 kDa	Endoplasmic reticulum	Membrane	3.850862
RRBP1_HUMAN	152 kDa	Cytoplasm	Soluble	57.80598
RTN3_HUMAN	113 kDa	Endoplasmic reticulum	Membrane	2.054191
SCRB1_HUMAN	61 kDa	Lysosome/Vacuole	Membrane	2.336866

S6A15_HUMAN	82 kDa	Cell membrane	Membrane	7.858622
SND1_HUMAN	102 kDa	Cytoplasm	Soluble	16.66589
SRP54_HUMAN	56 kDa	Cytoplasm	Soluble	4.391057
SRP68_HUMAN	71 kDa	Cytoplasm	Membrane	14.53623
SRP72_HUMAN	75 kDa	Nucleus	Soluble	5.829586
SYNE2_HUMAN	796 kDa	Endoplasmic reticulum	Membrane	21.96721
TAPT1_HUMAN	64 kDa	Endoplasmic reticulum	Membrane	4.391057
TBL2_HUMAN	50 kDa	Nucleus	Soluble	3.18489
TM214_HUMAN	77 kDa	Endoplasmic reticulum	Membrane	6.960286
MACOI_HUMAN	76 kDa	Endoplasmic reticulum	Membrane	19.54295
VDAC2_HUMAN	32 kDa	Mitochondrion	Membrane	2.387177
KAISO_HUMAN	74 kDa	Nucleus	Soluble	2.362021
ZCCHV_HUMAN	101 kDa	Cytoplasm	Soluble	31.05119
Sec62 Unique				
UniProt_ID	Molecular Weight	Localization	Type	SEC62-Normalized
ATF6A_HUMAN	75 kDa	Endoplasmic reticulum	Membrane	2.55273
ATPG_HUMAN	33 kDa	Mitochondrion	Soluble	1.633096
COR1B_HUMAN	54 kDa	Cytoplasm	Soluble	4.709399
DLDH_HUMAN	54 kDa	Mitochondrion	Soluble	1.633096
E41L3_HUMAN	121 kDa	Nucleus	Soluble	3.282476
FLNA_HUMAN	281 kDa	Cytoplasm	Soluble	27.94037
DHE3_HUMAN	61 kDa	Mitochondrion	Soluble	3.076303
HNRPM_HUMAN	78 kDa	Nucleus	Soluble	8.545256
PDIA3_HUMAN	57 kDa	Endoplasmic reticulum	Soluble	4.931855
PRDX4_HUMAN	31 kDa	Endoplasmic reticulum	Soluble	5.0268
SEC62_HUMAN	46 kDa	Endoplasmic reticulum	Membrane	36.5331
Sec61β Unique				
UniProt_ID	Molecular Weight	Localization	Type	SEC61B-Normalized
AAAS_HUMAN	60 kDa	Nucleus	Soluble	0.833828

GCP60_HUMAN	61 kDa	Cytoplasm	Soluble	1.415609
ARFG1_HUMAN	45 kDa	Golgi apparatus	Membrane	0.712638
AT2B1_HUMAN	139 kDa	Cell membrane	Membrane	1.434944
CLMN_HUMAN	112 kDa	Nucleus	Soluble	1.560968
DHR13_HUMAN	41 kDa	Endoplasmic reticulum	Membrane	1.066541
FDFT_HUMAN	48 kDa	Endoplasmic reticulum	Membrane	1.434944
ITPR3_HUMAN	304 kDa	Endoplasmic reticulum	Membrane	5.914138
PCAT2_HUMAN	60 kDa	Endoplasmic reticulum	Membrane	0.712638
MSPD2_HUMAN	60 kDa	Endoplasmic reticulum	Membrane	2.375461
NOTC2_HUMAN	265 kDa	Cell membrane	Membrane	0.833828
NU153_HUMAN	154 kDa	Nucleus	Membrane	8.91005
PMYT1_HUMAN	55 kDa	Cytoplasm	Soluble	1.919704
ACOD_HUMAN	42 kDa	Endoplasmic reticulum	Membrane	1.192564
SCFD1_HUMAN	72 kDa	Cytoplasm	Soluble	0.833828
S61A1_HUMAN	52 kDa	Endoplasmic reticulum	Membrane	0.950184
SC61B_HUMAN	10 kDa	Endoplasmic reticulum	Membrane	6.297388
STX8_HUMAN	27 kDa	Golgi apparatus	Membrane	1.30892
TMX3_HUMAN	52 kDa	Endoplasmic reticulum	Membrane	1.192564
Ribophorin I Unique				
UniProt_ID	Molecular Weight	Localization	Type	RPN1-Normalized
ABCA3_HUMAN	191 kDa	Lysosome/Vacuole	Membrane	1.751422
ANO10_HUMAN	76 kDa	Cell membrane	Membrane	1.415038
ANO6_HUMAN	106 kDa	Cell membrane	Membrane	2.442493
A4_HUMAN	87 kDa	Cell membrane	Membrane	2.877563
BET1_HUMAN	13 kDa	Golgi apparatus	Membrane	1.68563
CLCN7_HUMAN	89 kDa	Lysosome/Vacuole	Membrane	0.775167
CLGN_HUMAN	70 kDa	Endoplasmic reticulum	Membrane	2.702076
CLP1L_HUMAN	62 kDa	Endoplasmic	Membrane	2.003709

		reticulum		
DHRS1_HUMAN	34 kDa	Peroxisome	Membrane	1.415038
DJC16_HUMAN	91 kDa	Endoplasmic reticulum	Membrane	7.715062
ERGI3_HUMAN	43 kDa	Lysosome/Vacuole	Membrane	1.11155
FKBP8_HUMAN	45 kDa	Mitochondrion	Membrane	7.813749
FRAS1_HUMAN	443 kDa	Cell membrane	Membrane	4.22681
FZD6_HUMAN	79 kDa	Cell membrane	Membrane	1.447934
HMDH_HUMAN	97 kDa	Lysosome/Vacuole	Membrane	1.246846
ITPR2_HUMAN	308 kDa	Endoplasmic reticulum	Membrane	2.391293
LMF2_HUMAN	80 kDa	Endoplasmic reticulum	Membrane	2.120701
NBAS_HUMAN	269 kDa	Cytoplasm	Soluble	1.447934
NETO2_HUMAN	59 kDa	Cell membrane	Membrane	1.027455
PIGU_HUMAN	50 kDa	Endoplasmic reticulum	Membrane	3.031164
RPN1_HUMAN	69 kDa	Endoplasmic reticulum	Membrane	101.3676
RPN2_HUMAN	69 kDa	Endoplasmic reticulum	Membrane	3.572348
ZNT9_HUMAN	64 kDa	Nucleus	Membrane	1.937918
B3A2_HUMAN	137 kDa	Cell membrane	Membrane	1.440638
SL9A1_HUMAN	91 kDa	Cell membrane	Membrane	0.943359
SOAT1_HUMAN	65 kDa	Endoplasmic reticulum	Membrane	3.360251
SSRA_HUMAN	32 kDa	Endoplasmic reticulum	Membrane	3.075068
STT3A_HUMAN	81 kDa	Endoplasmic reticulum	Membrane	4.607098
STT3B_HUMAN	94 kDa	Endoplasmic reticulum	Membrane	10.15755
SURF4_HUMAN	30 kDa	Endoplasmic reticulum	Membrane	1.11155
TM109_HUMAN	26 kDa	Endoplasmic reticulum	Membrane	1.616126
STING_HUMAN	42 kDa	Endoplasmic reticulum	Membrane	1.279742
TRPM7_HUMAN	213 kDa	Cell membrane	Membrane	1.667326

UB2J1_HUMAN	35 kDa	Endoplasmic reticulum	Membrane	12.76094
WFS1_HUMAN	100 kDa	Cell membrane	Membrane	2.080509

Shared Analysis							
UniProt_ID	Molecular Weight	Localization	Type	Covariance	First	Second	Third
LCAP_HUMAN	117 kDa	Cell membrane	Membrane	127.4835	SEC61B	RPN1	
EMC8_HUMAN	24 kDa	Cytoplasm	Soluble	127.418	LRRC59	SEC61B	
PLD3_HUMAN	55 kDa	Endoplasmic reticulum	Membrane	125.6364	RPN1	SEC61B	
SRPRB_HUMAN	30 kDa	Endoplasmic reticulum	Membrane	123.6475	LRRC59	RPN1	
PTSS1_HUMAN	56 kDa	Endoplasmic reticulum	Membrane	123.6096	LRRC59	SEC61B	
NONO_HUMAN	54 kDa	Nucleus	Soluble	123.298	LRRC59	SEC62	
GORS2_HUMAN	47 kDa	Nucleus	Soluble	122.7882	RPN1	SEC61B	
ACBD5_HUMAN	60 kDa	Peroxisome	Membrane	122.4957	LRRC59	SEC61B	
TMX4_HUMAN	39 kDa	Endoplasmic reticulum	Membrane	122.3877	LRRC59	SEC61B	
RAGP1_HUMAN	64 kDa	Cytoplasm	Soluble	122.0294	LRRC59	SEC61B	
KDIS_HUMAN	197 kDa	Cell membrane	Membrane	121.5446	SEC62	RPN1	
UFL1_HUMAN	90 kDa	Nucleus	Soluble	120.796	LRRC59	SEC62	
OAT_HUMAN	49 kDa	Mitochondrion	Soluble	120.3138	SEC62	SEC61B	
SC6A8_HUMAN	71 kDa	Cell membrane	Membrane	119.072	RPN1	SEC61B	
UBIA1_HUMAN	37 kDa	Lysosome/Vacuole	Membrane	118.2226	RPN1	SEC61B	
NDC1_HUMAN	76 kDa	Endoplasmic reticulum	Membrane	117.6663	SEC61B	RPN1	
TM230_HUMAN	13 kDa	Mitochondrion	Membrane	117.1854	RPN1	SEC61B	

TM209_HUMAN	63 kDa	Endoplasmic reticulum	Membrane	116.7777	RPN1	SEC61B	
UBXN8_HUMAN	31 kDa	Endoplasmic reticulum	Membrane	116.3423	RPN1	SEC61B	
DHRS7_HUMAN	38 kDa	Endoplasmic reticulum	Membrane	116.1533	RPN1	SEC61B	
RAB7A_HUMAN	23 kDa	Cytoplasm	Soluble	116.007	SEC62	SEC61B	
MMGT1_HUMAN	15 kDa	Endoplasmic reticulum	Membrane	115.9312	SEC61B	RPN1	
PGRC1_HUMAN	22 kDa	Endoplasmic reticulum	Membrane	115.8737	SEC61B	RPN1	
EMC7_HUMAN	26 kDa	Endoplasmic reticulum	Membrane	115.8165	RPN1	SEC61B	
SNX19_HUMAN	109 kDa	Endoplasmic reticulum	Membrane	115.4892	RPN1	SEC61B	
GRP78_HUMAN	72 kDa	Endoplasmic reticulum	Soluble	115.479	RPN1	SEC61B	
NPM_HUMAN	33 kDa	Nucleus	Soluble	91.80167	LRRC59	SEC62	SEC61B
NCPR_HUMAN	77 kDa	Endoplasmic reticulum	Membrane	91.54305	SEC61B	LRRC59	RPN1
WLS_HUMAN	62 kDa	Golgi apparatus	Membrane	88.5648	LRRC59	RPN1	SEC61B
CALX_HUMAN	68 kDa	Endoplasmic reticulum	Membrane	87.77246	LRRC59	SEC61B	RPN1
UBP33_HUMAN	107 kDa	Cytoplasm	Soluble	85.98291	LRRC59	SEC61B	RPN1
RBP2_HUMAN	358 kDa	Cytoplasm	Soluble	81.5881	LRRC59	SEC62	SEC61B
TEX2_HUMAN	125 kDa	Endoplasmic reticulum	Membrane	80.99225	SEC62	LRRC59	SEC61B

ESYT2_HUMAN	102 kDa	Endoplasmic reticulum	Membrane	79.79758	LRRC59	SEC62	SEC61B
ACATN_HUMAN	61 kDa	Endoplasmic reticulum	Membrane	78.66311	LRRC59	RPN1	SEC61B
CBPD_HUMAN	153 kDa	Cell membrane	Membrane	77.91285	LRRC59	SEC61B	RPN1
SC22B_HUMAN	25 kDa	Golgi apparatus	Membrane	77.88479	LRRC59	RPN1	SEC61B
SEC63_HUMAN	88 kDa	Endoplasmic reticulum	Membrane	77.02612	LRRC59	SEC61B	SEC62
NU155_HUMAN	155 kDa	Nucleus	Soluble	76.19039	SEC61B	SEC62	LRRC59
TOIP2_HUMAN	51 kDa	Endoplasmic reticulum	Membrane	76.17013	LRRC59	SEC61B	RPN1
CA043_HUMAN	29 kDa	Golgi apparatus	Membrane	73.9542	LRRC59	SEC61B	RPN1
S12A2_HUMAN	131 kDa	Cell membrane	Membrane	72.80736	LRRC59	SEC61B	RPN1
LRIG2_HUMAN	119 kDa	Cell membrane	Membrane	71.79342	LRRC59	SEC61B	RPN1
4F2_HUMAN	68 kDa	Endoplasmic reticulum	Membrane	70.94001	LRRC59	SEC61B	RPN1
MBOA7_HUMAN	53 kDa	Endoplasmic reticulum	Membrane	69.67967	LRRC59	SEC61B	RPN1
AT1A1_HUMAN	113 kDa	Cell membrane	Membrane	69.65447	LRRC59	RPN1	SEC61B
LNP_HUMAN	48 kDa	Endoplasmic reticulum	Membrane	68.91816	LRRC59	RPN1	SEC61B
TX264_HUMAN	34 kDa	Endoplasmic reticulum	Membrane	68.69555	LRRC59	SEC61B	
VEZA_HUMAN	89 kDa	Mitochondrion	Membrane	67.42219	LRRC59	SEC61B	RPN1
RTN4_HUMAN	130 kDa	Endoplasmic reticulum	Membrane	67.40823	SEC62	LRRC59	SEC61B
PREB_HUMAN	45 kDa	Endoplasmic	Membrane	66.91173	LRRC59	SEC61B	SEC62

		reticulum					
STIM2_HUMAN	84 kDa	Endoplasmic reticulum	Membrane	63.85283	LRRC59	SEC62	
CCD47_HUMAN	56 kDa	Endoplasmic reticulum	Membrane	63.50649	LRRC59	SEC61B	SEC62
OSBL8_HUMAN	101 kDa	Endoplasmic reticulum	Membrane	63.42706	LRRC59	SEC62	
TACC1_HUMAN	88 kDa	Cytoplasm	Soluble	61.41415	LRRC59	SEC62	
CK5P3_HUMAN	57 kDa	Cytoplasm	Soluble	60.55665	LRRC59	SEC62	SEC61B
AL3A2_HUMAN	55 kDa	Peroxisome	Membrane	59.01832	LRRC59	SEC62	
DNJC1_HUMAN	64 kDa	Endoplasmic reticulum	Membrane	58.52406	LRRC59	SEC61B	
LBR_HUMAN	71 kDa	Endoplasmic reticulum	Membrane	55.88778	LRRC59	SEC62	SEC61B
MAN1_HUMAN	100 kDa	Nucleus	Membrane	53.66749	LRRC59	SEC61B	
TRI13_HUMAN	47 kDa	Cytoplasm	Soluble	53.38305	SEC61B	LRRC59	SEC62
ANKL2_HUMAN	104 kDa	Endoplasmic reticulum	Membrane	52.7134	LRRC59	SEC62	
COPG2_HUMAN	98 kDa	Nucleus	Soluble	52.44602	LRRC59	SEC62	SEC61B
STBD1_HUMAN	39 kDa	Endoplasmic reticulum	Membrane	51.39241	LRRC59	SEC62	
STIM1_HUMAN	77 kDa	Endoplasmic reticulum	Membrane	51.03579	LRRC59	SEC62	
MPRI_HUMAN	274 kDa	Cell membrane	Membrane	50.10611	LRRC59	SEC62	
JPH1_HUMAN	72 kDa	Cell membrane	Soluble	49.95096	LRRC59	SEC62	SEC61B
PDZD8_HUMAN	129 kDa	Endoplasmic reticulum	Membrane	49.93891			

ACSL3_HUMAN	80 kDa	Endoplasmic reticulum	Membrane	49.86708			
VAPB_HUMAN	27 kDa	Endoplasmic reticulum	Membrane	48.98445			
LAP2B_HUMAN	51 kDa	Nucleus	Soluble	47.31382			
TMEM9_HUMAN	21 kDa	Cell membrane	Membrane	46.23176			
DHCR7_HUMAN	54 kDa	Endoplasmic reticulum	Membrane	45.40611			
WWOX_HUMAN	47 kDa	Cytoplasm	Soluble	44.58871			
LMAN1_HUMAN	58 kDa	Endoplasmic reticulum	Membrane	44.58642			
NSMA3_HUMAN	93 kDa	Endoplasmic reticulum	Membrane	44.09391			
BAP31_HUMAN	28 kDa	Endoplasmic reticulum	Membrane	44.06569			
TOIP1_HUMAN	66 kDa	Nucleus	Membrane	43.11196			
E2AK3_HUMAN	125 kDa	Cell membrane	Membrane	42.81621			
EMD_HUMAN	29 kDa	Endoplasmic reticulum	Membrane	42.11389			
PGRC2_HUMAN	24 kDa	Endoplasmic reticulum	Membrane	41.60882			
VRK2_HUMAN	58 kDa	Cell membrane	Membrane	41.26459			
VAPA_HUMAN	28 kDa	Endoplasmic reticulum	Membrane	40.80098			
STX5_HUMAN	40 kDa	Golgi apparatus	Membrane	40.53806			

Appendix B

RNA-seq DESeq output analysis files corresponding to Figure 12 in the text.

LRRC59 Enriched - Unique								
Gene	baseMean	log2FoldChange	lfcSE	Wald.stat	pvalue	padj	Localization	Type
DNER	21.27	2.82	0.59	4.76	1.97E-06	6.78E-05	Cell membrane	Membrane
CDCP1	23.08	2.18	0.43	5.04	4.59E-07	2.02E-05	Cell membrane	Membrane
PCDH17	57.85	2.00	0.29	6.79	1.14E-11	1.76E-09	Cell membrane	Membrane
TMEM200B	18.00	1.91	0.49	3.90	9.49E-05	1.53E-03	Cell membrane	Membrane
HTR3A	11.23	1.90	0.64	2.96	3.11E-03	2.05E-02	Cell membrane	Membrane
NALCN	169.65	1.87	0.24	7.84	4.57E-15	1.28E-12	Cell membrane	Membrane
LGR6	20.62	1.80	0.50	3.63	2.82E-04	3.49E-03	Cell membrane	Membrane
GHR	17.19	1.73	0.51	3.43	6.13E-04	6.25E-03	Cell membrane	Membrane
CACNG6	19.72	1.73	0.52	3.32	8.85E-04	8.17E-03	Cell membrane	Membrane
LRRN1	49.31	1.68	0.31	5.38	7.34E-08	4.15E-06	Cell membrane	Membrane
ADRA2C	834.98	1.66	0.18	9.06	1.31E-19	5.83E-17	Cell membrane	Membrane
CD82	17.93	1.66	0.51	3.27	1.07E-03	9.42E-03	Cell membrane	Membrane
CHRM3	16.77	1.60	0.49	3.29	9.91E-04	8.92E-03	Cell membrane	Membrane
PROM1	57.81	1.58	0.33	4.84	1.31E-06	4.87E-05	Cell membrane	Membrane
CLSTN2	92.72	1.50	0.27	5.60	2.09E-08	1.38E-06	Cell membrane	Membrane
SLC24A2	44.91	1.49	0.45	3.31	9.19E-04	8.41E-03	Cell membrane	Membrane
GPR88	29.49	1.46	0.44	3.30	9.50E-04	8.64E-03	Cell membrane	Membrane
SLC7A5	4445.31	1.45	0.21	7.06	1.67E-12	3.04E-10	Cell membrane	Membrane
NTRK2	23.31	1.45	0.48	3.05	2.32E-03	1.65E-02	Cell membrane	Membrane
PRSS8	16.77	1.41	0.54	2.63	8.50E-03	4.21E-02	Cell membrane	Membrane

OSMR	114.03	1.36	0.25	5.48	4.33E-06	2.58E-06	Cell membrane	Membrane
FGFRL1	1713.34	1.35	0.20	6.69	2.19E-11	3.16E-09	Cell membrane	Membrane
MAL2	367.14	1.34	0.27	5.04	4.64E-07	2.04E-05	Cell membrane	Membrane
GFRA1	394.55	1.34	0.21	6.50	8.09E-11	9.69E-09	Cell membrane	Membrane
CNR1	22.51	1.32	0.40	3.27	1.09E-03	9.58E-03	Cell membrane	Membrane
EVA1A	26.06	1.30	0.46	2.85	4.33E-03	2.59E-02	Cell membrane	Membrane
LRP1	1174.20	1.30	0.22	5.91	3.36E-09	2.79E-07	Cell membrane	Membrane
FAM155B	238.07	1.30	0.20	6.52	7.09E-11	8.67E-09	Cell membrane	Membrane
NOTCH2	4346.62	1.29	0.23	5.52	3.48E-08	2.13E-06	Cell membrane	Membrane
SLCO2A1	75.30	1.29	0.29	4.46	8.38E-06	2.22E-04	Cell membrane	Membrane
ADRA2A	39.25	1.29	0.38	3.38	7.28E-04	7.04E-03	Cell membrane	Membrane
EDA	189.99	1.28	0.20	6.29	3.08E-10	3.31E-08	Cell membrane	Membrane
KIT	249.16	1.27	0.28	4.48	7.50E-06	2.03E-04	Cell membrane	Membrane
MMP15	648.30	1.27	0.21	5.95	2.74E-09	2.35E-07	Cell membrane	Membrane
GABBR2	146.18	1.22	0.23	5.26	1.48E-07	7.60E-06	Cell membrane	Membrane
IGF2R	2515.55	1.22	0.22	5.51	3.62E-08	2.20E-06	Cell membrane	Membrane
CDH22	33.29	1.22	0.41	3.01	2.61E-03	1.81E-02	Cell membrane	Membrane
CDH2	1345.88	1.21	0.22	5.55	2.88E-08	1.83E-06	Cell membrane	Membrane
SLCO4C1	71.68	1.19	0.32	3.66	2.53E-04	3.21E-03	Cell membrane	Membrane
PIEZO2	33.33	1.18	0.35	3.35	8.17E-04	7.72E-03	Cell membrane	Membrane
CNTN1	442.94	1.18	0.28	4.19	2.78E-05	5.84E-04	Cell membrane	Membrane
SLC44A3	62.23	1.17	0.30	3.86	1.13E-04	1.77E-03	Cell membrane	Membrane
ADAM9	943.82	1.17	0.22	5.34	9.44E-08	5.13E-06	Cell membrane	Membrane
EPHB2	814.43	1.16	0.21	5.56	2.67E-08	1.72E-06	Cell membrane	Membrane
ITGB5	585.73	1.15	0.23	4.97	6.71E-07	2.76E-05	Cell membrane	Membrane
CD9	766.13	1.15	0.23	4.94	7.83E-07	3.12E-05	Cell membrane	Membrane
NUP210	7410.40	1.15	0.19	6.16	7.08E-10	6.98E-08	Cell membrane	Membrane

FREM2	1178.59	1.14	0.23	4.90	9.58E-07	3.72E-05	Cell membrane	Membrane
FRAS1	1221.82	1.12	0.22	5.01	5.58E-07	2.37E-05	Cell membrane	Membrane
ITM2C	1616.76	1.12	0.21	5.24	1.63E-07	8.22E-06	Cell membrane	Membrane
MOXD1	585.90	1.11	0.21	5.38	7.30E-08	4.15E-06	Cell membrane	Membrane
ERBB3	221.61	1.11	0.22	5.11	3.26E-07	1.48E-05	Cell membrane	Membrane
LAPTM4B	3607.04	1.11	0.25	4.45	8.63E-06	2.27E-04	Cell membrane	Membrane
SLC16A1	3663.44	1.11	0.26	4.26	2.06E-05	4.62E-04	Cell membrane	Membrane
SDC1	717.55	1.10	0.18	6.29	3.17E-10	3.37E-08	Cell membrane	Membrane
SLC1A5	8374.39	1.09	0.22	4.88	1.05E-06	4.00E-05	Cell membrane	Membrane
KCNH2	513.72	1.08	0.23	4.71	2.48E-06	8.24E-05	Cell membrane	Membrane
SLC1A2	46.91	1.08	0.36	2.97	2.97E-03	1.98E-02	Cell membrane	Membrane
KLRG2	40.82	1.08	0.41	2.63	8.44E-03	4.19E-02	Cell membrane	Membrane
HTR7	37.90	1.07	0.34	3.14	1.70E-03	1.32E-02	Cell membrane	Membrane
RAMP1	135.32	1.07	0.25	4.24	2.26E-05	4.99E-04	Cell membrane	Membrane
FAM174A	197.66	1.07	0.26	4.15	3.26E-05	6.65E-04	Cell membrane	Membrane
CHRNA4	80.95	1.07	0.29	3.67	2.43E-04	3.12E-03	Cell membrane	Membrane
SLC18B1	516.93	1.07	0.22	4.92	8.58E-07	3.38E-05	Cell membrane	Membrane
GABRB3	854.10	1.07	0.18	5.81	6.31E-09	5.00E-07	Cell membrane	Membrane
COL23A1	38.69	1.06	0.36	2.93	3.40E-03	2.18E-02	Cell membrane	Membrane
CLSTN3	636.15	1.06	0.19	5.61	2.03E-08	1.35E-06	Cell membrane	Membrane
MCAM	465.39	1.06	0.20	5.27	1.34E-07	7.00E-06	Cell membrane	Membrane
IL27RA	153.89	1.06	0.24	4.35	1.35E-05	3.25E-04	Cell membrane	Membrane
FAM234A	741.35	1.06	0.20	5.40	6.57E-08	3.78E-06	Cell membrane	Membrane
TMBIM1	338.19	1.06	0.19	5.52	3.44E-08	2.12E-06	Cell membrane	Membrane
TMEM132A	1145.47	1.05	0.19	5.57	2.56E-08	1.66E-06	Cell membrane	Membrane
ITGB1	1660.31	1.05	0.22	4.67	3.09E-06	9.73E-05	Cell membrane	Membrane
ITGA6	640.65	1.04	0.22	4.83	1.37E-06	5.04E-05	Cell membrane	Membrane

NOTCH1	1374.93	1.04	0.18	5.71	1.16E-08	8.28E-07	Cell membrane	Membrane
CADM4	582.07	1.04	0.20	5.33	1.01E-07	5.42E-06	Cell membrane	Membrane
TSPAN3	4472.40	1.04	0.21	4.98	6.42E-07	2.68E-05	Cell membrane	Membrane
SLC39A6	1122.15	1.03	0.22	4.73	2.20E-06	7.43E-05	Cell membrane	Membrane
GNAO1	200.70	1.03	0.23	4.49	7.08E-06	1.95E-04	Cell membrane	Membrane
NGFR	63.81	1.03	0.32	3.24	1.18E-03	1.01E-02	Cell membrane	Membrane
MET	1267.11	1.03	0.24	4.21	2.55E-05	5.47E-04	Cell membrane	Membrane
SLC16A2	583.99	1.03	0.21	4.89	1.03E-06	3.94E-05	Cell membrane	Membrane
DSC2	521.06	1.02	0.21	4.84	1.27E-06	4.77E-05	Cell membrane	Membrane
TMEFF1	200.81	1.02	0.24	4.17	3.03E-05	6.25E-04	Cell membrane	Membrane
HPCAL4	43.63	1.01	0.38	2.64	8.35E-03	4.16E-02	Cell membrane	Membrane
MMP17	184.97	1.01	0.27	3.70	2.19E-04	2.88E-03	Cell membrane	Membrane
DSG2	1316.93	1.01	0.22	4.51	6.46E-06	1.82E-04	Cell membrane	Membrane
NEO1	1737.68	1.01	0.21	4.90	9.68E-07	3.74E-05	Cell membrane	Membrane
SLC39A1	1617.85	1.01	0.21	4.84	1.27E-06	4.77E-05	Cell membrane	Membrane
ABCC4	1139.56	1.01	0.23	4.39	1.14E-05	2.83E-04	Cell membrane	Membrane
NPC1L1	33.79	1.01	0.38	2.65	8.05E-03	4.06E-02	Cell membrane	Membrane
SGCE	451.47	1.00	0.22	4.50	6.94E-06	1.92E-04	Cell membrane	Membrane
SCN3B	74.02	1.00	0.31	3.19	1.44E-03	1.18E-02	Cell membrane	Membrane
DAB1	11.41	2.86	0.68	4.23	2.32E-05	5.08E-04	Cytoplasm	Soluble
COLCA2	24.53	2.52	0.52	4.86	1.17E-06	4.43E-05	Cytoplasm	Soluble
MYH14	1809.72	2.39	0.82	2.92	3.52E-03	2.24E-02	Cytoplasm	Soluble
VAT1L	8.43	2.39	0.74	3.23	1.22E-03	1.04E-02	Cytoplasm	Soluble
EPRS	3404.79	2.25	0.57	3.92	8.94E-05	1.46E-03	Cytoplasm	Soluble
SH2D7	10.07	2.12	0.65	3.26	1.11E-03	9.71E-03	Cytoplasm	Soluble
FAM49A	9.05	2.02	0.72	2.83	4.71E-03	2.74E-02	Cytoplasm	Soluble
NOS1	13.17	1.89	0.60	3.17	1.55E-03	1.24E-02	Cytoplasm	Soluble

DTX1	13.64	1.89	0.63	3.00	2.74E-03	1.87E-02	Cytoplasm	Soluble
PLA2G4A	25.79	1.78	0.52	3.43	5.99E-04	6.15E-03	Cytoplasm	Soluble
S100P	16.41	1.71	0.57	2.98	2.84E-03	1.91E-02	Cytoplasm	Soluble
KTN1	5347.09	1.62	0.28	5.76	8.59E-09	6.41E-07	Cytoplasm	Membrane
CPLX1	189.06	1.57	0.26	6.07	1.27E-09	1.19E-07	Cytoplasm	Soluble
RRBP1	699.46	1.51	0.31	4.96	7.17E-07	2.90E-05	Cytoplasm	Soluble
GSAP	16.96	1.48	0.53	2.81	5.03E-03	2.88E-02	Cytoplasm	Soluble
FNDC1	80.15	1.41	0.28	5.01	5.49E-07	2.35E-05	Cytoplasm	Soluble
PIK3R5	15.25	1.40	0.54	2.58	9.93E-03	4.69E-02	Cytoplasm	Soluble
NCKAP1L	29.17	1.31	0.40	3.25	1.14E-03	9.87E-03	Cytoplasm	Soluble
AK5	32.85	1.28	0.40	3.19	1.41E-03	1.16E-02	Cytoplasm	Soluble
PRKCB	234.08	1.24	0.21	5.83	5.50E-09	4.38E-07	Cytoplasm	Soluble
PRKDC	8172.76	1.23	0.27	4.52	6.21E-06	1.76E-04	Cytoplasm	Soluble
RBP7	42.96	1.21	0.41	2.98	2.85E-03	1.92E-02	Cytoplasm	Soluble
IFI35	26.52	1.21	0.42	2.88	4.04E-03	2.46E-02	Cytoplasm	Soluble
ALOX12B	44.12	1.18	0.34	3.46	5.31E-04	5.64E-03	Cytoplasm	Soluble
PSMB3	233.83	1.13	0.24	4.77	1.87E-06	6.43E-05	Cytoplasm	Soluble
CNN2	706.43	1.12	0.21	5.41	6.24E-08	3.62E-06	Cytoplasm	Soluble
FBXL16	655.30	1.11	0.23	4.79	1.67E-06	5.86E-05	Cytoplasm	Soluble
SLC9A3R2	456.57	1.10	0.21	5.18	2.19E-07	1.06E-05	Cytoplasm	Soluble
TRAPPC1	764.17	1.09	0.19	5.64	1.69E-08	1.14E-06	Cytoplasm	Soluble
PLEKHA4	50.48	1.09	0.41	2.68	7.44E-03	3.83E-02	Cytoplasm	Soluble
BLMH	731.17	1.09	0.20	5.46	4.82E-08	2.86E-06	Cytoplasm	Soluble
CARS	455.78	1.08	0.22	5.00	5.83E-07	2.45E-05	Cytoplasm	Soluble
PITPNA	1094.35	1.08	0.17	6.55	5.90E-11	7.42E-09	Cytoplasm	Soluble
CTBP1	2248.16	1.07	0.17	6.23	4.55E-10	4.71E-08	Cytoplasm	Soluble
SMTNL2	81.95	1.06	0.36	2.93	3.39E-03	2.18E-02	Cytoplasm	Soluble

CAPG	25.62	1.06	0.40	2.65	8.01E-03	4.05E-02	Cytoplasm	Soluble
RIMS3	582.02	1.06	0.20	5.35	8.98E-08	4.92E-06	Cytoplasm	Soluble
S100A11	169.63	1.05	0.22	4.70	2.63E-06	8.65E-05	Cytoplasm	Soluble
ACTR3	577.69	1.05	0.25	4.13	3.58E-05	7.17E-04	Cytoplasm	Soluble
EEF1A2	1276.86	1.04	0.23	4.53	5.83E-06	1.67E-04	Cytoplasm	Soluble
KIF26A	1135.30	1.04	0.20	5.30	1.17E-07	6.15E-06	Cytoplasm	Soluble
NRIP3	63.63	1.03	0.30	3.41	6.48E-04	6.52E-03	Cytoplasm	Soluble
HDAC11	120.08	1.03	0.25	4.20	2.66E-05	5.66E-04	Cytoplasm	Soluble
DAB2	92.88	1.01	0.28	3.55	3.83E-04	4.41E-03	Cytoplasm	Soluble
STK32C	277.88	1.01	0.21	4.72	2.32E-06	7.79E-05	Cytoplasm	Soluble
GIT1	1734.80	1.00	0.19	5.17	2.37E-07	1.14E-05	Cytoplasm	Soluble
KIF1A	4538.75	1.00	0.23	4.30	1.69E-05	3.92E-04	Cytoplasm	Soluble
LRRC59	11614.02	4.30	0.20	21.62	########	1.02E-99	Endoplasmic reticulum	Membrane
CYP4F22	9.70	2.61	0.74	3.54	4.06E-04	4.61E-03	Endoplasmic reticulum	Membrane
LAMB3	12.84	1.53	0.58	2.65	8.07E-03	4.07E-02	Endoplasmic reticulum	Soluble
NAT8L	1943.33	1.52	0.18	8.41	4.11E-17	1.45E-14	Endoplasmic reticulum	Membrane
TMEM129	1904.93	1.32	0.17	7.59	3.27E-14	8.00E-12	Endoplasmic reticulum	Membrane
CYP51A1	243.65	1.31	0.26	5.10	3.37E-07	1.53E-05	Endoplasmic reticulum	Membrane
FA2H	58.03	1.29	0.32	4.04	5.43E-05	9.91E-04	Endoplasmic reticulum	Membrane
EMC7	592.97	1.25	0.21	6.05	1.48E-09	1.35E-07	Endoplasmic	Membrane

							reticulum	
ZMPSTE24	1005.00	1.23	0.24	5.11	3.20E-07	1.47E-05	Endoplasmic reticulum	Membrane
STT3A	2394.60	1.21	0.27	4.54	5.64E-06	1.63E-04	Endoplasmic reticulum	Membrane
HYOU1	1852.87	1.21	0.21	5.86	4.69E-09	3.82E-07	Endoplasmic reticulum	Soluble
TMEM109	1017.44	1.19	0.22	5.37	8.04E-08	4.48E-06	Endoplasmic reticulum	Membrane
LAMB1	4293.91	1.16	0.21	5.54	3.06E-08	1.92E-06	Endoplasmic reticulum	Soluble
SMIM1	60.21	1.16	0.45	2.60	9.42E-03	4.52E-02	Endoplasmic reticulum	Membrane
TMEM38A	226.52	1.14	0.20	5.69	1.27E-08	9.00E-07	Endoplasmic reticulum	Membrane
GANAB	6242.86	1.13	0.19	5.85	4.87E-09	3.93E-07	Endoplasmic reticulum	Soluble
DHRS7B	311.11	1.12	0.22	5.05	4.48E-07	1.98E-05	Endoplasmic reticulum	Membrane
RNFT2	533.62	1.12	0.23	4.80	1.59E-06	5.66E-05	Endoplasmic reticulum	Membrane
PDIA3	1134.45	1.11	0.23	4.89	1.03E-06	3.95E-05	Endoplasmic reticulum	Soluble
ATP6AP2	963.56	1.10	0.25	4.49	7.19E-06	1.96E-04	Endoplasmic reticulum	Membrane
GPAT3	168.15	1.10	0.29	3.82	1.32E-04	1.98E-03	Endoplasmic reticulum	Membrane

PTDSS1	2042.91	1.10	0.20	5.38	7.50E-08	4.23E-06	Endoplasmic reticulum	Membrane
UGGT1	1606.05	1.10	0.22	5.02	5.19E-07	2.23E-05	Endoplasmic reticulum	Soluble
PLPP7	42.78	1.09	0.33	3.35	8.16E-04	7.71E-03	Endoplasmic reticulum	Membrane
FADS2	1681.20	1.09	0.24	4.54	5.56E-06	1.61E-04	Endoplasmic reticulum	Membrane
DEGS2	95.61	1.08	0.26	4.10	4.10E-05	7.98E-04	Endoplasmic reticulum	Membrane
PDIA6	1550.67	1.08	0.24	4.51	6.46E-06	1.82E-04	Endoplasmic reticulum	Soluble
SCD	6442.97	1.06	0.22	4.83	1.36E-06	5.03E-05	Endoplasmic reticulum	Membrane
UBAC2	900.41	1.05	0.20	5.34	9.47E-08	5.13E-06	Endoplasmic reticulum	Membrane
SERINC1	1151.44	1.05	0.29	3.67	2.44E-04	3.13E-03	Endoplasmic reticulum	Membrane
PCYOX1	973.67	1.05	0.24	4.33	1.52E-05	3.61E-04	Endoplasmic reticulum	Soluble
CYP2S1	121.92	1.05	0.25	4.17	2.99E-05	6.20E-04	Endoplasmic reticulum	Membrane
FOXRED2	2498.60	1.05	0.18	5.85	4.78E-09	3.88E-07	Endoplasmic reticulum	Soluble
LRPAP1	1954.49	1.04	0.18	5.68	1.36E-08	9.57E-07	Endoplasmic reticulum	Soluble
PLD3	4097.56	1.04	0.20	5.21	1.89E-07	9.35E-06	Endoplasmic	Membrane

							reticulum	
PIGU	296.38	1.03	0.24	4.38	1.19E-05	2.95E-04	Endoplasmic reticulum	Membrane
P4HA1	490.01	1.03	0.21	4.90	9.35E-07	3.65E-05	Endoplasmic reticulum	Soluble
MT-ND6	168.82	1.02	0.30	3.39	7.07E-04	6.90E-03	Mitochondrion	Membrane
ORMDL3	592.20	1.02	0.17	5.93	3.01E-09	2.54E-07	Endoplasmic reticulum	Membrane
P4HA2	276.85	1.01	0.19	5.26	1.46E-07	7.55E-06	Endoplasmic reticulum	Soluble
MFSD1	159.50	1.01	0.32	3.17	1.52E-03	1.22E-02	Endoplasmic reticulum	Membrane
SERPINE2	550.10	1.01	0.20	4.96	6.99E-07	2.86E-05	Endoplasmic reticulum	Soluble
ATP13A2	2726.33	1.00	0.19	5.36	8.25E-08	4.58E-06	Endoplasmic reticulum	Membrane
MT1F	9.46	1.85	0.69	2.67	7.62E-03	3.90E-02	Extracellular	Soluble
NTF3	30.83	1.83	0.40	4.63	3.61E-06	1.11E-04	Extracellular	Soluble
GDF6	50.54	1.70	0.31	5.52	3.30E-08	2.05E-06	Extracellular	Soluble
TAC1	49.26	1.67	0.33	5.14	2.74E-07	1.29E-05	Extracellular	Soluble
HTRA3	81.39	1.67	0.34	4.96	7.05E-07	2.87E-05	Extracellular	Soluble
FAM150B	12.37	1.66	0.60	2.78	5.37E-03	3.02E-02	Extracellular	Soluble
C4orf48	590.47	1.64	0.26	6.41	1.46E-10	1.67E-08	Extracellular	Soluble
RSPO2	15.17	1.61	0.54	3.00	2.74E-03	1.87E-02	Extracellular	Soluble
EGFLAM	89.74	1.57	0.27	5.79	6.97E-09	5.42E-07	Extracellular	Soluble
FBN2	4401.83	1.55	0.27	5.78	7.30E-09	5.60E-07	Extracellular	Soluble
SVEP1	133.44	1.47	0.25	5.99	2.12E-09	1.87E-07	Extracellular	Soluble

SPINK2	17.96	1.42	0.50	2.83	4.63E-03	2.71E-02	Extracellular	Soluble
LTBP1	836.31	1.39	0.24	5.68	1.37E-08	9.57E-07	Extracellular	Soluble
LPL	136.99	1.38	0.24	5.64	1.66E-08	1.13E-06	Extracellular	Soluble
NID1	3864.34	1.36	0.21	6.61	3.75E-11	5.25E-09	Extracellular	Soluble
FAM163A	25.30	1.35	0.43	3.13	1.77E-03	1.36E-02	Extracellular	Membrane
HMCN1	125.26	1.30	0.25	5.18	2.23E-07	1.08E-05	Extracellular	Soluble
BRINP2	20.53	1.30	0.45	2.85	4.37E-03	2.60E-02	Extracellular	Soluble
SEZ6L2	258.74	1.28	0.25	5.21	1.86E-07	9.22E-06	Extracellular	Soluble
LAMC1	5553.60	1.27	0.21	6.15	7.81E-10	7.49E-08	Extracellular	Soluble
PXDN	1745.24	1.24	0.18	6.85	7.44E-12	1.20E-09	Extracellular	Soluble
APLN	43.44	1.19	0.38	3.12	1.83E-03	1.40E-02	Extracellular	Soluble
QDPR	194.74	1.18	0.22	5.30	1.13E-07	5.98E-06	Extracellular	Soluble
SEMA3F	270.63	1.17	0.21	5.52	3.34E-08	2.07E-06	Extracellular	Soluble
CST3	2704.82	1.17	0.24	4.96	7.07E-07	2.87E-05	Extracellular	Soluble
ADAMTS9	108.71	1.17	0.24	4.79	1.67E-06	5.86E-05	Extracellular	Soluble
HPSE	68.99	1.16	0.31	3.78	1.59E-04	2.27E-03	Extracellular	Soluble
DKK3	33.24	1.16	0.41	2.83	4.63E-03	2.71E-02	Extracellular	Soluble
EDIL3	475.76	1.14	0.27	4.27	1.95E-05	4.41E-04	Extracellular	Soluble
VEGFC	34.29	1.14	0.38	3.02	2.50E-03	1.75E-02	Extracellular	Soluble
SMOC1	706.35	1.12	0.22	5.08	3.82E-07	1.71E-05	Extracellular	Soluble
COL6A1	1488.00	1.12	0.19	6.02	1.75E-09	1.59E-07	Extracellular	Soluble
IFI6	155.71	1.09	0.25	4.41	1.02E-05	2.58E-04	Extracellular	Membrane
PSAP	5132.02	1.08	0.21	5.21	1.86E-07	9.22E-06	Extracellular	Soluble
CPVL	642.87	1.06	0.28	3.81	1.40E-04	2.08E-03	Extracellular	Soluble
PCSK1N	828.80	1.05	0.25	4.25	2.16E-05	4.81E-04	Extracellular	Soluble
CTSZ	774.91	1.05	0.19	5.56	2.72E-08	1.74E-06	Extracellular	Soluble
PROS1	138.75	1.04	0.24	4.31	1.65E-05	3.86E-04	Extracellular	Soluble

TNC	211.71	1.03	0.24	4.24	2.23E-05	4.92E-04	Extracellular	Soluble
PGF	268.04	1.02	0.23	4.37	1.21E-05	2.98E-04	Extracellular	Soluble
DNASE2	616.78	1.01	0.22	4.51	6.39E-06	1.81E-04	Extracellular	Soluble
CRIM1	629.69	1.01	0.18	5.55	2.92E-08	1.85E-06	Extracellular	Soluble
RAB3C	18.01	3.04	0.55	5.57	2.54E-08	1.65E-06	Golgi apparatus	Membrane
RAB32	27.85	2.62	0.42	6.18	6.59E-10	6.54E-08	Golgi apparatus	Membrane
HS3ST5	15.28	2.45	0.55	4.43	9.48E-06	2.45E-04	Golgi apparatus	Membrane
SLC35F3	22.37	1.77	0.45	3.95	7.90E-05	1.33E-03	Golgi apparatus	Membrane
MFSD10	925.72	1.46	0.19	7.61	2.66E-14	7.11E-12	Golgi apparatus	Membrane
CHST2	137.04	1.23	0.22	5.65	1.60E-08	1.09E-06	Golgi apparatus	Membrane
STX8	158.91	1.15	0.27	4.17	3.00E-05	6.21E-04	Golgi apparatus	Membrane
JAKMIP1	62.68	1.13	0.27	4.21	2.52E-05	5.42E-04	Golgi apparatus	Soluble
B4GAT1	1168.93	1.11	0.23	4.84	1.30E-06	4.83E-05	Golgi apparatus	Membrane
SLC35F1	713.65	1.10	0.22	4.94	7.62E-07	3.06E-05	Golgi apparatus	Membrane
WSCD1	970.78	1.10	0.16	7.00	2.51E-12	4.37E-10	Golgi apparatus	Membrane
EXT2	1148.48	1.10	0.22	5.09	3.55E-07	1.60E-05	Golgi apparatus	Membrane
B3GALT5	46.30	1.09	0.34	3.18	1.45E-03	1.19E-02	Golgi apparatus	Membrane
MAN1A1	835.06	1.07	0.23	4.68	2.82E-06	9.08E-05	Golgi apparatus	Membrane
GLG1	2297.32	1.05	0.19	5.57	2.48E-08	1.62E-06	Golgi apparatus	Membrane
WLS	2064.73	1.02	0.24	4.29	1.82E-05	4.17E-04	Golgi apparatus	Membrane
GALNT2	2327.65	1.00	0.20	5.07	4.02E-07	1.79E-05	Golgi apparatus	Membrane
PLBD2	599.83	1.15	0.18	6.38	1.73E-10	1.94E-08	Lysosome/Vacuole	Soluble
TM9SF2	2066.85	1.12	0.25	4.46	8.21E-06	2.18E-04	Lysosome/Vacuole	Membrane
MFSD2B	61.85	1.10	0.29	3.75	1.78E-04	2.46E-03	Lysosome/Vacuole	Membrane
PPT1	1112.77	1.03	0.23	4.38	1.21E-05	2.98E-04	Lysosome/Vacuole	Soluble
MT-CYB	6915.48	1.00	0.29	3.45	5.68E-04	5.91E-03	Mitochondrion	Membrane
AC004556.1	8.17	4.80	1.68	2.86	4.18E-03	2.52E-02	Mitochondrion	Soluble

SUGCT	18.87	1.79	0.47	3.85	1.18E-04	1.83E-03	Mitochondrion	Soluble
LDHD	16.30	1.44	0.55	2.64	8.38E-03	4.17E-02	Mitochondrion	Soluble
CHSY3	260.80	1.23	0.25	4.97	6.65E-07	2.75E-05	Mitochondrion	Membrane
MT-ND3	139.93	1.12	0.29	3.82	1.36E-04	2.03E-03	Mitochondrion	Membrane
GLDC	316.47	1.11	0.33	3.38	7.34E-04	7.07E-03	Mitochondrion	Soluble
IARS2	2166.29	1.10	0.25	4.48	7.52E-06	2.04E-04	Mitochondrion	Soluble
OAT	859.44	1.08	0.25	4.33	1.52E-05	3.61E-04	Mitochondrion	Soluble
SPNS1	65.06	1.02	0.33	3.10	1.93E-03	1.45E-02	Mitochondrion	Membrane
GK	750.92	1.00	0.17	6.06	1.39E-09	1.29E-07	Mitochondrion	Membrane
BAG6	9.60	5.62	1.96	2.87	4.05E-03	2.47E-02	Nucleus	Membrane
PGR	23.63	2.99	0.46	6.52	6.82E-11	8.46E-09	Nucleus	Soluble
DDX39B	13.05	2.32	0.85	2.72	6.58E-03	3.49E-02	Nucleus	Soluble
ZIC1	16.72	2.03	0.50	4.08	4.55E-05	8.67E-04	Nucleus	Soluble
C2CD4B	20.85	1.86	0.48	3.85	1.16E-04	1.81E-03	Nucleus	Soluble
HMX2	10.83	1.60	0.62	2.57	1.02E-02	4.79E-02	Nucleus	Soluble
ETV4	224.58	1.56	0.27	5.85	5.06E-09	4.06E-07	Nucleus	Soluble
PTF1A	20.48	1.56	0.52	2.99	2.84E-03	1.91E-02	Nucleus	Soluble
HMX1	714.04	1.23	0.20	6.10	1.07E-09	1.01E-07	Nucleus	Soluble
FEZ1	224.19	1.23	0.25	4.97	6.83E-07	2.80E-05	Nucleus	Soluble
TMEM98	720.80	1.22	0.20	6.16	7.48E-10	7.21E-08	Nucleus	Soluble
OLIG1	199.11	1.20	0.24	4.90	9.55E-07	3.72E-05	Nucleus	Soluble
HIST2H2AA4	173.09	1.19	0.25	4.87	1.11E-06	4.20E-05	Nucleus	Soluble
MYCN	36.57	1.19	0.41	2.87	4.07E-03	2.48E-02	Nucleus	Soluble
SPAG16	154.86	1.18	0.23	5.17	2.39E-07	1.14E-05	Nucleus	Soluble
FAM131C	135.72	1.16	0.34	3.45	5.57E-04	5.81E-03	Nucleus	Membrane
FBLL1	55.63	1.15	0.29	3.94	8.07E-05	1.35E-03	Nucleus	Soluble
OSTF1	56.08	1.14	0.32	3.58	3.37E-04	4.01E-03	Nucleus	Soluble

PKIB	111.10	1.14	0.28	4.03	5.46E-04	9.94E-04	Nucleus	Soluble
UNCX	86.05	1.13	0.32	3.57	3.51E-04	4.13E-03	Nucleus	Soluble
CITED1	57.90	1.13	0.33	3.46	5.40E-04	5.70E-03	Nucleus	Soluble
PPP2R2C	937.82	1.12	0.17	6.75	1.46E-11	2.21E-09	Nucleus	Soluble
H2BFS	55.94	1.11	0.34	3.25	1.15E-03	9.97E-03	Nucleus	Soluble
SOX3	25.64	1.10	0.42	2.62	8.79E-03	4.31E-02	Nucleus	Membrane
LGALS3	112.13	1.08	0.27	4.05	5.14E-05	9.49E-04	Nucleus	Soluble
WDR1	1435.00	1.07	0.20	5.35	8.71E-08	4.80E-06	Nucleus	Soluble
ELP5	1086.47	1.06	0.20	5.31	1.07E-07	5.66E-06	Nucleus	Soluble
MCMBP	1222.90	1.05	0.22	4.89	1.03E-06	3.94E-05	Nucleus	Soluble
COTL1	1015.68	1.04	0.22	4.84	1.29E-06	4.82E-05	Nucleus	Soluble
CYS1	62.45	1.03	0.35	2.93	3.35E-03	2.16E-02	Nucleus	Soluble
HES7	205.48	1.02	0.25	4.08	4.57E-05	8.69E-04	Nucleus	Soluble
HIST2H3D	569.04	1.01	0.27	3.75	1.80E-04	2.47E-03	Nucleus	Soluble
LRRC59 Enriched - Shared								
Gene	baseMean	log2FoldChange	lfcSE	Wald.stat	pvalue	padj	Localization	Type
NRSN1	19.39	6.40	1.12	5.73	1.01E-08	7.37E-07	Cell membrane	Membrane
OPRK1	9.71	4.64	1.01	4.57	4.81E-06	1.42E-04	Cell membrane	Membrane
AGTR1	8.10	4.53	1.20	3.77	1.61E-04	2.29E-03	Cell membrane	Membrane
PTPRO	18.61	4.45	0.68	6.58	4.79E-11	6.26E-09	Cell membrane	Membrane
SLC4A10	10.08	4.44	0.92	4.80	1.59E-06	5.66E-05	Cell membrane	Membrane
SLC24A3	14.85	4.17	0.78	5.32	1.01E-07	5.42E-06	Cell membrane	Membrane
KCND2	30.52	3.66	0.50	7.27	3.57E-13	7.54E-11	Cell membrane	Membrane
LSAMP	41.96	3.52	0.53	6.58	4.58E-11	6.08E-09	Cell membrane	Membrane
EPHA6	109.27	3.50	0.35	10.12	4.55E-24	2.84E-21	Cell membrane	Membrane
GABRA5	69.03	3.47	0.35	9.95	2.53E-23	1.47E-20	Cell membrane	Membrane
PTPRZ1	49.97	3.46	0.41	8.45	3.01E-17	1.08E-14	Cell membrane	Membrane

ANO4	20.86	3.30	0.57	5.75	8.91E-09	6.59E-07	Cell membrane	Membrane
SLC7A3	57.84	3.01	0.44	6.86	6.91E-12	1.12E-09	Cell membrane	Membrane
KCNJ3	25.21	3.00	0.50	6.05	1.44E-09	1.33E-07	Cell membrane	Membrane
ASTN1	385.18	2.94	0.20	14.42	3.78E-47	1.06E-43	Cell membrane	Membrane
TMEFF2	22.40	2.91	0.51	5.70	1.20E-08	8.53E-07	Cell membrane	Membrane
ALPL	31.56	2.88	0.47	6.15	7.98E-10	7.60E-08	Cell membrane	Membrane
CCKBR	24.56	2.86	0.50	5.73	1.01E-08	7.37E-07	Cell membrane	Membrane
C2CD2	26.25	2.84	0.45	6.33	2.44E-10	2.69E-08	Cell membrane	Membrane
NPR1	26.16	2.74	0.48	5.72	1.06E-08	7.64E-07	Cell membrane	Membrane
SYT1	23.37	2.68	0.59	4.54	5.72E-06	1.64E-04	Cell membrane	Membrane
ATP2B3	157.82	2.68	0.29	9.24	2.49E-20	1.17E-17	Cell membrane	Membrane
PTGFR	8.09	2.54	0.91	2.79	5.23E-03	2.97E-02	Cell membrane	Membrane
RAC2	18.91	2.45	0.58	4.26	2.06E-05	4.62E-04	Cell membrane	Membrane
SLITRK3	25.40	2.45	0.52	4.70	2.63E-06	8.65E-05	Cell membrane	Membrane
SLC16A7	54.60	2.42	0.32	7.55	4.38E-14	1.03E-11	Cell membrane	Membrane
CD6	8.30	2.31	0.75	3.07	2.14E-03	1.57E-02	Cell membrane	Membrane
HTR6	111.22	2.30	0.29	7.91	2.64E-15	7.67E-13	Cell membrane	Membrane
NOTCH3	1429.35	2.22	0.23	9.63	5.92E-22	2.85E-19	Cell membrane	Membrane
PVRL3	59.87	2.17	0.33	6.52	7.09E-11	8.67E-09	Cell membrane	Membrane
SSPN	25.24	2.16	0.50	4.35	1.34E-05	3.24E-04	Cell membrane	Membrane
GFRA2	17.89	2.13	0.58	3.65	2.60E-04	3.27E-03	Cell membrane	Membrane
SYNGR4	17.66	2.08	0.51	4.06	5.00E-05	9.30E-04	Cell membrane	Membrane
IL18R1	38.45	2.01	0.36	5.54	3.11E-08	1.94E-06	Cell membrane	Membrane
CLDN7	56.77	2.01	0.30	6.61	3.88E-11	5.32E-09	Cell membrane	Membrane
PLPPR3	402.15	1.96	0.26	7.48	7.60E-14	1.69E-11	Cell membrane	Membrane
ACVR1C	57.15	1.96	0.33	5.92	3.20E-09	2.67E-07	Cell membrane	Membrane
GSG1L	20.25	1.87	0.53	3.52	4.39E-04	4.88E-03	Cell membrane	Membrane

TMEM130	16.15	1.86	0.61	3.03	2.43E-03	1.72E-02	Cell membrane	Membrane
VSTM2B	288.88	1.85	0.28	6.58	4.75E-11	6.26E-09	Cell membrane	Membrane
RAMP2	37.51	1.80	0.36	4.96	7.09E-07	2.88E-05	Cell membrane	Membrane
CXCL16	493.41	1.78	0.21	8.64	5.44E-18	2.13E-15	Cell membrane	Membrane
SCARA5	191.21	1.74	0.23	7.49	6.76E-14	1.52E-11	Cell membrane	Membrane
LRP2	1023.31	1.74	0.25	7.04	1.86E-12	3.27E-10	Cell membrane	Membrane
MFI2	423.67	1.71	0.19	9.03	1.68E-19	7.26E-17	Cell membrane	Membrane
EFNB3	229.43	1.67	0.20	8.25	1.60E-16	5.20E-14	Cell membrane	Membrane
P2RX5	178.14	1.67	0.23	7.17	7.44E-13	1.48E-10	Cell membrane	Membrane
ADCYAP1R1	126.35	1.67	0.24	7.05	1.79E-12	3.21E-10	Cell membrane	Membrane
ADAM12	14.80	1.65	0.63	2.61	8.97E-03	4.38E-02	Cell membrane	Membrane
SUSD4	190.67	1.62	0.23	7.08	1.41E-12	2.64E-10	Cell membrane	Membrane
PCDH10	60.66	1.61	0.35	4.64	3.47E-06	1.07E-04	Cell membrane	Membrane
NSG1	128.55	1.61	0.25	6.51	7.77E-11	9.36E-09	Cell membrane	Membrane
L1CAM	74.07	1.61	0.30	5.30	1.14E-07	6.02E-06	Cell membrane	Membrane
ATP10A	23.50	1.59	0.48	3.29	9.88E-04	8.90E-03	Cell membrane	Membrane
RET	94.37	1.59	0.33	4.80	1.62E-06	5.76E-05	Cell membrane	Membrane
FAM171A2	689.59	1.58	0.21	7.60	3.02E-14	7.72E-12	Cell membrane	Membrane
ATP1B2	143.21	1.57	0.23	6.71	1.92E-11	2.84E-09	Cell membrane	Membrane
IGSF11	19.87	1.55	0.47	3.28	1.05E-03	9.34E-03	Cell membrane	Membrane
SLC9A2	53.40	1.54	0.32	4.80	1.59E-06	5.66E-05	Cell membrane	Membrane
NELL2	931.04	1.53	0.24	6.33	2.45E-10	2.69E-08	Cell membrane	Membrane
MPP2	300.52	1.53	0.23	6.78	1.21E-11	1.85E-09	Cell membrane	Soluble
PTH1R	37.59	1.48	0.39	3.83	1.30E-04	1.97E-03	Cell membrane	Membrane
CDH1	80.57	1.44	0.31	4.70	2.66E-06	8.73E-05	Cell membrane	Membrane
PMP22	233.25	1.44	0.26	5.59	2.26E-08	1.48E-06	Cell membrane	Membrane
ATG9A	1575.92	1.44	0.21	6.75	1.50E-11	2.26E-09	Cell membrane	Membrane

CNTFR	71.43	1.43	0.28	5.10	3.46E-07	1.56E-05	Cell membrane	Membrane
CPD	3639.40	1.41	0.21	6.59	4.38E-11	5.90E-09	Cell membrane	Membrane
COL9A2	55.45	1.41	0.36	3.96	7.50E-05	1.28E-03	Cell membrane	Membrane
RND2	670.12	1.41	0.19	7.21	5.49E-13	1.10E-10	Cell membrane	Membrane
SLC47A1	620.00	1.40	0.21	6.60	4.13E-11	5.63E-09	Cell membrane	Membrane
SLC52A2	566.44	1.36	0.22	6.13	8.62E-10	8.17E-08	Cell membrane	Membrane
TP53I13	1521.10	1.35	0.18	7.36	1.90E-13	4.06E-11	Cell membrane	Membrane
ATP1A3	1311.32	1.35	0.21	6.56	5.32E-11	6.80E-09	Cell membrane	Membrane
ATP1A1	9358.34	1.32	0.24	5.55	2.93E-08	1.85E-06	Cell membrane	Membrane
KCNK6	42.87	1.32	0.34	3.88	1.06E-04	1.69E-03	Cell membrane	Membrane
IGSF8	417.92	1.32	0.23	5.75	8.70E-09	6.47E-07	Cell membrane	Membrane
RASL10B	2147.40	1.30	0.21	6.21	5.47E-10	5.59E-08	Cell membrane	Membrane
SLC7A1	4024.27	1.29	0.22	5.76	8.30E-09	6.25E-07	Cell membrane	Membrane
COL4A2	1366.00	1.29	0.26	5.01	5.52E-07	2.36E-05	Cell membrane	Membrane
NKAIN1	153.07	1.28	0.29	4.47	7.81E-06	2.10E-04	Cell membrane	Membrane
HLA-B	617.38	1.23	0.23	5.42	5.90E-08	3.44E-06	Cell membrane	Membrane
FXYD6	63.86	1.23	0.31	3.91	9.21E-05	1.50E-03	Cell membrane	Membrane
FLOT2	1826.85	1.22	0.20	6.00	2.03E-09	1.82E-07	Cell membrane	Membrane
PTPRU	2061.46	1.22	0.18	6.71	1.95E-11	2.86E-09	Cell membrane	Membrane
PTPRF	5828.35	1.21	0.19	6.30	3.06E-10	3.31E-08	Cell membrane	Membrane
FGFR4	317.76	1.20	0.22	5.51	3.62E-08	2.20E-06	Cell membrane	Membrane
SLC19A1	1938.94	1.19	0.22	5.54	3.07E-08	1.92E-06	Cell membrane	Membrane
SLC38A3	45.80	1.18	0.35	3.41	6.50E-04	6.53E-03	Cell membrane	Membrane
IGF2	104.20	1.18	0.34	3.46	5.50E-04	5.76E-03	Cell membrane	Membrane
AMHR2	54.67	1.14	0.32	3.59	3.29E-04	3.93E-03	Cell membrane	Membrane
SECTM1	29.42	1.13	0.43	2.63	8.44E-03	4.19E-02	Cell membrane	Membrane
JAG2	3598.57	1.08	0.20	5.52	3.48E-08	2.13E-06	Cell membrane	Membrane

ATP12A	30.39	1.04	0.40	2.57	1.03E-02	4.82E-02	Cell membrane	Membrane
TMEM99	211.97	1.02	0.22	4.72	2.36E-06	7.91E-05	Cell membrane	Membrane
ITGA2B	66.60	1.00	0.27	3.68	2.37E-04	3.07E-03	Cell membrane	Membrane
VCL	12257.00	4.68	0.65	7.25	4.05E-13	8.43E-11	Cytoplasm	Soluble
MARS	29536.12	4.65	0.61	7.60	2.86E-14	7.42E-12	Cytoplasm	Soluble
AIMP1	3559.27	4.32	0.57	7.54	4.54E-14	1.05E-11	Cytoplasm	Soluble
RIMS1	8.51	3.83	0.87	4.40	1.08E-05	2.69E-04	Cytoplasm	Soluble
QARS	12490.75	3.35	0.53	6.30	2.90E-10	3.16E-08	Cytoplasm	Soluble
OAS3	48.84	2.92	0.39	7.52	5.52E-14	1.26E-11	Cytoplasm	Soluble
RERG	33.77	2.50	0.39	6.47	9.85E-11	1.15E-08	Cytoplasm	Soluble
MYRIP	43.99	2.50	0.34	7.44	1.00E-13	2.20E-11	Cytoplasm	Soluble
ACTL8	9.10	2.36	0.85	2.77	5.66E-03	3.14E-02	Cytoplasm	Soluble
HSPB1	122.44	1.97	0.28	7.05	1.85E-12	3.27E-10	Cytoplasm	Soluble
GAS7	90.82	1.87	0.30	6.25	4.00E-10	4.19E-08	Cytoplasm	Soluble
HPGD	30.15	1.86	0.40	4.62	3.82E-06	1.17E-04	Cytoplasm	Soluble
RPL39L	106.45	1.72	0.29	5.94	2.89E-09	2.45E-07	Cytoplasm	Soluble
TNS1	27.59	1.52	0.44	3.47	5.28E-04	5.62E-03	Cytoplasm	Soluble
TSTD1	98.96	1.50	0.31	4.91	9.11E-07	3.56E-05	Cytoplasm	Soluble
PNMT	32.00	1.44	0.39	3.71	2.09E-04	2.78E-03	Cytoplasm	Soluble
PALM3	28.99	1.39	0.40	3.44	5.86E-04	6.05E-03	Cytoplasm	Soluble
RLTPR	289.19	1.34	0.23	5.73	9.87E-09	7.27E-07	Cytoplasm	Soluble
FAM101B	1456.77	1.33	0.23	5.77	8.16E-09	6.19E-07	Cytoplasm	Soluble
KIF1C	2877.43	1.33	0.20	6.69	2.17E-11	3.15E-09	Cytoplasm	Soluble
RASGRP2	51.73	1.32	0.41	3.23	1.26E-03	1.07E-02	Cytoplasm	Soluble
DPYSL4	235.86	1.30	0.20	6.59	4.41E-11	5.90E-09	Cytoplasm	Soluble
MYO1D	662.58	1.25	0.25	4.99	6.04E-07	2.53E-05	Cytoplasm	Soluble
SHANK2	154.74	1.19	0.25	4.82	1.43E-06	5.20E-05	Cytoplasm	Soluble

ARHGAP44	364.54	1.18	0.18	6.61	3.77E-11	5.25E-09	Cytoplasm	Soluble
RAB11FIP4	576.59	1.16	0.20	5.95	2.74E-09	2.35E-07	Cytoplasm	Soluble
NLRP1	211.11	1.15	0.21	5.58	2.34E-08	1.53E-06	Cytoplasm	Soluble
SYT16	40.75	1.14	0.36	3.14	1.66E-03	1.30E-02	Cytoplasm	Soluble
GSTP1	476.50	1.12	0.20	5.52	3.30E-08	2.05E-06	Cytoplasm	Soluble
FRMPD3	45.21	1.10	0.36	3.02	2.54E-03	1.77E-02	Cytoplasm	Soluble
NDRG1	2474.35	1.08	0.21	5.13	2.95E-07	1.37E-05	Cytoplasm	Soluble
LLGL1	1568.50	1.04	0.19	5.48	4.30E-08	2.57E-06	Cytoplasm	Soluble
PHYHD1	62.95	1.02	0.31	3.29	1.00E-03	8.99E-03	Cytoplasm	Soluble
DCAKD	627.08	1.02	0.17	5.88	4.20E-09	3.46E-07	Cytoplasm	Soluble
FKBP1C	26.52	1.01	0.39	2.58	9.86E-03	4.66E-02	Cytoplasm	Soluble
UGT3A2	39.92	2.05	0.40	5.17	2.30E-07	1.11E-05	Endoplasmic reticulum	Membrane
GHDC	251.86	1.74	0.22	7.75	9.02E-15	2.49E-12	Endoplasmic reticulum	Membrane
GSN	213.61	1.59	0.33	4.78	1.72E-06	6.01E-05	Endoplasmic reticulum	Soluble
LAMC3	372.39	1.47	0.21	6.91	4.93E-12	8.24E-10	Endoplasmic reticulum	Soluble
DHRS13	265.89	1.46	0.24	6.19	6.11E-10	6.14E-08	Endoplasmic reticulum	Membrane
CYP2J2	56.17	1.40	0.31	4.59	4.52E-06	1.35E-04	Endoplasmic reticulum	Membrane
ATP2A3	115.92	1.37	0.28	4.88	1.05E-06	4.00E-05	Endoplasmic reticulum	Membrane
CYP26B1	257.07	1.37	0.24	5.79	7.15E-09	5.51E-07	Endoplasmic reticulum	Membrane

G6PC3	1166.94	1.25	0.22	5.72	1.06E-08	7.64E-07	Endoplasmic reticulum	Membrane
CERS1	94.27	1.23	0.26	4.69	2.73E-06	8.86E-05	Endoplasmic reticulum	Membrane
FAM134C	1176.53	1.20	0.20	6.02	1.77E-09	1.60E-07	Endoplasmic reticulum	Membrane
PEMT	575.29	1.14	0.20	5.66	1.54E-08	1.06E-06	Endoplasmic reticulum	Membrane
NUCB1	1941.73	1.14	0.19	6.06	1.35E-09	1.26E-07	Endoplasmic reticulum	Soluble
PIGS	2020.70	1.14	0.18	6.34	2.25E-10	2.49E-08	Endoplasmic reticulum	Membrane
CTDNEP1	1193.57	1.10	0.21	5.25	1.49E-07	7.64E-06	Endoplasmic reticulum	Membrane
APLP1	760.35	1.09	0.21	5.24	1.58E-07	8.00E-06	Endoplasmic reticulum	Membrane
TMEM256	213.85	1.08	0.24	4.58	4.73E-06	1.40E-04	Endoplasmic reticulum	Membrane
KIAA0100	4081.07	1.05	0.20	5.19	2.11E-07	1.04E-05	Endoplasmic reticulum	Membrane
ZDHHC24	568.08	1.05	0.21	5.07	4.01E-07	1.79E-05	Endoplasmic reticulum	Membrane
PROCR	333.21	1.01	0.25	4.07	4.67E-05	8.81E-04	Endoplasmic reticulum	Membrane
B3GALT1	42.69	3.70	0.41	9.06	1.28E-19	5.83E-17	Extracellular	Soluble
PDGFD	28.00	3.13	0.48	6.49	8.35E-11	9.85E-09	Extracellular	Soluble
IGSF21	122.09	2.54	0.36	7.14	9.38E-13	1.80E-10	Extracellular	Soluble

IGFBP4	40.53	2.33	0.38	6.16	7.13E-10	7.00E-08	Extracellular	Soluble
CRTAC1	116.04	2.16	0.28	7.59	3.25E-14	8.00E-12	Extracellular	Soluble
HTRA1	254.14	2.08	0.27	7.72	1.13E-14	3.09E-12	Extracellular	Soluble
SFRP1	652.53	1.99	0.20	9.85	6.84E-23	3.72E-20	Extracellular	Soluble
SERPINF1	309.75	1.96	0.23	8.54	1.33E-17	4.89E-15	Extracellular	Soluble
LAMA1	931.50	1.94	0.23	8.39	4.98E-17	1.71E-14	Extracellular	Soluble
BCHE	48.64	1.90	0.40	4.70	2.66E-06	8.73E-05	Extracellular	Soluble
APOC1	91.14	1.88	0.33	5.63	1.85E-08	1.24E-06	Extracellular	Soluble
GRN	1491.03	1.84	0.24	7.57	3.79E-14	9.01E-12	Extracellular	Soluble
CR2	96.70	1.81	0.26	6.91	4.82E-12	8.14E-10	Extracellular	Soluble
CILP2	234.35	1.80	0.26	6.86	6.65E-12	1.09E-09	Extracellular	Soluble
SFRP5	121.69	1.76	0.30	5.86	4.57E-09	3.75E-07	Extracellular	Soluble
LGI3	43.10	1.73	0.39	4.46	8.14E-06	2.17E-04	Extracellular	Soluble
STC1	30.66	1.72	0.42	4.14	3.51E-05	7.05E-04	Extracellular	Soluble
CBLN1	17.35	1.69	0.51	3.28	1.05E-03	9.33E-03	Extracellular	Soluble
FSIP2	20.75	1.66	0.52	3.19	1.41E-03	1.16E-02	Extracellular	Soluble
SPOCK1	79.83	1.65	0.33	4.94	7.89E-07	3.14E-05	Extracellular	Soluble
EGFL7	996.29	1.64	0.23	7.07	1.50E-12	2.79E-10	Extracellular	Soluble
SERPINI1	25.13	1.60	0.42	3.78	1.59E-04	2.27E-03	Extracellular	Soluble
NTN1	1175.47	1.56	0.21	7.61	2.73E-14	7.19E-12	Extracellular	Soluble
COL21A1	88.71	1.55	0.32	4.81	1.51E-06	5.42E-05	Extracellular	Soluble
FAM19A5	231.12	1.48	0.24	6.16	7.35E-10	7.13E-08	Extracellular	Soluble
C1QL1	409.03	1.47	0.26	5.67	1.41E-08	9.86E-07	Extracellular	Soluble
HSPG2	1731.60	1.45	0.23	6.18	6.42E-10	6.41E-08	Extracellular	Soluble
FGF21	27.81	1.44	0.46	3.17	1.52E-03	1.22E-02	Extracellular	Soluble
HHIP	173.71	1.44	0.23	6.20	5.54E-10	5.63E-08	Extracellular	Soluble
FN1	1477.61	1.39	0.20	6.92	4.53E-12	7.73E-10	Extracellular	Soluble

CLPSL2	24.60	1.37	0.42	3.25	1.14E-03	9.93E-03	Extracellular	Soluble
APOE	391.12	1.36	0.27	5.04	4.69E-07	2.05E-05	Extracellular	Soluble
COL4A1	935.83	1.33	0.26	5.00	5.60E-07	2.37E-05	Extracellular	Soluble
MMP2	123.49	1.31	0.24	5.44	5.34E-08	3.13E-06	Extracellular	Soluble
MDK	2494.83	1.27	0.22	5.89	3.97E-09	3.28E-07	Extracellular	Soluble
NXPH4	808.47	1.26	0.22	5.65	1.64E-08	1.12E-06	Extracellular	Soluble
NTN3	121.44	1.25	0.28	4.49	7.13E-06	1.96E-04	Extracellular	Soluble
IGFBP2	1490.75	1.24	0.24	5.24	1.64E-07	8.23E-06	Extracellular	Soluble
FBLN1	939.09	1.21	0.26	4.64	3.53E-06	1.09E-04	Extracellular	Soluble
WNT3A	171.17	1.17	0.28	4.15	3.26E-05	6.65E-04	Extracellular	Soluble
COL2A1	2247.66	1.17	0.24	4.94	7.91E-07	3.14E-05	Extracellular	Soluble
ADAMTS2	482.86	1.11	0.22	5.04	4.74E-07	2.07E-05	Extracellular	Soluble
COL5A2	45.75	1.10	0.33	3.38	7.34E-04	7.07E-03	Extracellular	Soluble
ITIH5	35.13	1.09	0.37	2.93	3.41E-03	2.19E-02	Extracellular	Soluble
VWA1	326.09	1.08	0.23	4.67	3.05E-06	9.66E-05	Extracellular	Soluble
VSTM2L	67.31	1.08	0.34	3.14	1.69E-03	1.32E-02	Extracellular	Soluble
GPX3	213.24	1.07	0.24	4.50	6.76E-06	1.88E-04	Extracellular	Soluble
SPARC	96.63	1.04	0.34	3.02	2.53E-03	1.76E-02	Extracellular	Soluble
CHST9	38.78	3.76	0.46	8.23	1.85E-16	5.89E-14	Golgi apparatus	Membrane
GALNT13	92.74	3.19	0.29	11.05	2.10E-28	2.09E-25	Golgi apparatus	Membrane
PLEKHB1	44.98	1.45	0.35	4.12	3.86E-05	7.59E-04	Golgi apparatus	Membrane
B4GALT1	1040.88	1.15	0.21	5.61	2.06E-08	1.37E-06	Golgi apparatus	Membrane
MGAT3	562.05	1.09	0.19	5.71	1.14E-08	8.18E-07	Golgi apparatus	Membrane
TUSC1	111.20	2.64	0.31	8.57	1.04E-17	3.88E-15	Lysosome/Vacuole	Soluble
MME	77.13	1.80	0.29	6.16	7.24E-10	7.06E-08	Lysosome/Vacuole	Membrane
DPP4	54.02	1.70	0.32	5.27	1.36E-07	7.07E-06	Lysosome/Vacuole	Membrane
PLPP4	81.30	1.54	0.35	4.41	1.01E-05	2.57E-04	Lysosome/Vacuole	Membrane

AQP3	45.18	1.36	0.36	3.77	1.62E-04	2.30E-03	Lysosome/Vacuole	Membrane
CTSD	964.65	1.34	0.23	5.79	7.10E-09	5.49E-07	Lysosome/Vacuole	Soluble
TCIRG1	151.50	1.06	0.24	4.45	8.40E-06	2.22E-04	Lysosome/Vacuole	Membrane
DECR1	22.91	3.76	0.54	6.97	3.20E-12	5.52E-10	Mitochondrion	Membrane
VAT1	1154.00	1.68	0.20	8.28	1.28E-16	4.22E-14	Mitochondrion	Soluble
MT-ND5	5396.02	1.38	0.23	6.05	1.48E-09	1.35E-07	Mitochondrion	Membrane
C1QBP	4271.77	1.31	0.20	6.50	8.28E-11	9.84E-09	Mitochondrion	Soluble
POLDIP2	1606.49	1.29	0.19	6.73	1.68E-11	2.52E-09	Mitochondrion	Soluble
ECHS1	1025.90	1.28	0.20	6.43	1.30E-10	1.50E-08	Mitochondrion	Soluble
MRPL45	42.83	1.28	0.36	3.56	3.68E-04	4.28E-03	Mitochondrion	Soluble
TSPO	224.36	1.24	0.28	4.40	1.08E-05	2.71E-04	Mitochondrion	Membrane
G0S2	25.51	1.22	0.44	2.79	5.29E-03	2.99E-02	Mitochondrion	Membrane
CHCHD10	128.57	1.20	0.28	4.26	2.05E-05	4.59E-04	Mitochondrion	Soluble
CPT1A	288.87	1.15	0.20	5.66	1.51E-08	1.05E-06	Mitochondrion	Membrane
MAP7D2	148.54	5.42	0.32	16.74	6.67E-63	2.82E-59	Nucleus	Soluble
ISL1	19.45	3.00	0.76	3.95	7.67E-05	1.30E-03	Nucleus	Soluble
SLC27A6	52.54	2.78	0.34	8.16	3.33E-16	1.04E-13	Nucleus	Membrane
UTF1	66.74	2.72	0.38	7.17	7.55E-13	1.48E-10	Nucleus	Soluble
HDX	39.45	2.68	0.43	6.25	4.06E-10	4.23E-08	Nucleus	Soluble
NKX6-2	53.09	2.58	0.37	6.90	5.15E-12	8.52E-10	Nucleus	Soluble
PAX1	50.13	2.17	0.35	6.29	3.11E-10	3.32E-08	Nucleus	Soluble
LHX1	10.52	2.15	0.68	3.17	1.51E-03	1.22E-02	Nucleus	Soluble
ZIC3	23.15	2.11	0.48	4.38	1.20E-05	2.95E-04	Nucleus	Soluble
IKZF1	26.93	2.02	0.50	4.03	5.47E-05	9.94E-04	Nucleus	Soluble
ZNF804A	13.25	2.00	0.67	2.97	2.95E-03	1.97E-02	Nucleus	Soluble
PRRX2	9.76	1.95	0.72	2.70	6.86E-03	3.60E-02	Nucleus	Soluble
JUP	766.25	1.61	0.27	5.99	2.11E-09	1.87E-07	Nucleus	Soluble

PPP1R1A	74.84	1.42	0.29	4.91	9.06E-07	3.56E-05	Nucleus	Soluble
HIST1H2AE	347.94	1.42	0.28	5.12	3.13E-07	1.44E-05	Nucleus	Soluble
PSMB6	503.11	1.38	0.20	6.83	8.50E-12	1.34E-09	Nucleus	Soluble
UBE2L6	104.43	1.37	0.31	4.36	1.32E-05	3.19E-04	Nucleus	Soluble
FGD5	18.57	1.34	0.47	2.83	4.62E-03	2.71E-02	Nucleus	Soluble
MYO1C	1456.66	1.28	0.20	6.48	9.35E-11	1.10E-08	Nucleus	Soluble
HIST2H4A	174.62	1.28	0.29	4.46	8.09E-06	2.16E-04	Nucleus	Soluble
PWWP2B	337.75	1.24	0.21	5.81	6.39E-09	5.03E-07	Nucleus	Soluble
THRA	662.33	1.23	0.22	5.72	1.07E-08	7.71E-07	Nucleus	Soluble
HIST2H4B	855.48	1.21	0.23	5.15	2.65E-07	1.26E-05	Nucleus	Soluble
DLGAP3	106.43	1.20	0.26	4.69	2.70E-06	8.82E-05	Nucleus	Soluble
COPRS	514.83	1.17	0.20	5.81	6.41E-09	5.03E-07	Nucleus	Soluble
KDF1	44.28	1.15	0.38	3.05	2.27E-03	1.63E-02	Nucleus	Soluble
HIST2H2AA3	678.44	1.13	0.27	4.17	3.10E-05	6.38E-04	Nucleus	Soluble
ZNF385C	53.42	1.13	0.41	2.80	5.18E-03	2.94E-02	Nucleus	Soluble
COPS3	1024.92	1.12	0.20	5.56	2.72E-08	1.74E-06	Nucleus	Soluble
AKNA	177.02	1.05	0.25	4.14	3.45E-05	6.96E-04	Nucleus	Soluble
RARG	328.68	1.01	0.19	5.38	7.53E-08	4.24E-06	Nucleus	Soluble
SEC61B Enriched - Unique								
Gene	baseMean	log2FoldChange	lfcSE	Wald.stat	pvalue	padj	Localization	Type
SSTR1	10.33	3.13	0.72	4.36	1.28E-05	4.92E-04	Cell membrane	Membrane
TENM1	153.84	1.85	0.20	9.18	4.38E-20	6.72E-17	Cell membrane	Membrane
GRIK3	117.10	1.47	0.27	5.53	3.14E-08	3.55E-06	Cell membrane	Membrane
SLC15A1	38.55	1.46	0.40	3.68	2.34E-04	4.05E-03	Cell membrane	Membrane
AQP4	24.58	1.27	0.47	2.67	7.59E-03	4.70E-02	Cell membrane	Membrane
SLITRK5	571.78	1.24	0.28	4.36	1.33E-05	5.05E-04	Cell membrane	Membrane
KCNN1	100.66	1.20	0.29	4.16	3.15E-05	9.40E-04	Cell membrane	Membrane

IFITM1	87.31	1.17	0.29	4.09	4.27E-05	1.19E-03	Cell membrane	Membrane
ADGRE2	23.56	1.13	0.42	2.68	7.45E-03	4.65E-02	Cell membrane	Membrane
MXRA8	193.54	1.08	0.26	4.13	3.68E-05	1.05E-03	Cell membrane	Membrane
SCARF2	1378.67	1.06	0.21	5.09	3.51E-07	2.78E-05	Cell membrane	Membrane
SPINT1	264.55	1.04	0.24	4.30	1.68E-05	6.10E-04	Cell membrane	Membrane
TTYH2	100.19	1.04	0.28	3.67	2.39E-04	4.12E-03	Cell membrane	Membrane
CACNA1G	116.90	1.04	0.25	4.15	3.37E-05	9.87E-04	Cell membrane	Membrane
ADAM11	619.21	1.03	0.19	5.42	5.81E-08	6.06E-06	Cell membrane	Membrane
KCNQ2	370.84	1.00	0.28	3.65	2.67E-04	4.44E-03	Cell membrane	Membrane
SEC61B	1308.44	3.30	0.27	12.03	2.48E-33	8.36E-30	Endoplasmic reticulum	Membrane
PTGES	21.89	1.37	0.46	3.01	2.62E-03	2.28E-02	Endoplasmic reticulum	Membrane
DIO3	25.13	1.31	0.40	3.23	1.23E-03	1.34E-02	Endoplasmic reticulum	Membrane
PTGIS	33.77	1.09	0.39	2.77	5.52E-03	3.78E-02	Endoplasmic reticulum	Membrane
NBL1	233.03	1.03	0.26	4.02	5.90E-05	1.51E-03	Extracellular	Membrane
FUT1	942.28	1.17	0.33	3.55	3.87E-04	5.78E-03	Golgi apparatus	Membrane
TMEM101	508.02	1.09	0.19	5.75	9.03E-09	1.30E-06	Golgi apparatus	Membrane
ST6GALNAC4	533.84	1.05	0.20	5.18	2.17E-07	1.84E-05	Golgi apparatus	Membrane
ST3GAL4	270.55	1.02	0.22	4.61	4.01E-06	1.96E-04	Golgi apparatus	Membrane
RHBDL3	366.08	1.04	0.19	5.58	2.35E-08	2.79E-06	Lysosome/Vacuole	Membrane
SFXN4	693.17	1.04	0.19	5.60	2.11E-08	2.56E-06	Mitochondrion	Membrane
PLA2G16	89.34	1.03	0.28	3.70	2.19E-04	3.87E-03	Mitochondrion	Membrane
MAFA	130.66	1.19	0.28	4.29	1.79E-05	6.41E-04	Nucleus	Membrane
PLCD3	1222.94	1.00	0.21	4.86	1.19E-06	7.38E-05	Nucleus	Membrane

ESPNL	8.02	2.50	0.73	3.44	5.86E-04	7.85E-03	Cytoplasm	Soluble
STAC2	15.83	1.63	0.54	3.02	2.56E-03	2.24E-02	Cytoplasm	Soluble
SOCS7	24.21	1.48	0.39	3.75	1.75E-04	3.31E-03	Cytoplasm	Soluble
TNK1	45.24	1.41	0.35	4.00	6.29E-05	1.58E-03	Cytoplasm	Soluble
CRIP2	80.32	1.29	0.32	4.00	6.24E-05	1.57E-03	Cytoplasm	Soluble
EPPK1	1137.66	1.27	0.28	4.54	5.57E-06	2.56E-04	Cytoplasm	Soluble
RGCC	42.68	1.19	0.38	3.16	1.58E-03	1.59E-02	Cytoplasm	Soluble
BIN1	57.74	1.19	0.30	3.91	9.09E-05	2.07E-03	Cytoplasm	Soluble
ALDOC	38.16	1.18	0.37	3.15	1.62E-03	1.61E-02	Cytoplasm	Soluble
CDC42BPG	99.02	1.12	0.29	3.88	1.02E-04	2.23E-03	Cytoplasm	Soluble
DUSP9	178.32	1.10	0.21	5.25	1.54E-07	1.40E-05	Cytoplasm	Soluble
PADI2	91.05	1.08	0.28	3.88	1.06E-04	2.29E-03	Cytoplasm	Soluble
ASS1	2323.85	1.07	0.24	4.43	9.61E-06	3.92E-04	Cytoplasm	Soluble
LSM12	62.37	1.05	0.31	3.33	8.70E-04	1.05E-02	Cytoplasm	Soluble
RASAL1	85.86	1.05	0.32	3.25	1.15E-03	1.29E-02	Cytoplasm	Soluble
MYO18A	637.08	1.04	0.33	3.14	1.69E-03	1.67E-02	Cytoplasm	Soluble
NXN	547.72	1.02	0.21	4.75	2.00E-06	1.12E-04	Cytoplasm	Soluble
RASSF4	88.13	1.02	0.27	3.73	1.91E-04	3.49E-03	Cytoplasm	Soluble
EMILIN3	709.03	1.02	0.19	5.39	6.90E-08	7.01E-06	Endoplasmic reticulum	Soluble
BMP2	156.08	3.60	0.25	14.67	9.57E-49	8.08E-45	Extracellular	Soluble
COL3A1	17.46	2.21	0.54	4.06	4.88E-05	1.31E-03	Extracellular	Soluble
ADAMTS4	28.81	1.35	0.42	3.25	1.16E-03	1.29E-02	Extracellular	Soluble
SEMA3G	41.03	1.26	0.34	3.70	2.16E-04	3.83E-03	Extracellular	Soluble
COL18A1	515.68	1.24	0.25	4.96	7.16E-07	4.95E-05	Extracellular	Soluble
LCN15	30.20	1.22	0.41	3.00	2.67E-03	2.31E-02	Extracellular	Soluble
SCUBE3	123.71	1.13	0.23	4.82	1.44E-06	8.55E-05	Extracellular	Soluble

SERPING1	29.03	1.08	0.40	2.72	6.50E-03	4.24E-02	Extracellular	Soluble
THBS4	63.43	1.02	0.28	3.68	2.36E-04	4.07E-03	Extracellular	Soluble
SLIT3	140.81	1.01	0.22	4.49	7.18E-06	3.10E-04	Extracellular	Soluble
CIB2	176.13	1.03	0.27	3.75	1.76E-04	3.31E-03	Lysosome/Vacuole	Soluble
HMGCLL1	31.39	1.07	0.39	2.77	5.62E-03	3.83E-02	Mitochondrion	Soluble
ERAL1	768.24	1.01	0.18	5.61	1.99E-08	2.46E-06	Mitochondrion	Soluble
ZNF738	9.37	3.70	0.82	4.52	6.26E-06	2.81E-04	Nucleus	Soluble
ZCCHC12	234.58	1.42	0.27	5.28	1.28E-07	1.19E-05	Nucleus	Soluble
AHNAK2	402.84	1.25	0.35	3.56	3.65E-04	5.54E-03	Nucleus	Soluble
RIPPLY3	28.73	1.25	0.39	3.21	1.31E-03	1.39E-02	Nucleus	Soluble
NEUROD2	35.64	1.24	0.40	3.11	1.88E-03	1.79E-02	Nucleus	Soluble
NOVA2	232.90	1.06	0.25	4.26	2.02E-05	6.87E-04	Nucleus	Soluble
SEC61B Enriched - Shared								
Gene	baseMean	log2FoldChange	lfcSE	Wald.stat	pvalue	padj	Localization	Type
LSAMP	41.96	4.87	0.51	9.50	2.16E-21	3.64E-18	Cell membrane	Membrane
NRSN1	19.39	4.84	1.13	4.30	1.68E-05	6.10E-04	Cell membrane	Membrane
AGTR1	8.10	4.66	1.19	3.93	8.50E-05	1.97E-03	Cell membrane	Membrane
ISL1	19.45	4.61	0.72	6.41	1.50E-10	3.39E-08	Nucleus	Soluble
OPRK1	9.71	3.72	1.02	3.65	2.61E-04	4.36E-03	Cell membrane	Membrane
PTGFR	8.09	3.68	0.85	4.31	1.66E-05	6.05E-04	Cell membrane	Membrane
SYT1	23.37	3.65	0.56	6.46	1.07E-10	2.57E-08	Cell membrane	Membrane
SLC24A3	14.85	3.46	0.78	4.42	9.98E-06	4.05E-04	Cell membrane	Membrane
KCND2	30.52	3.41	0.50	6.84	7.70E-12	2.36E-09	Cell membrane	Membrane
PTPRO	18.61	3.21	0.68	4.70	2.65E-06	1.40E-04	Cell membrane	Membrane
ALPL	31.56	3.11	0.46	6.81	9.80E-12	2.95E-09	Cell membrane	Membrane
ATP2B3	157.82	3.04	0.29	10.66	1.57E-26	3.79E-23	Cell membrane	Membrane
CHST9	38.78	2.94	0.46	6.43	1.29E-10	3.01E-08	Golgi apparatus	Membrane

HDX	39.45	2.91	0.42	6.98	2.89E-12	9.77E-10	Nucleus	Soluble
MAP7D2	148.54	2.90	0.33	8.68	3.83E-18	4.97E-15	Nucleus	Soluble
ANO4	20.86	2.87	0.57	5.05	4.42E-07	3.39E-05	Cell membrane	Membrane
SLITRK3	25.40	2.86	0.50	5.69	1.31E-08	1.76E-06	Cell membrane	Membrane
SLC4A10	10.08	2.85	0.94	3.02	2.52E-03	2.22E-02	Cell membrane	Membrane
AIMP1	3559.27	2.84	0.57	4.95	7.24E-07	4.99E-05	Cytoplasm	Soluble
VCL	12257.00	2.82	0.65	4.37	1.22E-05	4.75E-04	Cytoplasm	Soluble
PVRL3	59.87	2.81	0.32	8.84	9.69E-19	1.36E-15	Cell membrane	Membrane
EPHA6	109.27	2.76	0.35	7.97	1.58E-15	9.50E-13	Cell membrane	Membrane
GABRA5	69.03	2.69	0.35	7.68	1.55E-14	7.26E-12	Cell membrane	Membrane
NPR1	26.16	2.63	0.47	5.59	2.23E-08	2.69E-06	Cell membrane	Membrane
RAC2	18.91	2.59	0.56	4.62	3.85E-06	1.89E-04	Cell membrane	Membrane
ASTN1	385.18	2.58	0.20	12.68	7.66E-37	3.23E-33	Cell membrane	Membrane
TUSC1	111.20	2.49	0.30	8.17	3.10E-16	2.29E-13	Lysosome/Vacuole	Soluble
TMEFF2	22.40	2.46	0.51	4.87	1.09E-06	6.93E-05	Cell membrane	Membrane
UTF1	66.74	2.42	0.38	6.43	1.30E-10	3.01E-08	Nucleus	Soluble
RIMS1	8.51	2.41	0.89	2.71	6.76E-03	4.37E-02	Cytoplasm	Soluble
ACTL8	9.10	2.41	0.83	2.89	3.84E-03	2.98E-02	Cytoplasm	Soluble
CCKBR	24.56	2.38	0.49	4.81	1.48E-06	8.72E-05	Cell membrane	Membrane
MARS	29536.12	2.38	0.61	3.88	1.03E-04	2.23E-03	Cytoplasm	Soluble
GALNT13	92.74	2.32	0.29	8.01	1.19E-15	7.42E-13	Golgi apparatus	Membrane
PCDH10	60.66	2.30	0.33	6.91	4.77E-12	1.49E-09	Cell membrane	Membrane
BCHE	48.64	2.27	0.39	5.79	6.92E-09	1.01E-06	Extracellular	Soluble
NKX6-2	53.09	2.25	0.37	6.07	1.25E-09	2.32E-07	Nucleus	Soluble
OAS3	48.84	2.22	0.39	5.73	1.02E-08	1.44E-06	Cytoplasm	Soluble
HTRA1	254.14	2.22	0.27	8.30	1.06E-16	9.45E-14	Extracellular	Soluble
PTPRZ1	49.97	2.21	0.41	5.33	9.96E-08	9.71E-06	Cell membrane	Membrane

SSPN	25.24	2.12	0.49	4.36	1.30E-05	4.97E-04	Cell membrane	Membrane
FSIP2	20.75	2.10	0.50	4.23	2.35E-05	7.67E-04	Extracellular	Soluble
IGSF21	122.09	2.09	0.35	5.88	4.00E-09	6.31E-07	Extracellular	Soluble
PDGFD	28.00	2.08	0.49	4.26	2.08E-05	6.98E-04	Extracellular	Soluble
KCNJ3	25.21	2.07	0.50	4.15	3.36E-05	9.85E-04	Cell membrane	Membrane
IGFBP4	40.53	2.07	0.37	5.56	2.70E-08	3.08E-06	Extracellular	Soluble
GFRA2	17.89	2.06	0.57	3.61	3.02E-04	4.85E-03	Cell membrane	Membrane
LHX1	10.52	2.05	0.66	3.10	1.91E-03	1.81E-02	Nucleus	Soluble
QARS	12490.75	2.04	0.53	3.84	1.22E-04	2.52E-03	Cytoplasm	Soluble
PRRX2	9.76	2.04	0.70	2.92	3.45E-03	2.76E-02	Nucleus	Soluble
TMEM130	16.15	2.04	0.59	3.43	5.98E-04	7.94E-03	Cell membrane	Membrane
ZIC3	23.15	2.02	0.47	4.29	1.78E-05	6.37E-04	Nucleus	Soluble
LGI3	43.10	2.00	0.37	5.32	1.02E-07	9.84E-06	Extracellular	Soluble
RERG	33.77	1.99	0.38	5.19	2.14E-07	1.82E-05	Cytoplasm	Soluble
SLC7A3	57.84	1.99	0.44	4.49	7.08E-06	3.08E-04	Cell membrane	Membrane
B3GALT1	42.69	1.98	0.42	4.70	2.63E-06	1.40E-04	Extracellular	Soluble
CD6	8.30	1.98	0.74	2.67	7.48E-03	4.66E-02	Cell membrane	Membrane
G0S2	25.51	1.97	0.41	4.83	1.38E-06	8.32E-05	Mitochondrion	Membrane
PLPPR3	402.15	1.97	0.26	7.54	4.57E-14	1.98E-11	Cell membrane	Membrane
DECR1	22.91	1.94	0.56	3.47	5.19E-04	7.15E-03	Mitochondrion	Membrane
SLC27A6	52.54	1.93	0.34	5.62	1.86E-08	2.32E-06	Nucleus	Membrane
ZNF804A	13.25	1.91	0.66	2.91	3.60E-03	2.85E-02	Nucleus	Soluble
SERPINF1	309.75	1.89	0.23	8.32	8.73E-17	8.34E-14	Extracellular	Soluble
STC1	30.66	1.85	0.40	4.62	3.78E-06	1.88E-04	Extracellular	Soluble
CBLN1	17.35	1.85	0.49	3.76	1.73E-04	3.27E-03	Extracellular	Soluble
GSG1L	20.25	1.84	0.52	3.54	3.97E-04	5.89E-03	Cell membrane	Membrane
ATP10A	23.50	1.82	0.46	3.92	8.77E-05	2.02E-03	Cell membrane	Membrane

C2CD2	26.25	1.81	0.45	3.99	6.64E-05	1.64E-03	Cell membrane	Membrane
HTR6	111.22	1.80	0.29	6.22	5.00E-10	1.02E-07	Cell membrane	Membrane
HSPB1	122.44	1.75	0.28	6.34	2.27E-10	4.91E-08	Cytoplasm	Soluble
ATP2A3	115.92	1.75	0.27	6.40	1.51E-10	3.39E-08	Endoplasmic reticulum	Membrane
SFRP1	652.53	1.73	0.20	8.63	6.08E-18	7.33E-15	Extracellular	Soluble
NOTCH3	1429.35	1.73	0.23	7.51	6.11E-14	2.52E-11	Cell membrane	Membrane
PAX1	50.13	1.72	0.34	5.03	4.91E-07	3.63E-05	Nucleus	Soluble
SFRP5	121.69	1.70	0.30	5.73	9.88E-09	1.41E-06	Extracellular	Soluble
TSTD1	98.96	1.69	0.30	5.67	1.41E-08	1.88E-06	Cytoplasm	Soluble
ADAM12	14.80	1.69	0.61	2.76	5.85E-03	3.92E-02	Cell membrane	Membrane
GAS7	90.82	1.67	0.29	5.67	1.42E-08	1.88E-06	Cytoplasm	Soluble
FXYD6	63.86	1.65	0.30	5.47	4.56E-08	4.93E-06	Cell membrane	Membrane
P2RX5	178.14	1.65	0.23	7.20	5.88E-13	2.21E-10	Cell membrane	Membrane
TNS1	27.59	1.65	0.42	3.90	9.54E-05	2.14E-03	Cytoplasm	Soluble
ADCYAP1R1	126.35	1.65	0.23	7.12	1.08E-12	3.80E-10	Cell membrane	Membrane
VAT1	1154.00	1.62	0.20	8.02	1.08E-15	7.32E-13	Mitochondrion	Soluble
CLDN7	56.77	1.60	0.30	5.33	9.58E-08	9.39E-06	Cell membrane	Membrane
SLC9A2	53.40	1.59	0.31	5.12	2.99E-07	2.44E-05	Cell membrane	Membrane
VSTM2B	288.88	1.59	0.28	5.66	1.51E-08	1.96E-06	Cell membrane	Membrane
PLPP4	81.30	1.58	0.34	4.60	4.29E-06	2.08E-04	Lysosome/Vacuole	Membrane
MFI2	423.67	1.57	0.19	8.32	8.90E-17	8.34E-14	Cell membrane	Membrane
L1CAM	74.07	1.56	0.30	5.26	1.46E-07	1.33E-05	Cell membrane	Membrane
SCARA5	191.21	1.56	0.23	6.78	1.24E-11	3.48E-09	Cell membrane	Membrane
TSPO	224.36	1.55	0.28	5.57	2.58E-08	2.98E-06	Mitochondrion	Membrane
GRN	1491.03	1.54	0.24	6.36	2.06E-10	4.51E-08	Extracellular	Soluble
GHDC	251.86	1.54	0.22	6.92	4.44E-12	1.44E-09	Endoplasmic	Membrane

							reticulum	
APOC1	91.14	1.54	0.33	4.64	3.45E-06	1.75E-04	Extracellular	Soluble
SYNGR4	17.66	1.52	0.51	3.00	2.74E-03	2.35E-02	Cell membrane	Membrane
CXCL16	493.41	1.52	0.20	7.41	1.24E-13	4.99E-11	Cell membrane	Membrane
MME	77.13	1.51	0.29	5.23	1.69E-07	1.47E-05	Lysosome/Vacuole	Membrane
APOE	391.12	1.51	0.27	5.60	2.09E-08	2.55E-06	Extracellular	Soluble
RND2	670.12	1.51	0.19	7.78	6.98E-15	3.57E-12	Cell membrane	Membrane
MPP2	300.52	1.50	0.22	6.70	2.04E-11	5.56E-09	Cell membrane	Soluble
SPOCK1	79.83	1.47	0.33	4.45	8.48E-06	3.58E-04	Extracellular	Soluble
CILP2	234.35	1.46	0.26	5.61	1.99E-08	2.46E-06	Extracellular	Soluble
COL5A2	45.75	1.46	0.31	4.71	2.42E-06	1.31E-04	Extracellular	Soluble
DHRS13	265.89	1.46	0.23	6.25	4.08E-10	8.61E-08	Endoplasmic reticulum	Membrane
IL18R1	38.45	1.46	0.36	4.06	4.92E-05	1.31E-03	Cell membrane	Membrane
CRTAC1	116.04	1.46	0.28	5.14	2.79E-07	2.31E-05	Extracellular	Soluble
RAMP2	37.51	1.46	0.36	4.08	4.58E-05	1.26E-03	Cell membrane	Membrane
EGFL7	996.29	1.45	0.23	6.27	3.53E-10	7.54E-08	Extracellular	Soluble
RET	94.37	1.45	0.33	4.44	9.12E-06	3.76E-04	Cell membrane	Membrane
IKZF1	26.93	1.42	0.50	2.85	4.43E-03	3.27E-02	Nucleus	Soluble
CDH1	80.57	1.41	0.30	4.69	2.73E-06	1.44E-04	Cell membrane	Membrane
HIST1H2AE	347.94	1.41	0.28	5.12	3.08E-07	2.50E-05	Nucleus	Soluble
WNT3A	171.17	1.40	0.28	5.02	5.09E-07	3.73E-05	Extracellular	Soluble
ATP1A3	1311.32	1.39	0.20	6.80	1.05E-11	3.07E-09	Cell membrane	Membrane
UBE2L6	104.43	1.39	0.31	4.49	6.97E-06	3.06E-04	Nucleus	Soluble
JUP	766.25	1.39	0.27	5.16	2.42E-07	2.03E-05	Nucleus	Soluble
DPP4	54.02	1.38	0.32	4.35	1.38E-05	5.20E-04	Lysosome/Vacuole	Membrane
KDF1	44.28	1.37	0.36	3.79	1.48E-04	2.91E-03	Nucleus	Soluble

TCIRG1	151.50	1.37	0.23	5.91	3.46E-09	5.60E-07	Lysosome/Vacuole	Membrane
FGD5	18.57	1.35	0.46	2.97	2.94E-03	2.48E-02	Nucleus	Soluble
LAMA1	931.50	1.35	0.23	5.84	5.10E-09	7.76E-07	Extracellular	Soluble
PNMT	32.00	1.35	0.38	3.58	3.43E-04	5.26E-03	Cytoplasm	Soluble
RPL39L	106.45	1.33	0.29	4.63	3.58E-06	1.80E-04	Cytoplasm	Soluble
COL2A1	2247.66	1.33	0.24	5.66	1.52E-08	1.96E-06	Extracellular	Soluble
CNTFR	71.43	1.32	0.27	4.82	1.45E-06	8.60E-05	Cell membrane	Membrane
ATP1B2	143.21	1.32	0.23	5.72	1.09E-08	1.50E-06	Cell membrane	Membrane
SLC38A3	45.80	1.32	0.33	3.95	7.95E-05	1.85E-03	Cell membrane	Membrane
SLC47A1	620.00	1.31	0.21	6.21	5.20E-10	1.05E-07	Cell membrane	Membrane
LAMC3	372.39	1.31	0.21	6.21	5.41E-10	1.07E-07	Endoplasmic reticulum	Soluble
EFNB3	229.43	1.30	0.20	6.49	8.86E-11	2.17E-08	Cell membrane	Membrane
HPGD	30.15	1.30	0.40	3.25	1.15E-03	1.29E-02	Cytoplasm	Soluble
HSPG2	1731.60	1.29	0.23	5.50	3.88E-08	4.28E-06	Extracellular	Soluble
UGT3A2	39.92	1.29	0.40	3.24	1.21E-03	1.33E-02	Endoplasmic reticulum	Membrane
IGF2	104.20	1.28	0.34	3.82	1.36E-04	2.74E-03	Cell membrane	Membrane
FGFR4	317.76	1.28	0.21	5.95	2.65E-09	4.43E-07	Cell membrane	Membrane
RLTPR	289.19	1.28	0.23	5.50	3.85E-08	4.27E-06	Cytoplasm	Soluble
COL4A1	935.83	1.27	0.26	4.82	1.42E-06	8.52E-05	Extracellular	Soluble
PMP22	233.25	1.27	0.26	4.96	7.11E-07	4.93E-05	Cell membrane	Membrane
CLPSL2	24.60	1.26	0.41	3.09	2.02E-03	1.88E-02	Extracellular	Soluble
FAM171A2	689.59	1.26	0.21	6.11	9.85E-10	1.91E-07	Cell membrane	Membrane
PPP1R1A	74.84	1.26	0.28	4.44	8.87E-06	3.68E-04	Nucleus	Soluble
CPD	3639.40	1.26	0.21	5.87	4.25E-09	6.64E-07	Cell membrane	Membrane
KCNK6	42.87	1.26	0.33	3.80	1.42E-04	2.83E-03	Cell membrane	Membrane

PTH1R	37.59	1.25	0.38	3.29	1.00E-03	1.17E-02	Cell membrane	Membrane
COL21A1	88.71	1.25	0.32	3.89	9.99E-05	2.19E-03	Extracellular	Soluble
POLDIP2	1606.49	1.25	0.19	6.49	8.39E-11	2.08E-08	Mitochondrion	Soluble
IGSF11	19.87	1.24	0.46	2.68	7.46E-03	4.65E-02	Cell membrane	Membrane
ECHS1	1025.90	1.24	0.20	6.22	4.96E-10	1.02E-07	Mitochondrion	Soluble
ATP12A	30.39	1.24	0.39	3.21	1.35E-03	1.42E-02	Cell membrane	Membrane
SHANK2	154.74	1.24	0.24	5.08	3.74E-07	2.94E-05	Cytoplasm	Soluble
MMP2	123.49	1.24	0.24	5.24	1.57E-07	1.41E-05	Extracellular	Soluble
C1QBP	4271.77	1.23	0.20	6.11	1.02E-09	1.95E-07	Mitochondrion	Soluble
C1QL1	409.03	1.23	0.26	4.77	1.82E-06	1.04E-04	Extracellular	Soluble
NTN1	1175.47	1.22	0.20	5.97	2.33E-09	3.93E-07	Extracellular	Soluble
SLC16A7	54.60	1.22	0.33	3.74	1.83E-04	3.39E-03	Cell membrane	Membrane
PHYHD1	62.95	1.21	0.30	4.04	5.30E-05	1.39E-03	Cytoplasm	Soluble
FGF21	27.81	1.21	0.45	2.70	6.84E-03	4.40E-02	Extracellular	Soluble
MRPL45	42.83	1.20	0.35	3.43	6.03E-04	7.99E-03	Mitochondrion	Soluble
MYO1C	1456.66	1.20	0.20	6.10	1.09E-09	2.04E-07	Nucleus	Soluble
PSMB6	503.11	1.20	0.20	5.99	2.03E-09	3.50E-07	Nucleus	Soluble
ACVR1C	57.15	1.20	0.33	3.63	2.82E-04	4.60E-03	Cell membrane	Membrane
GSN	213.61	1.20	0.33	3.63	2.83E-04	4.61E-03	Endoplasmic reticulum	Soluble
COL4A2	1366.00	1.19	0.26	4.66	3.18E-06	1.64E-04	Cell membrane	Membrane
TP53I13	1521.10	1.19	0.18	6.51	7.76E-11	1.95E-08	Cell membrane	Membrane
KIF1C	2877.43	1.19	0.20	6.01	1.81E-09	3.17E-07	Cytoplasm	Soluble
SECTM1	29.42	1.19	0.42	2.85	4.35E-03	3.24E-02	Cell membrane	Membrane
PEMT	575.29	1.19	0.20	5.91	3.48E-09	5.60E-07	Endoplasmic reticulum	Membrane
SYT16	40.75	1.18	0.35	3.37	7.57E-04	9.45E-03	Cytoplasm	Soluble

RASGRP2	51.73	1.18	0.40	2.93	3.38E-03	2.72E-02	Cytoplasm	Soluble
RAB11FIP4	576.59	1.17	0.19	6.04	1.50E-09	2.71E-07	Cytoplasm	Soluble
ARHGAP44	364.54	1.17	0.18	6.62	3.63E-11	9.41E-09	Cytoplasm	Soluble
PALM3	28.99	1.17	0.39	2.96	3.09E-03	2.56E-02	Cytoplasm	Soluble
VWA1	326.09	1.16	0.23	5.06	4.26E-07	3.29E-05	Extracellular	Soluble
HIST2H2AA3	678.44	1.16	0.27	4.27	1.93E-05	6.72E-04	Nucleus	Soluble
ZNF385C	53.42	1.16	0.40	2.91	3.59E-03	2.84E-02	Nucleus	Soluble
COPRS	514.83	1.16	0.20	5.79	6.98E-09	1.02E-06	Nucleus	Soluble
MGAT3	562.05	1.15	0.19	6.06	1.33E-09	2.45E-07	Golgi apparatus	Membrane
G6PC3	1166.94	1.15	0.22	5.29	1.25E-07	1.19E-05	Endoplasmic reticulum	Membrane
PIGS	2020.70	1.15	0.18	6.40	1.58E-10	3.51E-08	Endoplasmic reticulum	Membrane
SERPINI1	25.13	1.15	0.42	2.74	6.14E-03	4.07E-02	Extracellular	Soluble
CYP26B1	257.07	1.15	0.23	4.88	1.06E-06	6.81E-05	Endoplasmic reticulum	Membrane
LRP2	1023.31	1.14	0.25	4.65	3.39E-06	1.73E-04	Cell membrane	Membrane
AQP3	45.18	1.14	0.35	3.22	1.26E-03	1.36E-02	Lysosome/Vacuole	Membrane
FAM101B	1456.77	1.14	0.23	4.97	6.66E-07	4.67E-05	Cytoplasm	Soluble
PWWP2B	337.75	1.14	0.21	5.35	8.77E-08	8.76E-06	Nucleus	Soluble
NDRG1	2474.35	1.14	0.21	5.38	7.43E-08	7.51E-06	Cytoplasm	Soluble
COPS3	1024.92	1.13	0.20	5.64	1.74E-08	2.19E-06	Nucleus	Soluble
ATG9A	1575.92	1.13	0.21	5.30	1.15E-07	1.10E-05	Cell membrane	Membrane
FAM134C	1176.53	1.13	0.20	5.64	1.66E-08	2.11E-06	Endoplasmic reticulum	Membrane
PTPRU	2061.46	1.12	0.18	6.19	5.92E-10	1.16E-07	Cell membrane	Membrane
MYRIP	43.99	1.12	0.35	3.24	1.18E-03	1.30E-02	Cytoplasm	Soluble

FAM19A5	231.12	1.12	0.24	4.71	2.44E-06	1.31E-04	Extracellular	Soluble
GPX3	213.24	1.12	0.23	4.77	1.85E-06	1.05E-04	Extracellular	Soluble
COL9A2	55.45	1.12	0.35	3.19	1.44E-03	1.48E-02	Cell membrane	Membrane
IGFBP2	1490.75	1.12	0.24	4.73	2.25E-06	1.23E-04	Extracellular	Soluble
AKNA	177.02	1.12	0.25	4.49	7.09E-06	3.08E-04	Nucleus	Soluble
CTSD	964.65	1.12	0.23	4.82	1.41E-06	8.44E-05	Lysosome/Vacuole	Soluble
MYO1D	662.58	1.11	0.25	4.48	7.61E-06	3.25E-04	Cytoplasm	Soluble
PLEKHB1	44.98	1.11	0.35	3.19	1.41E-03	1.47E-02	Golgi apparatus	Membrane
IGSF8	417.92	1.11	0.23	4.87	1.12E-06	7.03E-05	Cell membrane	Membrane
NELL2	931.04	1.10	0.24	4.55	5.40E-06	2.51E-04	Cell membrane	Membrane
SPARC	96.63	1.10	0.34	3.24	1.20E-03	1.32E-02	Extracellular	Soluble
ITGA2B	66.60	1.10	0.26	4.18	2.95E-05	8.93E-04	Cell membrane	Membrane
FRMPD3	45.21	1.09	0.35	3.09	2.01E-03	1.87E-02	Cytoplasm	Soluble
PTPRF	5828.35	1.09	0.19	5.66	1.55E-08	1.98E-06	Cell membrane	Membrane
CYP2J2	56.17	1.09	0.30	3.61	3.08E-04	4.93E-03	Endoplasmic reticulum	Membrane
SLC52A2	566.44	1.09	0.22	4.90	9.40E-07	6.15E-05	Cell membrane	Membrane
DLGAP3	106.43	1.08	0.25	4.31	1.66E-05	6.05E-04	Nucleus	Soluble
ATP1A1	9358.34	1.08	0.24	4.52	6.12E-06	2.78E-04	Cell membrane	Membrane
ADAMTS2	482.86	1.07	0.22	4.90	9.51E-07	6.19E-05	Extracellular	Soluble
CHCHD10	128.57	1.07	0.28	3.82	1.33E-04	2.70E-03	Mitochondrion	Soluble
CPT1A	288.87	1.06	0.20	5.31	1.12E-07	1.07E-05	Mitochondrion	Membrane
SUSD4	190.67	1.06	0.23	4.67	3.01E-06	1.56E-04	Cell membrane	Membrane
GSTP1	476.50	1.06	0.20	5.28	1.32E-07	1.21E-05	Cytoplasm	Soluble
FN1	1477.61	1.05	0.20	5.26	1.42E-07	1.30E-05	Extracellular	Soluble
FBLN1	939.09	1.05	0.26	4.05	5.11E-05	1.35E-03	Extracellular	Soluble
VSTM2L	67.31	1.05	0.34	3.13	1.76E-03	1.72E-02	Extracellular	Soluble

LLGL1	1568.50	1.05	0.19	5.57	2.48E-08	2.93E-06	Cytoplasm	Soluble
PROCR	333.21	1.05	0.25	4.27	1.93E-05	6.72E-04	Endoplasmic reticulum	Membrane
HLA-B	617.38	1.05	0.23	4.65	3.37E-06	1.72E-04	Cell membrane	Membrane
NSG1	128.55	1.05	0.25	4.28	1.91E-05	6.67E-04	Cell membrane	Membrane
APLP1	760.35	1.05	0.21	5.04	4.58E-07	3.45E-05	Endoplasmic reticulum	Membrane
ITIH5	35.13	1.05	0.36	2.90	3.72E-03	2.91E-02	Extracellular	Soluble
HIST2H4B	855.48	1.04	0.23	4.45	8.60E-06	3.62E-04	Nucleus	Soluble
FLOT2	1826.85	1.04	0.20	5.13	2.89E-07	2.38E-05	Cell membrane	Membrane
SLC19A1	1938.94	1.04	0.21	4.85	1.26E-06	7.67E-05	Cell membrane	Membrane
RASL10B	2147.40	1.04	0.21	4.95	7.60E-07	5.19E-05	Cell membrane	Membrane
DPYSL4	235.86	1.04	0.19	5.34	9.47E-08	9.34E-06	Cytoplasm	Soluble
NXPH4	808.47	1.04	0.22	4.65	3.24E-06	1.66E-04	Extracellular	Soluble
MT-ND5	5396.02	1.03	0.23	4.54	5.62E-06	2.58E-04	Mitochondrion	Membrane
TMEM256	213.85	1.03	0.23	4.44	8.81E-06	3.66E-04	Endoplasmic reticulum	Membrane
CERS1	94.27	1.03	0.26	3.99	6.54E-05	1.61E-03	Endoplasmic reticulum	Membrane
NTN3	121.44	1.03	0.27	3.75	1.79E-04	3.35E-03	Extracellular	Soluble
NUCB1	1941.73	1.03	0.19	5.46	4.72E-08	5.04E-06	Endoplasmic reticulum	Soluble
TMEM99	211.97	1.03	0.21	4.85	1.22E-06	7.50E-05	Cell membrane	Membrane
THRA	662.33	1.03	0.21	4.79	1.69E-06	9.78E-05	Nucleus	Soluble
JAG2	3598.57	1.02	0.20	5.24	1.61E-07	1.42E-05	Cell membrane	Membrane
CR2	96.70	1.02	0.26	3.90	9.72E-05	2.16E-03	Extracellular	Soluble
FKBP1C	26.52	1.02	0.38	2.73	6.42E-03	4.20E-02	Cytoplasm	Soluble

	AMHR2	54.67	1.02	0.31	3.30	9.65E-04	1.14E-02	Cell membrane	Membrane
	SLC7A1	4024.27	1.02	0.22	4.56	5.14E-06	2.42E-04	Cell membrane	Membrane
	HIST2H4A	174.62	1.02	0.28	3.59	3.32E-04	5.15E-03	Nucleus	Soluble
	NLRP1	211.11	1.01	0.20	5.00	5.70E-07	4.11E-05	Cytoplasm	Soluble
	CTDNEP1	1193.57	1.01	0.21	4.87	1.13E-06	7.11E-05	Endoplasmic reticulum	Membrane
	MDK	2494.83	1.01	0.22	4.68	2.80E-06	1.47E-04	Extracellular	Soluble
	KIAA0100	4081.07	1.01	0.20	4.98	6.33E-07	4.51E-05	Endoplasmic reticulum	Membrane
	B4GALT1	1040.88	1.01	0.20	4.92	8.64E-07	5.76E-05	Golgi apparatus	Membrane
	ZDHHC24	568.08	1.01	0.21	4.90	9.71E-07	6.28E-05	Endoplasmic reticulum	Membrane
	DCAKD	627.08	1.01	0.17	5.87	4.44E-09	6.87E-07	Cytoplasm	Soluble
	HHIP	173.71	1.00	0.23	4.34	1.40E-05	5.22E-04	Extracellular	Soluble
	NKAIN1	153.07	1.00	0.28	3.54	4.01E-04	5.92E-03	Cell membrane	Membrane
	RARG	328.68	1.00	0.18	5.43	5.58E-08	5.91E-06	Nucleus	Soluble

Appendix C

Supporting information for Figure 13: Differences in subsets of membrane bound ribosomes revealed under global disturbance of cellular translation.. **A)** Polysome traces for the whole cell treated with the indicated small molecule to ensure effectiveness of the dosage. **B)** India ink stains of the corresponding streptavidin blots.

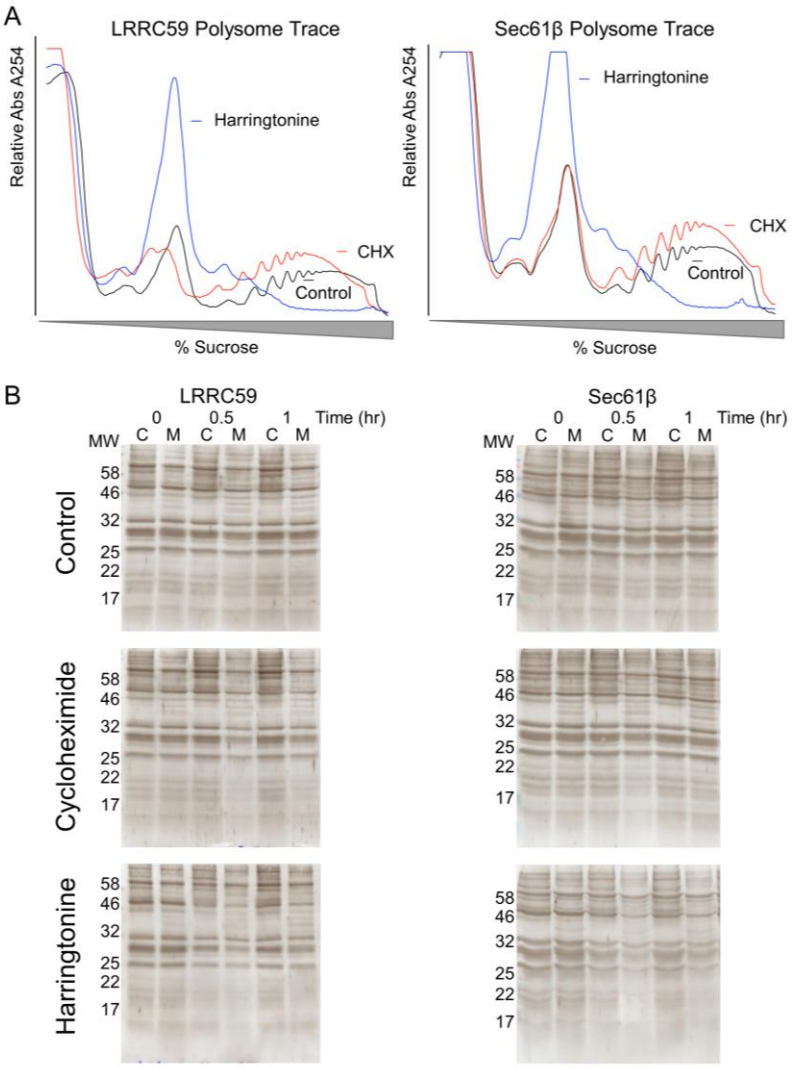

Appendix D

Supporting information for Figure 14. **A)** Scatterplots of the log2(count) for each indicated replicate with Pearson correlation coefficients in the lower right corner. **B)** Euclidean distance heatmap between each replicate to show that experimental samples are more similar to each other than to the EV control samples.

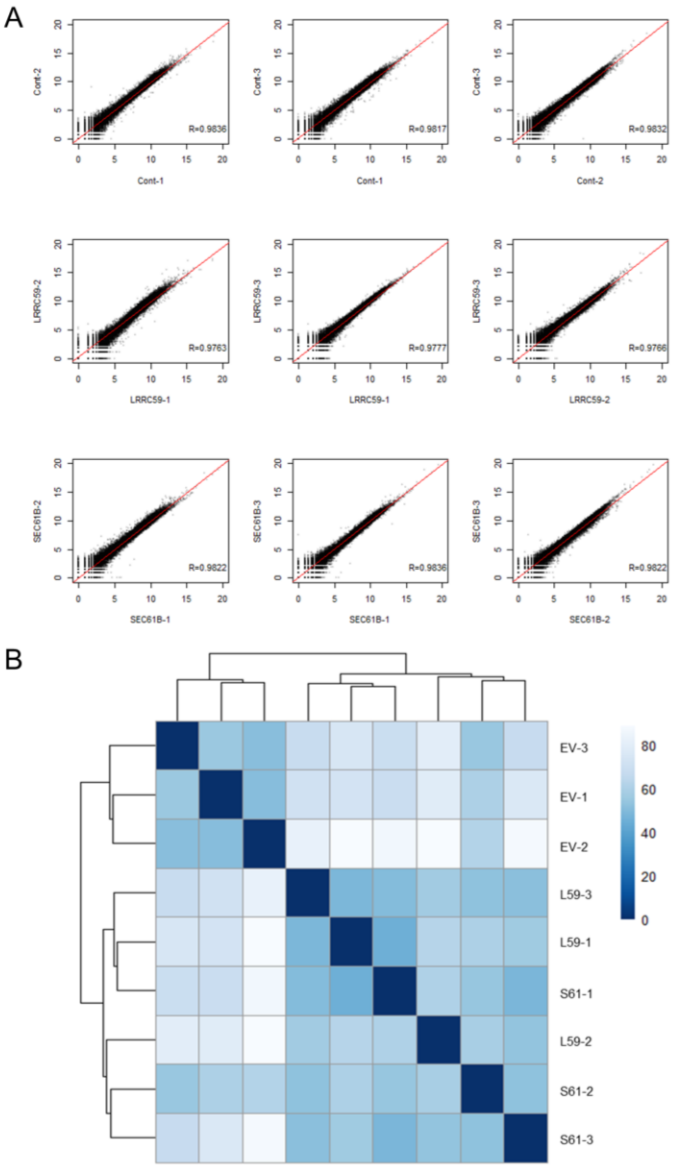
A
Cont-2
Cont-1
R=0.9836
Cont-3
Cont-1
R=0.9817
Cont-3
Cont-2
R=0.9832
LRRC59-2
LRRC59-1
R=0.9763
LRRC59-3
LRRC59-1
R=0.9777
LRRC59-3
LRRC59-2
R=0.9766
SEC61B-2
SEC61B-1
R=0.9822
SEC61B-3
SEC61B-1
R=0.9836
SEC61B-3
SEC61B-2
R=0.9822
B
EV-3
EV-1
EV-2
L59-3
L59-1
S61-1
L59-2
S61-2
S61-3
80
60
40
20
0

References

1. Porter, K. R., Claude, A. & Fullam, E. F. A STUDY OF TISSUE CULTURE CELLS BY ELECTRON MICROSCOPY: METHODS AND PRELIMINARY OBSERVATIONS. *J. Exp. Med.* **81,** 233–246 (1945).

2. Porter, K. R. & Kallman, F. L. SIGNIFICANCE OF CELL PARTICULATES AS SEEN BY ELECTRON MICROSCOPY. *Ann. N. Y. Acad. Sci.* **54,** 882–891 (1952).

3. Palade, G. E. & Siekevitz, P. Liver microsomes; an integrated morphological and biochemical study. *J. Biophys. Biochem. Cytol.* **2,** 171–200 (1956).

4. Dallner, G., Orrenius, S. & Bergstrand, A. Isolation and properties of rough and smooth vesicles from rat liver. *J. Cell Biol.* **16,** 426–30 (1963).

5. Blobel, G. & Dobberstein, B. Transfer of proteins across membranes. I. Presence of proteolytically processed and unprocessed nascent immunoglobulin light chains on membrane-bound ribosomes of murine myeloma. *J. Cell Biol.* **67,** 835–851 (1975).

6. Blobel, G. & Dobberstein, B. Transfer of protein across membranes. II. Reconstitution of functional rough microsomes from heterologous components. *J. Cell Biol.* **67,** 852–862 (1975).

7. Higgins, J. A. & Barrnett, R. J. STUDIES ON THE BIOGENESIS OF SMOOTH ENDOPLASMIC RETICULUM MEMBRANES IN LIVERS OF PHENOBARBITAL-TREATED RATS : I. The Site of Activity of Acyltransferases Involved in Synthesis of the Membrane Phospholipid. *J. Cell Biol.* **55,** 282–98 (1972).

8. Iseri, O. A., Lieber, C. S. & Gottlieb, L. S. The ultrastructure of fatty liver induced by prolonged ethanol ingestion. *Am. J. Pathol.* **48,** 535–55 (1966).

9. Lynes, E. M. & Simmen, T. Urban planning of the endoplasmic reticulum (ER): how diverse mechanisms segregate the many functions of the ER. *Biochim. Biophys. Acta - Mol. Cell Res.* **1813,** 1893–905 (2011).

10. Hayashi-Nishino, M. *et al.* A subdomain of the endoplasmic reticulum forms a cradle for autophagosome formation. *Nat. Cell Biol.* **11,** 1433–1437 (2009).

11. Reid, D. W. & Nicchitta, C. V. Primary Role for Endoplasmic Reticulum-bound Ribosomes in Cellular Translation Identified by Ribosome Profiling. *J. Biol. Chem.* **287,** 5518–5527 (2012).

12. Pépin, G., Perron, M. P. & Provost, P. Regulation of human Dicer by the resident ER membrane protein CLIMP-63. *Nucleic Acids Res.* **40,** 11603–11617 (2012).

13. Stalder, L. *et al.* The rough endoplasmatic reticulum is a central nucleation site of siRNA-mediated RNA silencing. *EMBO J.* **32,** 1115–27 (2013).

14. Humphreys, L. & Masters, C. On the differential release of glycolytic enzymes from cellular structure. *Biochem. Int.* **13,** 71–7 (1986).

15. McCloskey, M. A. & Poo, M. M. Rates of membrane-associated reactions: reduction of dimensionality revisited. *J. Cell Biol.* **102,** 88–96 (1986).

16. Cho, H. Y. *et al.* Assembly of Multi-tRNA Synthetase Complex via Heterotetrameric Glutathione Transferase-homology Domains. *J. Biol. Chem.* **290,** 29313–28 (2015).

17. Hu, J. *et al.* Size- and speed-dependent mechanical behavior in living mammalian cytoplasm. *Proc. Natl. Acad. Sci. U. S. A.* **114,** 9529–9534 (2017).

18. Singer, A. S. J. & Nicolson, G. L. The Fluid Mosaic Model of the Structure of Cell Membranes. *Science (80-.).* **175,** 720–731 (1972).

19. Kusumi, A., Suzuki, K. G. N., Kasai, R. S., Ritchie, K. & Fujiwara, T. K. Hierarchical mesoscale domain organization of the plasma membrane. *Trends Biochem. Sci.* **36,** 604–615 (2011).

20. Kusumi, A. *et al.* Dynamic Organizing Principles of the Plasma Membrane that Regulate Signal Transduction: Commemorating the Fortieth Anniversary of Singer and Nicolson's Fluid-Mosaic Model. *Annu. Rev. Cell Dev. Biol.* **28,** 215–250 (2012).

21. Kalay, Z., Fujiwara, T. K. & Kusumi, A. Confining Domains Lead to Reaction Bursts: Reaction Kinetics in the Plasma Membrane. *PLoS One* **7,** e32948 (2012).

22. Saka, S. K. *et al.* Multi-protein assemblies underlie the mesoscale organization of the plasma membrane. *Nat. Commun.* **5,** 4509 (2014).

23. Jagannathan, S., Reid, D. W., Cox, A. H. & Nicchitta, C. V. De novo translation initiation on membrane-bound ribosomes as a mechanism for localization of cytosolic protein mRNAs to the endoplasmic reticulum. *RNA* (2014). doi:10.1261/rna.045526.114

24. West, M., Zurek, N., Hoenger, A. & Voeltz, G. K. A 3D analysis of yeast ER structure reveals how ER domains are organized by membrane curvature. *J. Cell Biol.* **193,** 333–346 (2011).

25. Sandoz, P. A. & van der Goot, F. G. How many lives does CLIMP-63 have? *Biochem. Soc. Trans.* **43,** 222–8 (2015).

26. Klopfenstein, D. R. *et al.* Subdomain-specific localization of CLIMP-63 (p63) in the endoplasmic reticulum is mediated by its luminal alpha-helical segment. *J. Cell Biol.* **153,** 1287–300 (2001).

27. Shibata, Y. *et al.* Mechanisms Determining the Morphology of the Peripheral ER. *Cell* **143,** 774–788 (2010).

28. Schroeder, L. K. *et al.* Dynamic nanoscale morphology of the ER surveyed by STED microscopy. *J. Cell Biol.* **218,** 83–96 (2019).

29. Holcman, D. *et al.* Single particle trajectories reveal active endoplasmic reticulum luminal flow. *Nat. Cell Biol.* **20,** 1118–1125 (2018).

30. Rhee, H. *et al.* Proteomic Mapping of Mitochondria. *Science (80-.).* **339,** 1328 (2013).

31. Roux, K. J., Kim, D. I., Raida, M. & Burke, B. A promiscuous biotin ligase fusion protein identifies proximal and interacting proteins in mammalian cells. *J. Cell Biol.* **196,** 801–810 (2012).

32. Hung, V. *et al.* Proteomic mapping of cytosol-facing outer mitochondrial and ER membranes in living human cells by proximity biotinylation. *Elife* **6,** (2017).

33. Jing, J. *et al.* Proteomic mapping of ER-PM junctions identifies STIMATE as a regulator of Ca(2+) influx. *Nat. Cell Biol.* **17,** 1339–1347 (2015).

34. Spence, E. F. *et al.* In vivo proximity proteomics of nascent synapses reveals a novel regulator of cytoskeleton-mediated synaptic maturation. *Nat. Commun.* **10,**

386 (2019).

35. Paek, J. *et al.* Multidimensional Tracking of GPCR Signaling via Peroxidase-Catalyzed Proximity Labeling. *Cell* **169,** 338–349.e11 (2017).

36. Ellens, K. W. *et al.* Confronting the catalytic dark matter encoded by sequenced genomes. *Nucleic Acids Res.* **45,** 11495–11514 (2017).

37. Siekevitz, P. & Palade, G. E. A Cytochemical Study on the Pancreas of the Guinea Pig : V. In vivo Incorporation of Leucine-1-C(14) into the Chymotrypsinogen of Various Cell Fractions. *J. Biophys. Biochem. Cytol.* **7,** 619–630 (1960).

38. Blobel, G. & Sabatini, D. in *Biomembranes* (ed. Manson, L.) 193–195 (Springer US, 1971). doi:10.1007/978-1-4684-3330-2_16

39. Gilmore, R., Blobel, G. & Walter, P. Protein translocation across the endoplasmic reticulum. I. Detection in the microsomal membrane of a receptor for the signal recognition particle. *J. Cell Biol.* **95,** 463–469 (1982).

40. Gilmore, R., Walter, P. & Blobel, G. Protein translocation across the endoplasmic reticulum. II. Isolation and characterization of the signal recognition particle receptor. *J. Cell Biol.* **95,** 470–477 (1982).

41. Evans, E. A., Gilmore, R. & Blobel, G. Purification of microsomal signal peptidase as a complex. *Proc. Natl Acad. Sci. USA* **83,** 581–585 (1986).

42. Deshaies, R. J. & Schekman, R. A yeast mutant defective at an early stage in import of secretory protein precursors into the endoplasmic reticulum. *J. Cell Biol.* **105,** 633–645 (1987).

43. Gorlich, D. & Rapoport, T. A. Protein translocation into proteoliposomes reconstituted from purified components of the endoplasmic reticulum membrane. *Cell* **75,** 615–630 (1993).

44. Diehn, M., Eisen, M. B., Botstein, D. & Brown, P. O. Large-scale identification of secreted and membrane-associated gene products using DNA microarrays. *Nat. Genet.* **25,** 58–62 (2000).

45. Diehn, M., Bhattacharya, R., Botstein, D. & Brown, P. O. Genome-Scale Identification of Membrane-Associated Human mRNAs. *PLoS Genet.* **2,** 39–50

(2006).

46. Jagannathan, S., Chen, Q. & Nicchitta, C. Endoplasmic Reticulum (ER) Resident Protein-Encoding mRNAs Undergo Translation-Independent Localization to Subdomains of the ER Membrane. *Mol Biol Cell* **22,** (2011).

47. Jagannathan, S. *et al.* Multifunctional Roles for the Protein Translocation Machinery in RNA Anchoring to the Endoplasmic Reticulum. *J. Biol. Chem.* **289,** 25907–25924 (2014).

48. Kopczynski, C. C. *et al.* A high throughput screen to identify secreted and transmembrane proteins involved in Drosophila embryogenesis. *Proc Natl Acad Sci U S A* **95,** 9973–9978 (1998).

49. Lerner, R. S. & Nicchitta, C. V. mRNA translation is compartmentalized to the endoplasmic reticulum following physiological inhibition of cap-dependent translation. *Rna-a Publ. Rna Soc.* **12,** 775–789 (2006).

50. Stephens, S. B. & Nicchitta, C. V. Divergent regulation of protein synthesis in the cytosol and endoplasmic reticulum compartments of mammalian cells. *Mol. Biol. Cell* **19,** 623–632 (2008).

51. Voigt, F. *et al.* Single-Molecule Quantification of Translation-Dependent Association of mRNAs with the Endoplasmic Reticulum. *Cell Rep.* **21,** 3740–3753 (2017).

52. Potter, M. D. & Nicchitta, C. V. Endoplasmic reticulum-bound ribosomes reside in stable association with the translocon following termination of protein synthesis. *J. Biol. Chem.* **277,** 23314–23320 (2002).

53. Liu, L. *et al.* RNA interference of signal peptide-binding protein SRP54 elicits deleterious effects and protein sorting defects in trypanosomes. *J. Biol. Chem.* **277,** 47348–47357 (2002).

54. Mutka, S. C. & Walter, P. Multifaceted physiological response allows yeast to adapt to the loss of the signal recognition particle-dependent protein-targeting pathway. *Mol Biol Cell* **12,** 577–588 (2001).

55. Potter, M. D. & Nicchitta, C. V. Ribosome-independent regulation of translocon composition and Sec61 alpha conformation. *J. Biol. Chem.* **275,** 2037–2045 (2000).

56. Borgese, N., Mok, W., Kreibich, G. & Sabatini, D. D. Ribosomal-membrane interaction: In vitro binding of ribosomes to microsomal membranes. *J. Mol. Biol.* **88,** 559–580 (1974).

57. Kreibich, G., Freienstein, C. M., Pereyra, B. N., Ulrich, B. L. & Sabatini, D. D. Proteins of rough microsomal membranes related to ribosome binding. II. Cross-linking of bound ribosomes to specific membrane proteins exposed at the binding sites. *J. Cell Biol.* **77,** 488–506 (1978).

58. Tazawa, S. *et al.* Identification of a Membrane Protein Responsible for Ribosome Binding in Rough Microsomal Membranes. *J. Biochem.* **109,** 89–98 (1991).

59. Savitz, A. J. & Meyer, D. I. Identification of a ribosome receptor in the rough endoplasmic reticulum. *Nature* **346,** 540–544 (1990).

60. Kalies, K.-U., Görlich, D. & Rapoport, T. A. Binding of ribosomes to the rough endoplasmic reticulum mediated by the Sec61p-complex. *J. Cell Biol.* **126,** 925–934 (1994).

61. Beckmann, R. *et al.* Alignment of conduits for the nascent polypeptide chain in the Ribosome-Sec61 complex. *Science (80-.).* **278,** 2123–2126 (1997).

62. Voorhees, R. M., Fernández, I. S., Scheres, S. H. & Hegde, R. S. Structure of the Mammalian Ribosome-Sec61 Complex to 3.4 Å Resolution. *Cell* **157,** 1632–1643 (2014).

63. Meyer, H.-A. *et al.* Mammalian Sec61 Is Associated with Sec62 and Sec63. *J. Biol. Chem.* **275,** 14550–14557 (2000).

64. Zupicich, J., Brenner, S. E. & Skarnes, W. C. Computational prediction of membrane-tethered transcription factors. *Genome Biol.* **2,** research0050.1 (2001).

65. Kozutsumi, Y., Segal, M., Normington, K., Gething, M.-J. & Sambrook, J. The presence of malfolded proteins in the endoplasmic reticulum signals the induction of glucose-regulated proteins. *Nature* **332,** 462–464 (1988).

66. Cox, J. S. & Walter, P. A novel mechanism for regulating activity of a transcription factor that controls the unfolded protein response. *Cell* **87,** 391–404 (1996).

67. Harding, H. P., Zhang, Y. & Ron, D. Protein translation and folding are coupled

by an endoplasmic-reticulum-resident kinase. *Nature* **397,** 271–274 (1999).

68. Haze, K., Yoshida, H., Yanagi, H., Yura, T. & Mori, K. Mammalian Transcription Factor ATF6 Is Synthesized as a Transmembrane Protein and Activated by Proteolysis in Response to Endoplasmic Reticulum Stress. *Mol. Biol. Cell* **10,** (1999).

69. Reid, D. W., Chen, Q., Tay, A. S. L., Shenolikar, S. & Nicchitta, C. V. The Unfolded Protein Response Triggers Selective mRNA Release from the Endoplasmic Reticulum. *Cell* **158,** 1362–1374 (2014).

70. Unsworth, H., Raguz, S., Edwards, H. J., Higgins, C. F. & Yague, E. mRNA escape from stress granule sequestration is dictated by localization to the endoplasmic reticulum. *FASEB J.* **24,** 3370–3380 (2010).

71. Grootjans, J., Kaser, A., Kaufman, R. J. & Blumberg, R. S. The unfolded protein response in immunity and inflammation. *Nat. Rev. Immunol.* **16,** 469–84 (2016).

72. Corazzari, M., Gagliardi, M., Fimia, G. M. & Piacentini, M. Endoplasmic Reticulum Stress, Unfolded Protein Response, and Cancer Cell Fate. *Front. Oncol.* **7,** 78 (2017).

73. Jain, S. *et al.* ATPase-Modulated Stress Granules Contain a Diverse Proteome and Substructure. *Cell* **164,** 487–498 (2016).

74. Protter, D. S. W. & Parker, R. Principles and Properties of Stress Granules. *Trends Cell Biol.* **26,** 668–679 (2016).

75. Shin, Y. & Brangwynne, C. P. Liquid phase condensation in cell physiology and disease. *Science* **357,** eaaf4382 (2017).

76. Lin, Y., Protter, D. S. W. S. W., Rosen, M. K. K. & Parker, R. Formation and Maturation of Phase-Separated Liquid Droplets by RNA-Binding Proteins. *Mol. Cell* **60,** 208–219 (2015).

77. Kato, M. *et al.* Cell-free Formation of RNA Granules: Low Complexity Sequence Domains Form Dynamic Fibers within Hydrogels. *Cell* **149,** 753–767 (2012).

78. Reijns, M. A. M., Alexander, R. D., Spiller, M. P. & Beggs, J. D. A role for Q/N-rich aggregation-prone regions in P-body localization. *J. Cell Sci.* **121,** 2463–72 (2008).

79. Guo, W. *et al.* An ALS-associated mutation affecting TDP-43 enhances protein aggregation, fibril formation and neurotoxicity. *Nat. Struct. Mol. Biol.* **18,** 822–830 (2011).

80. Wheeler, J. R., Matheny, T., Jain, S., Abrisch, R. & Parker, R. Distinct stages in stress granule assembly and disassembly. *Elife* **5,** 1–25 (2016).

81. Zhang, H. *et al.* RNA Controls PolyQ Protein Phase Transitions. *Mol. Cell* **60,** 220–230 (2015).

82. Shin, Y. *et al.* Spatiotemporal Control of Intracellular Phase Transitions Using Light-Activated optoDroplets. *Cell* **168,** 159–171.e14 (2017).

83. Zhang, P. *et al.* Chronic optogenetic induction of stress granules is cytotoxic and reveals the evolution of ALS-FTD pathology. *Elife* **8,** (2019).

84. Mateju, D. *et al.* An aberrant phase transition of stress granules triggered by misfolded protein and prevented by chaperone function. *EMBO J.* e201695957 (2017). doi:10.15252/EMBJ.201695957

85. Patel, A. *et al.* A Liquid-to-Solid Phase Transition of the ALS Protein FUS Accelerated by Disease Mutation. *Cell* **162,** 1066–77 (2015).

86. Buchan, J. R., Kolaitis, R.-M., Taylor, J. P. & Parker, R. Eukaryotic stress granules are cleared by autophagy and Cdc48/VCP function. *Cell* **153,** 1461–74 (2013).

87. Van Treeck, B. *et al.* RNA self-assembly contributes to stress granule formation and defining the stress granule transcriptome. *Proc. Natl. Acad. Sci. U. S. A.* **115,** 2734–2739 (2018).

88. Khong, A. *et al.* The Stress Granule Transcriptome Reveals Principles of mRNA Accumulation in Stress Granules. *Mol. Cell* **68,** 808–820.e5 (2017).

89. Moon, S. L. *et al.* Multicolour single-molecule tracking of mRNA interactions with RNP granules. *Nat. Cell Biol.* **21,** 162–168 (2019).

90. Stoecklin, G. *et al.* MK2-induced tristetraprolin:14-3-3 complexes prevent stress granule association and ARE-mRNA decay. *EMBO J.* **23,** 1313–1324 (2004).

91. Bakheet, T., Williams, B. R. G. & Khabar, K. S. A. ARED 2.0: an update of AU-rich

element mRNA database. *Nucleic Acids Res.* **31,** 421–423 (2003).

92. Li, G.-W., Burkhardt, D., Gross, C. & Weissman, J. S. Quantifying absolute protein synthesis rates reveals principles underlying allocation of cellular resources. *Cell* **157,** 624–35 (2014).

93. Damgaard, C. K. & Lykke-Andersen, J. Translational coregulation of 5'TOP mRNAs by TIA-1 and TIAR. *Genes Dev.* **25,** 2057–68 (2011).

94. Zid, B. M. & O'Shea, E. K. Promoter sequences direct cytoplasmic localization and translation of mRNAs during starvation in yeast. *Nature* **514,** 117–121 (2014).

95. English, A. R. & Voeltz, G. K. Endoplasmic reticulum structure and interconnections with other organelles. *Cold Spring Harb. Perspect. Biol.* **5,** 1–16 (2013).

96. Schwarz, D. S. & Blower, M. D. The endoplasmic reticulum: structure, function and response to cellular signaling. *Cell. Mol. Life Sci.* **73,** 79–94 (2016).

97. Fawcett, D. W. *An Atlas of Fine Structure: the cell, its organelles, and inclusions*. (WB Suanders Co, 1966).

98. Valm, A. M. *et al.* Applying systems-level spectral imaging and analysis to reveal the organelle interactome. *Nature* **546,** 162–167 (2017).

99. Helle, S. C. J. *et al.* Organization and function of membrane contact sites. *Biochim. Biophys. Acta - Mol. Cell Res.* **1833,** 2526–2541 (2013).

100. Vance, J. E. MAM (mitochondria-associated membranes) in mammalian cells: Lipids and beyond. *Biochim. Biophys. Acta - Mol. Cell Biol. Lipids* **1841,** 595–609 (2014).

101. de Brito, O. M. & Scorrano, L. An intimate liaison: spatial organization of the endoplasmic reticulum-mitochondria relationship. *EMBO J.* **29,** 2715–23 (2010).

102. Reid, D. W. & Nicchitta, C. V. Diversity and selectivity in mRNA translation on the endoplasmic reticulum. *Nat. Rev. Mol. Cell Biol.* **16,** 221–231 (2015).

103. Mueckler, M. M. & Pitot, H. C. Structure and function of rat liver polysome populations. I. Complexity, frequency distribution, and degree of uniqueness of

free and membrane-bound polysomal polyadenylate-containing RNA populations. *J. Cell Biol.* **90,** 495–506 (1981).

104. Schaletzky, J. & Rapoport, T. A. Ribosome Binding to and Dissociation from Translocation Sites of the Endoplasmic Reticulum Membrane. *Mol. Biol. Cell* **17,** 3860–3869 (2006).

105. Becker, T. *et al.* Structure of monomeric yeast and mammalian Sec61 complexes interacting with the translating ribosome. *Science (80-.).* **326,** 1369–1373 (2009).

106. Prinz, A., Behrens, C., Rapoport, T. A., Hartmann, E. & Kalies, K. Evolutionarily conserved binding of ribosomes to the translocation channel via the large ribosomal RNA. *Eur. Mol. Biol. Organ.* **19,** 1900–1906 (2000).

107. Pfeffer, S. *et al.* Structure of the native Sec61 protein-conducting channel. *Nat. Commun.* **6,** 8403 (2015).

108. Pfeffer, S. *et al.* Structure of the mammalian oligosaccharyl-transferase complex in the native ER protein translocon. *Nat. Commun.* **5,** 3072 (2014).

109. Gamerdinger, M., Hanebuth, M. A., Frickey, T. & Deuerling, E. The principle of antagonism ensures protein targeting specificity at the endoplasmic reticulum. *Science (80-.).* **348,** 201–207 (2015).

110. Cui, X. A., Zhang, H. & Palazzo, A. F. p180 Promotes the Ribosome-Independent Localization of a Subset of mRNA to the Endoplasmic Reticulum. *PLoS Biol.* **10,** (2012).

111. Harada, Y., Li, H., Li, H. & Lennarz, W. J. Oligosaccharyltransferase directly binds to ribosome at a location near the translocon-binding site. *Proc. Natl. Acad. Sci.* **106,** 6945–6949 (2009).

112. Sommer, N., Junne, T., Kalies, K.-U., Spiess, M. & Hartmann, E. TRAP assists membrane protein topogenesis at the mammalian ER membrane. *Biochim. Biophys. Acta - Mol. Cell Res.* **1833,** 3104–3111 (2013).

113. Voigt, S., Jungnickel, B., Hartmann, E. & Rapoport, T. A. Signal sequence-dependent function of the TRAM protein during early phases of protein transport across the endoplasmic reticulum membrane. *J. Cell Biol.* **134,** 25–35 (1996).

114. Cai, L., Fritz, D., Stefanovic, L. & Stefanovic, B. Binding of LARP6 to the Conserved 5′ Stem–Loop Regulates Translation of mRNAs Encoding Type I Collagen. *J. Mol. Biol.* **395,** 309–326 (2010).

115. Wilson, C. M. *et al.* Ribophorin I associates with a subset of membrane proteins after their integration at the Sec61 translocon. *J. Biol. Chem.* **280,** 4195–4206 (2005).

116. Wild, R. *et al.* Structure of the yeast oligosaccharyltransferase complex gives insight into eukaryotic N-glycosylation. *Science (80-.).* **359,** 545–550 (2018).

117. Pfeffer, S. *et al.* Dissecting the molecular organization of the translocon-associated protein complex. *Nat. Commun.* **8,** 14516 (2017).

118. Levy, R., Wiedmann, M. & Kreibich, G. In Vitro Binding of Ribosomes to the β Subunit of the Sec61p Protein Translocation Complex. *J. Biol. Chem.* **276,** 2340–2346 (2001).

119. Deshaies, R. J., Sanders, S. L., Feldheim, D. A. & Schekman, R. Assembly of yeast Sec proteins involved in translocation into the endoplasmic reticulum into a membrane-bound multisubunit complex. *Nature* **349,** 806–808 (1991).

120. Müller, L. *et al.* Evolutionary Gain of Function for the ER Membrane Protein Sec62 from Yeast to Humans. *Mol. Biol. Cell* **21,** 691–703 (2010).

121. Lang, S. *et al.* Different effects of Sec61α, Sec62 and Sec63 depletion on transport of polypeptides into the endoplasmic reticulum of mammalian cells. *J. Cell Sci.* **125,** 1958–1969 (2012).

122. Ichimura, T. *et al.* Anti-(p34 protein) antibodies inhibit ribosome binding to and protein translocation across the rough microsomal membrane. *FEBS Lett.* **326,** 241–245 (1993).

123. Jagannathan, S., Nwosu, C. & Nicchitta, C. V. in *RNA Detection and Visualization: Methods and Protocols* (ed. Gerst, J. E.) **714,** 301–321 (2011).

124. Stephens, S. B. & Nicchitta, C. V. in *Translation Initiation: Cell Biology, High-Throughput Methods, and Chemical-Based Approaches* (ed. Lorsch, J.) **431,** 47–60 (2007).

125. Choi-Rhee, E., Schulman, H. & Cronan, J. E. Promiscuous protein biotinylation by

Escherichia coli biotin protein ligase. *Protein Sci.* **13,** 3043–3050 (2004).

126. Kim, D. I. *et al.* Probing nuclear pore complex architecture with proximity-dependent biotinylation. *Proc. Natl. Acad. Sci.* **111,** E2453–E2461 (2014).

127. Nikonov, A. V., Snapp, E., Lippincott-Schwartz, J. & Kreibich, G. Active translocon complexes labeled with GFP-Dad1 diffuse slowly as large polysome arrays in the endoplasmic reticulum. *J. Cell Biol.* **158,** 497–506 (2002).

128. Jan, C. H., Williams, C. C. & Weissman, J. S. Principles of ER cotranslational translocation revealed by proximity-specific ribosome profiling. *Science (80-.).* **346,** (2014).

129. Varnaitė, R. & MacNeill, S. A. Meet the neighbors: Mapping local protein interactomes by proximity-dependent labeling with BioID. *Proteomics* **16,** 2503–2518 (2016).

130. Kwon, K. & Beckett, D. Function of a conserved sequence motif in biotin holoenzyme synthetases. *Protein Sci.* **9,** 1530–1539 (2000).

131. Rees, J. S., Li, X.-W., Perrett, S., Lilley, K. S. & Jackson, A. P. Protein Neighbors and Proximity Proteomics. *Mol. Cell. Proteomics* **14,** 2848–2856 (2015).

132. Ueda, S., Blee, A. M., Macway, K. G., Renner, D. J. & Yamada, S. Force Dependent Biotinylation of Myosin IIA by α-Catenin Tagged with a Promiscuous Biotin Ligase. *PLoS One* **10,** e0122886 (2015).

133. Gupta, G. D. *et al.* A Dynamic Protein Interaction Landscape of the Human Centrosome-Cilium Interface. *Cell* **163,** 1484–99 (2015).

134. Goyette, J. & Gaus, K. Mechanisms of protein nanoscale clustering. *Curr. Opin. Cell Biol.* **44,** 86–92 (2017).

135. Cross, B. C. S., Sinning, I., Luirink, J. & High, S. Delivering proteins for export from the cytosol. *Nat. Rev. Mol. Cell Biol.* **10,** 255–264 (2009).

136. Gardner, B. M., Pincus, D., Gotthardt, K., Gallagher, C. M. & Walter, P. Endoplasmic reticulum stress sensing in the unfolded protein response. *Cold Spring Harb. Perspect. Biol.* **5,** a013169 (2013).

137. Vembar, S. S. & Brodsky, J. L. One step at a time: endoplasmic reticulum-associated degradation. *Nat. Rev. Mol. Cell Biol.* **9,** 944–957 (2008).

138. Shannon, P. *et al.* Cytoscape: a software environment for integrated models of biomolecular interaction networks. *Genome Res.* **13,** 2498–504 (2003).

139. Szklarczyk, D. *et al.* The STRING database in 2017: quality-controlled protein–protein association networks, made broadly accessible. *Nucleic Acids Res.* **45,** D362–D368 (2017).

140. Castello, A. *et al.* Insights into RNA biology from an atlas of mammalian mRNA-binding proteins. *Cell* **149,** 1393–406 (2012).

141. Castello, A. *et al.* Comprehensive Identification of RNA-Binding Domains in Human Cells. *Mol. Cell* **63,** 696–710 (2016).

142. Hentze, M. W., Castello, A., Schwarzl, T. & Preiss, T. A brave new world of RNA-binding proteins. *Nat. Rev. Mol. Cell Biol.* **19,** 327–341 (2018).

143. Hsu, J. C. C., Reid, D. W., Hoffman, A. M., Sarkar, D. & Nicchitta, C. V. Oncoprotein AEG-1 is an endoplasmic reticulum RNA-binding protein whose interactome is enriched in organelle resident protein-encoding mRNAs. *RNA* **24,** 688–703 (2018).

144. Ueno, T., Kaneko, K., Sata, T., Hattori, S. & Ogawa-Goto, K. Regulation of polysome assembly on the endoplasmic reticulum by a coiled-coil protein, p180. *Nucleic Acids Res.* **40,** 3006–3017 (2012).

145. Chiantia, S. *et al.* Role of ceramide in membrane protein organization investigated by combined AFM and FCS. *Biochim. Biophys. Acta - Biomembr.* **1778,** 1356–1364 (2008).

146. Ogawa-Goto, K. *et al.* p180 Is Involved in the Interaction between the Endoplasmic Reticulum and Microtubules through a Novel Microtubule-binding and Bundling Domain. *Mol. Biol. Cell* **18,** 3741–3751 (2007).

147. Savitz, A. J. & Meyer, D. I. Receptor-mediated Ribosome Binding to Liposomes Depends on Lipid Composition. *J. Biol. Chem.* **272,** 13140–13145 (1997).

148. Chartron, J. W., Hunt, K. C. L. & Frydman, J. Cotranslational signal-independent

SRP preloading during membrane targeting. *Nature* **536,** 224–8 (2016).

149. Gorlich, D., Prehn, S., Hartmann, E., Kalies, K. U. & Rapoport, T. A. A mammalian homolog of SEC61p and SECYp is associated with ribosomes and nascent polypeptides during translocation. *Cell* **71,** 489–503 (1992).

150. Lingappa, V. R. & Blobel, G. Early Events in the Biosynthesis of Secretory and Membrane Proteins: The Signal Hypothesis. in *Proceedings of the 1979 Laurentian Hormone Conference* 451–475 (Academic Press, 1980). doi:10.1016/B978-0-12-571136-4.50018-8

151. Blobel, G. Protein Targeting (Nobel Lecture). *ChemBioChem* **1,** 86–102 (2000).

152. Braunger, K. *et al.* Structural basis for coupling protein transport and N-glycosylation at the mammalian endoplasmic reticulum. *Science (80-.).* **360,** 215–219 (2018).

153. Wilson, D. N. & Doudna Cate, J. H. The structure and function of the eukaryotic ribosome. *Cold Spring Harb. Perspect. Biol.* **4,** a011536 (2012).

154. Zhang, Y., Wölfle, T. & Rospert, S. Interaction of nascent chains with the ribosomal tunnel proteins Rpl4, Rpl17, and Rpl39 of Saccharomyces cerevisiae. *J. Biol. Chem.* **288,** 33697–707 (2013).

155. Lin, P. J., Jongsma, C. G., Pool, M. R. & Johnson, A. E. Polytopic membrane protein folding at L17 in the ribosome tunnel initiates cyclical changes at the translocon. *J. Cell Biol.* **195,** 55–70 (2011).

156. Cui, K., Coutts, M., Stahl, J. & Sytkowski, A. J. Novel interaction between the transcription factor CHOP (GADD153) and the ribosomal protein FTE/S3a modulates erythropoiesis. *J. Biol. Chem.* **275,** 7591–6 (2000).

157. Ingolia, N. T., Lareau, L. F. & Weissman, J. S. Ribosome profiling of mouse embryonic stem cells reveals the complexity and dynamics of mammalian proteomes. *Cell* **147,** 789–802 (2011).

158. Schneider-Poetsch, T. *et al.* Inhibition of eukaryotic translation elongation by cycloheximide and lactimidomycin. *Nat. Chem. Biol.* **6,** 209–217 (2010).

159. Walter, P. & Blobel, G. Signal recognition particle contains a 7S RNA essential for

protein translocation across the endoplasmic reticulum. *Nature* **299,** 691–698 (1982).

160. Baltz, A. G. *et al.* The mRNA-Bound Proteome and Its Global Occupancy Profile on Protein-Coding Transcripts. *Mol. Cell* **46,** 674–690 (2012).

161. Jan, C. H., Williams, C. C. & Weissman, J. S. Response to Comment on 'Principles of ER cotranslational translocation revealed by proximity-specific ribosome profiling'. *Science (80-.).* **348,** 1217–b (2015).

162. Hsu, J. C.-C. & Nicchitta, C. V. Proteome Expression: The Subcellular Organisation of Protein Synthesis. *eLS* 1–8 (2018). doi:10.1002/9780470015902.a0005718

163. Ohsumi, T. *et al.* Ribosome-binding protein p34 is a member of the leucine-rich-repeat-protein superfamily. *Biochem. J.* **294,** 465–472 (1993).

164. Shibatani, T., David, L. L., McCormack, A. L., Frueh, K. & Skach, W. R. Proteomic Analysis of Mammalian Oligosaccharyltransferase Reveals Multiple Subcomplexes that Contain Sec61, TRAP, and Two Potential New Subunits. *Biochemistry* **44,** 5982–5992 (2005).

165. Wang, H. & Stefanovic, B. Role of LARP6 and Nonmuscle Myosin in Partitioning of Collagen mRNAs to the ER Membrane. *PLoS One* **9,** e108870 (2014).

166. Blau, M. *et al.* ERj1p uses a universal ribosomal adaptor site to coordinate the 80S ribosome at the membrane. *Nat. Struct. Mol. Biol.* **12,** 1015–1016 (2005).

167. Benedix, J. *et al.* BiP Modulates the Affinity of Its Co-chaperone ERj1 for Ribosomes. *J. Biol. Chem.* **285,** 36427–36433 (2010).

168. Johnson, A. E. & van Waes, M. A. The translocon: a dynamic gateway at the ER membrane. *Annu. Rev. Cell Dev. Biol.* **15,** 799–842 (1999).

169. Mauro, V. P. & Edelman, G. M. The ribosome filter hypothesis. *Proc. Natl. Acad. Sci.* **99,** 12031–12036 (2002).

170. Gilbert, W. V. Functional specialization of ribosomes? *Trends Biochem. Sci.* **36,** 127–32 (2011).

171. Wu, B., Eliscovich, C., Yoon, Y. J. & Singer, R. H. Translation dynamics of single mRNAs in live cells and neurons. *Science (80-.).* **352,** 1430–1435 (2016).

172. Shi, Z. *et al.* Heterogeneous Ribosomes Preferentially Translate Distinct Subpools of mRNAs Genome-wide. *Mol. Cell* **67,** 71–83.e7 (2017).

173. Banani, S. F., Lee, H. O., Hyman, A. A. & Rosen, M. K. Biomolecular condensates: Organizers of cellular biochemistry. *Nat. Rev. Mol. Cell Biol.* **18,** 285–298 (2017).

174. Hudder, A., Nathanson, L. & Deutscher, M. P. Organization of Mammalian Cytoplasm. *Mol. Cell. Biol.* **23,** 9318–9326 (2003).

175. Youn, J.-Y. *et al.* High-Density Proximity Mapping Reveals the Subcellular Organization of mRNA-Associated Granules and Bodies. *Mol. Cell* 1–16 (2018). doi:10.1016/j.molcel.2017.12.020

176. Uezu, A. *et al.* Identification of an elaborate complex mediating postsynaptic inhibition. *Science (80-.).* **353,** 960–962 (2016).

177. Migliaccio, G., Nicchitta, C. V & Blobel, G. The signal sequence receptor, unlike the signal recognition particle receptor, is not essential for protein translocation. *J. Cell Biol.* **117,** 15–25 (1992).

178. Walter, P. & Blobel, G. Purification of a membrane-associated protein complex required for protein translocation across the endoplasmic reticulum. *Proc. Natl. Acad. Sci.* **77,** 7112–6 (1980).

179. Chomczynski, P. & Sacchi, N. The single-step method of RNA isolation by acid guanidinium thiocyanate–phenol–chloroform extraction: twenty-something years on. *Nat. Protoc.* **1,** 581–585 (2006).

180. Firat-Karalar, E. N. & Stearnsx, T. in *Methods in Cell Biology* **129,** 153–170 (2015).

181. Matasova, N. B. *et al.* Isolation of ribosomal subunits containing intact rRNA from human placenta: Estimation of functional activity of 80S ribosomes. *Anal. Biochem.* **198,** 219–223 (1991).

182. Ritchie, C., Cylinder, I., Platt, E. J. & Barklis, E. Analysis of HIV-1 Gag Protein Interactions via Biotin Ligase Tagging. *J. Virol.* **89,** 3988–4001 (2015).

183. Bolger, A. M., Lohse, M. & Usadel, B. Trimmomatic: a flexible trimmer for Illumina sequence data. *Bioinformatics* **30,** 2114–20 (2014).

184. Kim, D., Langmead, B. & Salzberg, S. L. HISAT: a fast spliced aligner with low memory requirements. *Nat. Methods* **12,** 357–360 (2015).

185. Anders, S., Pyl, P. T. & Huber, W. HTSeq-A Python framework to work with high-throughput sequencing data. *Bioinformatics* **31,** 166–169 (2015).

186. Love, M. I., Huber, W. & Anders, S. Moderated estimation of fold change and dispersion for RNA-seq data with DESeq2. *Genome Biol.* **15,** 550 (2014).

187. Benjamini, Y. & Hochberg, Y. Controlling the False Discovery Rate: A Practical and Powerful Approach to Multiple Controlling the False Discovery Rate: a Practical and Powerful Approach to Multiple Testing. *Source J. R. Stat. Soc. Ser. B* **57,** 289–300 (1995).

188. Almagro Armenteros, J. J. *et al.* DeepLoc: prediction of protein subcellular localization using deep learning. *Bioinformatics* **33,** 3387–3395 (2017).

189. Walter, P. & Ron, D. The unfolded protein response: from stress pathway to homeostatic regulation. *Science* **334,** 1081–6 (2011).

190. Kedersha, N. & Anderson, P. *Regulation of Translation by Stress Granules and Processing Bodies*. *Progress in Molecular Biology and Translational Science* **90,** (Elsevier Inc., 2009).

191. Macejak, D. G. & Sarnow, P. Internal initiation of translation mediated by the 5′ leader of a cellular mRNA. *Nature* **353,** 90–94 (1991).

192. Yoshida, H., Haze, K., Yanagi, H., Yura, T. & Mori, K. Identification of the cis-acting endoplasmic reticulum stress response element responsible for transcriptional induction of mammalian glucose-regulated proteins. Involvement of basic leucine zipper transcription factors. *J. Biol. Chem.* **273,** 33741–9 (1998).

193. Bensaude, O. Inhibiting eukaryotic transcription: Which compound to choose? How to evaluate its activity? *Transcription* **2,** 103–108 (2011).

194. Elbarbary, R. A. *et al.* Tudor-SN – mediated endonucleolytic decay of human cell microRNAs promotes G 1 /S phase transition. **862,** 859–862 (2017).

195. Keene, J. D. RNA regulons: coordination of post-transcriptional events. *Nat. Rev. Genet.* **8,** 533–543 (2007).

196. Zimmermann, R., Eyrisch, S., Ahmad, M. & Helms, V. Protein translocation across the ER membrane. *Biochim. Biophys. Acta - Biomembr.* **1808,** 912–924 (2011).

197. Jiang, Y., Cheng, Z., Mandon, E. C. & Gilmore, R. An interaction between the SRP receptor and the translocon is critical during cotranslational protein translocation. *J. Cell Biol.* **180,** 1149–61 (2008).

198. Snapp, E. L., Reinhart, G. A., Bogert, B. A., Lippincott-Schwartz, J. & Hegde, R. S. The organization of engaged and quiescent translocons in the endoplasmic reticulum of mammalian cells. *J. Cell Biol.* **164,** 997–1007 (2004).

199. Hegde, R. S., Voigt, S., Rapoport, T. A. & Lingappa, V. R. TRAM Regulates the Exposure of Nascent Secretory Proteins to the Cytosol during Translocation into the Endoplasmic Reticulum. *Cell* **92,** 621–631 (1998).

200. Abell, B. M. *et al.* Tail-anchored and Signal-anchored Proteins Utilize Overlapping Pathways during Membrane Insertion. *J. Biol. Chem.* **278,** 5669–5678 (2003).

201. Duncan, C. D. S. & Mata, J. Widespread Cotranslational Formation of Protein Complexes. *PLoS Genet.* **7,** e1002398 (2011).

202. Shiber, A. *et al.* Cotranslational assembly of protein complexes in eukaryotes revealed by ribosome profiling. *Nature* **561,** 268–272 (2018).

203. Korkmazhan, E., Teimouri, H., Peterman, N. & Levine, E. Dynamics of translation can determine the spatial organization of membrane-bound proteins and their mRNA. *Proc. Natl. Acad. Sci. U. S. A.* **114,** 13424–13429 (2017).

204. Sakahira, H. & Nagata, S. Co-translational folding of caspase-activated DNase with Hsp70, Hsp40, and inhibitor of caspase-activated DNase. *J. Biol. Chem.* **277,** 3364–70 (2002).

205. Halbach, A. *et al.* Cotranslational assembly of the yeast SET1C histone methyltransferase complex. *EMBO J.* **28,** 2959–2970 (2009).

206. Gahlmann, A. & Moerner, W. E. Exploring bacterial cell biology with single-molecule tracking and super-resolution imaging. *Nat. Rev. Microbiol.* **12,** 9–22

(2014).

207. Rassam, P. *et al.* Supramolecular assemblies underpin turnover of outer membrane proteins in bacteria. *Nature* **523,** 333–336 (2015).

208. Maurizio, E. *et al.* Translating Proteomic Into Functional Data: An High Mobility Group A1 (HMGA1) Proteomic Signature Has Prognostic Value in Breast Cancer. *Mol. Cell. Proteomics* **15,** 109–23 (2016).

209. Maquat, L. E., Hwang, J., Sato, H. & Tang, Y. CBP80-promoted mRNP rearrangements during the pioneer round of translation, nonsense-mediated mRNA decay, and thereafter. *Cold Spring Harb. Symp. Quant. Biol.* **75,** 127–34 (2010).

210. Zhang, K. *et al.* Stress granule assembly disrupts nucleocytoplasmic transport. *Cell* **173,** 1–14 (2018).

211. Markmiller, S. *et al.* Context-Dependent and Disease-Specific Diversity in Protein Interactions within Stress Granules. *Cell* **172,** 590–604.e13 (2018).

212. Fan, X. C. & Steitz, J. A. HNS, a nuclear-cytoplasmic shuttling sequence in HuR. *Proc. Natl. Acad. Sci. U. S. A.* **95,** 15293–8 (1998).

213. Myer, V. E., Fan, X., Steitz, J. & Shyu, A. Identification of HuR as a protein implicated in AUUUA-mediated mRNA decay. *EMBO J.* **16,** 2130–2139 (1997).

214. Fialcowitz-White, E. J. *et al.* Specific protein domains mediate cooperative assembly of HuR oligomers on AU-rich mRNA-destabilizing sequences. *J. Biol. Chem.* **282,** 20948–59 (2007).

215. Tie, H. C., Ludwig, A., Sandin, S. & Lu, L. The spatial separation of processing and transport functions to the interior and periphery of the Golgi stack. *Elife* **7,** (2018).

216. Feric, M. *et al.* Coexisting Liquid Phases Underlie Nucleolar Subcompartments. *Cell* **165,** 1686–1697 (2016).

Biography

I attended Williams College in Williamstown, MA and graduated with a Bachelor's degree in Chemistry in 2010. Here I performed undergraduate research in the chemistry department which helped encourage an interest in basic science, but I had a desire to gain experience outside of academia before perusing this further. After a few years of working as a Chemist at DuPont's famed Experimental Station campus in Wilmington, DE, many of the PhDs I worked for started encouraging me to apply for graduate programs. I chose to pursue a PhD in Biochemistry at Duke University matriculating in 2013. In 2014, I started my research in Dr. Christopher Nicchitta's lab where I have been studying the organization of complex biochemical processes within cells.